République Algérienne Démocratique et Populaire
Ministère de l'Enseignement Supérieur et de la Recherche Scientifique

Ecole Nationale Polytechnique
Electronic Department
Communications and Photovoltaic Conversation
Devices Laboratory (LDCCP)

Doctoral Thesis in Electronic

Option : Telecommunications

Presented by :

Soufiane TEBACHE

Magister in Electronic

Title

Contribution to Performance Improvement in Antenna-System-Design for Advanced Wireless Communications

---

Defended publicly on 2021/07/08, in front of the following dissertation committee:

President:	Mme TOUHAMI Rachida	Professor	ENP
Supervisors:	Mr BELOUCHRANI Adel	Professor	ENP
	Mr GHANEM Farid	Doctor	Right Innov
Examiners:	Mr DENIDNI Tayeb.A	Professor	INRS-Canada
	Mr TOUNSI Mohamed.L	Professor	USTHB
	Mr CHALLAL Mouloud	Professor	UMBB
	Mr ADNANE Mourad	Professor	ENP

ENP 2021

Communications and Photovoltaic Conversation Devices Laboratory (LDCCP)
Ecole Nationale Polytechnique (ENP)
10, Avenue Frères Oudek,Hassen Badi,BP.182,16200 El Harrach, Algiers, Algeria
www.enp.edu.dz

République Algérienne Démocratique et Populaire
Ministère de l'Enseignement Supérieur et de la Recherche Scientifique

Ecole Nationale Polytechnique
Electronic Department
Communications and Photovoltaic Conversation
Devices Laboratory (LDCCP)

Doctoral Thesis in Electronic

Option : Telecommunications

Presented by :

Soufiane TEBACHE

Magister in Electronic

Title

Contribution to Performance Improvement in Antenna-System-Design for Advanced Wireless Communications

---

Defended publicly on 2021/07/08, in front of the following dissertation committee:

President:	Mme TOUHAMI Rachida	Professor	ENP
Supervisors:	Mr BELOUCHRANI Adel	Professor	ENP
	Mr GHANEM Farid	Doctor	Right Innov
Examiners:	Mr DENIDNI Tayeb.A	Professor	INRS-Canada
	Mr TOUNSI Mohamed.L	Professor	USTHB
	Mr CHALLAL Mouloud	Professor	UMBB
	Mr ADNANE Mourad	Professor	ENP

ENP 2021

Communications and Photovoltaic Conversation Devices Laboratory (LDCCP)
Ecole Nationale Polytechnique (ENP)
10, Avenue Frères Oudek,Hassen Badi,BP.182,16200 El Harrach, Algiers, Algeria
www.enp.edu.dz

République Algérienne Démocratique et Populaire
Ministère de l'Enseignement Supérieur et de la Recherche Scientifique

Ecole Nationale Polytechnique
Département d'Electronique
Laboratoire des Dispositifs de Communications
et de Conversations Photovoltaïques (LDCCP)

Thèse de Doctorat en Electronique

Option : Télécommunications

Présentée par :

TEBACHE Soufiane

Magister en Electronique

Thème

Contribution to Performance Improvement in Antenna-System-Design for Advanced Wireless Communications

---

Soutenue publiquement le 08/07/2021, devant le jury composé de:

Président:	Mme TOUHAMI Rachida	Professeur	ENP
Rapporteurs:	Mr BELOUCHRANI Adel	Professeur	ENP
	Mr GHANEM Farid	Maitre de Recherche/A	Right Innov
Examinateurs:	Mr DENIDNI Tayeb.A	Professeur	INRS-Canada
	Mr TOUNSI Mohamed.L	Professeur	USTHB
	Mr CHALLAL Mouloud	Professeur	UMBB
	Mr ADNANE Mourad	Professeur	ENP

ENP 2021

Laboratoire des Dispositifs de Communications et de Conversations Photovoltaïques (LDCCP)
Ecole Nationale Polytechnique (ENP)
10, Avenue des Frères Oudek,Hassen Badi,BP.182,16200 El Harrach, Alger, Algérie
www.enp.edu.dz

"An invasion of armies can be resisted, but not an idea whose time has come".

Victor Hugo (1852).

Dedication

This thesis is dedicated to

My lovely Family

My dear Wife

My Son Iyad (Amyas)

My Daughter Anya

My Friends

My Professors from beginning until Now and

Forever...

Soufiane TEBACHE.

"Great goals deserve painful sacrifices"

Acknowledgments

First and the foremost, I would like to thank ***"Almighty ALLAH"*** *for bestowing His blessings upon me to achieve and complete this humble work.*

I am extremely grateful to my supervisors: ***Dr. Farid GHANEM*** *and* ***Pr. Adel BELOUCHRANI*** *for all of the help, moral and scientific support they provided during this work.*

A special gratitude is devoted to ***Dr. Ali MANSOU****L for his availability, his precious advices, suggestions and fruitful discussions we conducted together. Ali was and still is very generous in sharing knowledge.*

My sincere thanks to the ***Dissertation Committee: Pr. TOUHAMI Rachida*** *as president,* ***Pr. TOUNSI Mohamed Lamine, Pr. CHALLAL Mouloud*** *and* ***Pr. ADNANE Mourad*** *for reviewing and handling this work, for their advices and insightful comments, with great and many recognitions to* ***Pr. DENIDNI Tayeb.A*** *from* ***INRS-Canada*** *for devoting his time to review this thesis and advising me with valuable suggestions.*

Many thanks are also devoted to ***Dr. El Korso Mohammed Nabil*** *and to* ***Dr. Ratni Badreddine*** *from* ***LEME Laboratory, France*** *for their kindness and help.*

I would like to express my deep gratitude to all my friends and colleagues, notably: ***Dr. Lyes AMARA****,* ***Dr. Abdelheq BOUKARKAR*** *who are very motivating and supporting. I am also grateful to* ***Dr. Samy LABANDJI*** *for helping in antenna measurements. Great thanks go also to* ***Dr. Khalida GHANEM*** *for her kindness and sharing knowledge.*

I am extremely grateful to my colleague ***Mr. Rabah ABDI*** *for his multiple advices, suggestions, knowledge and encouragement. He is of special mind and I am very glade to be with him at work. Great respect for him.*

Finally, my gratitudes go also to all who contribute to complete this thesis work.

ملخص

تتناول هذه الأطروحة تصميم مكونات الأنظمة اللاسلكية الحديثة في ميدان الموجات الدقيقة. الهدف الرئيسي لذلك هو المساهمة في تحسين أداء هذه الأنظمة. يتكون عمل هذه الأطروحة من اقتراح تصاميم جديدة للتغلب على بعض التحديات في الهيمنة اللاسلكية. إعادة تشكيل إشعاع الهوائي كان الموضوع الأول الذي تم تناوله. يتعلق الأمر بالهوائيات أحادية القطب مع تطوير نهج بسيط لتحقيق إعادة التشكل. تعتبر وحدات تبديل الطور من المكونات الهامة في التطبيقات المختلفة التي تتطلب اطوار مختلفة، وبالتالي اقتراح ثلاثة تصاميم جديدة بعد دراسة شاملة. بالإضافة إلى ذلك، فإن تقنية MIMO واعدة جداً في التقنيات الحديثة، ومع ذلك فإن وجود اقتران متبادل بين الهوائيات يؤدي إلى تدهور كبير في أداء النظام. وقد تم تناول هذه المشكلة باقتراح آلية فعالة لفك ارتباط الهوائيات القريبة.

كلمات مفتاحية

الأنظمة اللاسلكية، إعادة تشكيل الإشعاع، مغيرات الطور، عزل الهوائيات.

Résumé

Titre: "Contribution à l'Amélioration des Performances en Conception de Systèmes d'Antennes pour les Communications Sans-Fil Avancées."

La présente thèse traite de la conception d'antennes pour les systèmes modernes sans fil, dans l'objectif de contribuer à l'amélioration de leurs performances. Le travail de cette thèse consiste en la proposition de nouvelles conceptions pour surmonter quelques défis dans le domaine sans fil. La reconfiguration du rayonnement des antennes est le premier sujet traité. Il concerne les antennes monopoles avec le développement d'une approche pour atteindre la reconfigurabilité. Les déphaseurs sont aussi des composants importants dans diverses applications, d'où la proposition de trois nouvelles conceptions suite à une étude approfondie. En outre, la technique MIMO est très prometteuse dans les technologies récentes, cependant la présence du couplage mutuel entre les antennes dégrade les performances du système. Ce problème est également traité avec la proposition d'un mécanisme efficace pour le découplage des antennes.

Mots-clés

Systèmes sans fil, Reconfiguration du rayonnement, Déphaseurs, Découplage des antennes.

Abstract

The present thesis deals with antenna design for modern wireless devices. The main goal is then to contribute in the performance improvement of those communications systems. Hence, the thesis suggests and investigates new designs to overcome some wireless challenges. Antenna pattern reconfiguration is the first subject treated. It concerns CPW-Fed monopole antennas where a simple approach is developed to achieve this purpose. Phase shifters are also key components in many advanced applications, hence they are deeply studied in this work and three novel designs have been proposed. Moreover, MIMO technique is very promising in recent technologies, however with the presence of antenna coupling the overall performances are drastically degraded. This challenge has also been tackled, and an efficient decoupling mechanism of closely spaced antennas is proposed.

Keywords

Wireless systems, Antenna pattern reconfiguration, Phase shifters, Antenna decoupling.

Contents

List of Tables

List of Figures

Acronyms

SDR	**S**oftware **D**efined **R**adio
CR	**C**ognitive **R**adio
GSM	**G**lobal **S**ystems for **M**obile telecommunications
UWB	**U**ltra **W**ide **B**and
ADC	**A**nalog to **D**igital **C**onverter
DAC	**D**igital to **A**nalog **C**onverter
LNA	**L**ow **N**oise **A**mplifier
USRP	**U**niversal **S**oftware **R**adio **P**eripheral
PC	**P**ersonal **C**omputer
NI	**N**ational **I**nstrument
FPGA	**F**ield **P**programmable **G**ate **A**rrays
MIMO	**M**ultiple **I**nput **M**ultiple **O**utput
CPW	**C**oplanar **W**ave-guide
SINR	**S**ignal to **I**nterference **N**oise **R**atio
TL	**T**ransmission **L**ine
DGS	**D**efected **G**round **S**tructure
CSRR	**C**omplementary **S**plit **R**ing **R**esonator
PCB	**P**rinted **C**ircuit **B**oard
EBG	**E**lectromagnetic **B**and **G**ap
DMN	**D**ecoupling and **M**atching **N**etwork
DRA	**D**ielectric **R**esonator **A**ntenna
ECC	**E**nvelope **C**orrelation **C**oefficient
DG	**D**iversity **G**ain
TARC	**T**otal **A**ctive **R**eflection **C**oefficient
CST	**C**omputer **S**imulation **T**echnology

ADS	**A**dvanced **D**esign **S**ystem
AWGN	**A**dditive **W**hite **G**aussian **N**oise
DOA	**D**irection **O**f **A**rrival
MCM	**M**utual **C**oupling **M**atrix
NI	**N**ational **I**nstruments
CDTA	**C**entre de **D**éveloppement des **T**echnologies **A**vancées

General Introduction

"Highlight the difference makes you a genius"

General Introduction

Tremendous advances in wireless communications systems have been noticed, every decade. Starting from analogue technology based systems as first generation (1G) developed in 1980s, then 2G systems in 1990s as Global Systems for Mobile Telecommunications (GSM) which benefits from digital technology. Several wireless systems have been therefore subject of permanent investigation and development such as 3G, 4G and 5G where first smart-phone devices available in the market in 2021.

The most targeted purposes in such systems are higher speed for increased data rate, more channel capacity and lower latency for real-time interaction as new applications appear day after day. Severe requirements are then raised, as example, important leap is expected by 2022 where 10 Gbits/s data rates for mobile terminals are projected, 73% of all mobile data traffic is expected to be video traffic by 2023 and new format 360-degree video will require five times the bandwidth of today's videos as well.

Tedious and long-term efforts are generally required to success advanced services. Indeed, integrating diverse wireless services and applications in one communications system is not an easy challenge. Software Defined Radio (SDR) and Cognitive Radio (CR) are new introduced promising concepts, since they allow large flexibility by software reconfiguration of their main features, for instance: frequency band, antenna specifications and roughly their whole front-end which must follow the reconfiguration requirements.

But, what will be the implication of RF system design (microwave devices, antennas, etc) in those future technologies? A key answer is the integration of multi-antenna systems for increasing transmission data rate, exploiting diversity and multi-services in limited bandwidth. Eventual new radio interface components are then part of the challenge.

Conventionally, antennas are considered as passive devices used to collect electromagnetic energy from free space, hence they look like sources or generators in the overall system. However, in the modern approach, antenna can provide novel aspects of filtering (fre-

quency filtering and space filtering) as well as radiating aspect. These new challenging aspects are achieved through reconfiguration concept. Consequently, modern antenna design may be very promising in reducing cost-design, avoiding bulk and offering more attractive services and improved performances.

Miniaturization of systems is also another crucial constraint in modern wireless devices. Indeed, industrials are excessively endeavouring to provide efficient systems in small and compact volume such as smart-phones, tablets and many others. This purpose has so far some technical limitations, notably when antennas are closely packed in limited space, thus electromagnetic coupling phenomenon rises. Consequently, the overall system performances are drastically degraded.

In the outlook of the aforementioned challenges, the work done in the present thesis aims at solving some antenna design tasks in order to achieve requirements of modern wireless devices. Hence, three main challenges are addressed: antenna radiation pattern reconfiguration, phase shifters design for multi-element systems and array antenna decoupling.

Reconfigurability is one of the most attractive and promising concept in emergent wireless systems such as SDR. It is particularly involved in RF front end, notably in antennas including frequency and pattern reconfiguration. This last task is treated and a solution is then proposed. It concerns CPW-Fed monopoles which are known to be omnidirectional antennas. However, in many cases, tilting the main beam in desired direction is fairly requested to achieve specific performances as diversity, fading and interference combat. Although, diverse techniques and methods are presented in the literature, the developed approach is simply based on judicious slotting of the ground plane of such antennas.

Phased arrays are also of great interest in several applications such as beam-forming and source localization. Need of specific devices is then raised. Phase shifters are crucial components in such hot topic. They allow steering the array main beam in wanted direction. This task is treated as well in this thesis, and different phase shifter designs are proposed as a solution to the raised problem.

Another most challenging subject is the antenna decoupling. Since MIMOs are promising solution in recent systems, important priority is then specially devoted to this kind of architectures. As stated before, antenna mutual coupling is found to be very harmful notably in closely packed elements. Therefore, this topic is addressed as well and a novel decoupling technique is studied and developed.

For summarizing, during this thesis work, we proposed novel designs related to microwave devices and antennas. We believe that proposed designs contribute significantly in the improvement of advanced wireless systems. Further, achieved works have been published, as research papers, in renown journals and in international conferences. Namely, achievements concern:

- Pattern reconfiguration of CPW-Fed monopoles,
- Three design approaches of phase shifters for UWB applications,
- Antenna decoupling technique of strongly coupled monopoles.

The thesis is organized in four chapters. The first one is devoted to introducing the challenges of modern wireless communications systems, SDR concept and USRP equipments based on software radio. In addition, a state of the art is established on three topics: antenna pattern reconfiguration, phase shifters design and antenna decoupling. Most of techniques and methods available in the literature are then presented and discussed.
The second chapter deals with the proposed approach for antenna pattern reconfiguration. Details of the approach with obtained results are then presented and discussed. The third chapter concerns design of microwave phase shifters. Frequency independent phase shift is obtained with two different methods. Additional achievements are discussed as well. The final chapter is related to the proposed decoupling mechanism of closely spaced antennas. Interesting results are obtained through a tapered slot integrated in the ground plane of the array. The thesis is finally ended with a general conclusion.

Chapter 1

Chapter 1

Modern Wireless Communications Challenges

1.1 Introduction

Nowadays, wireless communications have become a versatile domain involved in whole human-life. Indeed, signals, data and different informations are mostly transmitted between users by radio-waves technology, exploiting the free-space (wireless path) as a channel of communications.

Since the inception of wireless systems, researchers, engineers and industrials have constantly devoted tremendous efforts for developing efficient and smart systems with improved performances: more data-rate, compact size, lower manufacturing cost, and most importantly integration of multi-services. Consequently, the basic wireless system components — that is, the antenna and the analog and digital front ends — have been deeply investigated and attractive outcomes have been achieved in recent decades [1].

Software defined radio (SDR) is one of the revolutionary development which opened new perspectives in wireless communications. The SDR is based on th reconfiguration concept (frequency, radiation pattern or both of them), hence the antenna and the front-end should integrate this adaptability to provide a total reconfigurable wireless system.

Moreover, in next-generation wireless devices, higher performances are critically needed, for instance: high data rate, improved efficiency and compact size, to meet the new communications requirements as in 5G systems and beyond. MIMOs are one of the most promising solution for such purposes. However, gathering number of MIMO antennas in small surface is very challenging due to the rise of mutual coupling phenomenon, which degrades drastically the MIMO performances. Hence, decoupling techniques have been of

great interest for researches, in recent years.

1.2 Software defined radio (SDR)

1.2.1 Overview

Software defined radio (SDR) is a hot emergent topic in the telecommunications field. SDR is considered as a platform for integrating new technologies, many of today's separate systems and different services into existing networks with the same hardware platform. It therefore allows larger flexibility into mobile communications. Further, SDR is involved in both software development and digital signal processing [2]. SDR concept is very promising in actual and future technologies (cognitive radio, 5G and beyond).
A software defined radio system is then a radio communications system in where certain hardware components are implemented in software. They include namely: filters, amplifiers, modulators, demodulators etc. Since these components are software defined, they can be adjusted as needed without making significant hardware modifications. The universal software radio peripheral (USRP) is an attractive SDR transceiver which can be used to develop software defined radio applications.

1.2.2 SDR system architecture

The general structure of a Radio Communications Device is illustrated in Figure 1.1. It is a complicated hardware structure with almost fixed and defined features.
The SDR evolution aims to simplify this structure. Efforts have been devoted mainly to software side trying to replace some of the hardware with software. The question is then: Which part of the hardware can be replaced by software? The ideal solution is replacing almost all the hardware except irreplaceable ones, as antennas and ADC/DAC (Figure 1.2).
Hardware is still required in SDR radio, however it is just limited to receiving and transmitting radio signals. Hence, an SDR system is globally composed of antenna, transmitter/receiver, and a host (PC computer) for running the software.

1.2.3 Benefits and limitations of SDR

Replacing software by hardware leads to reducing the manufacturing cost and the maintenance time, also allows developing more flexible systems. Further, using a processor

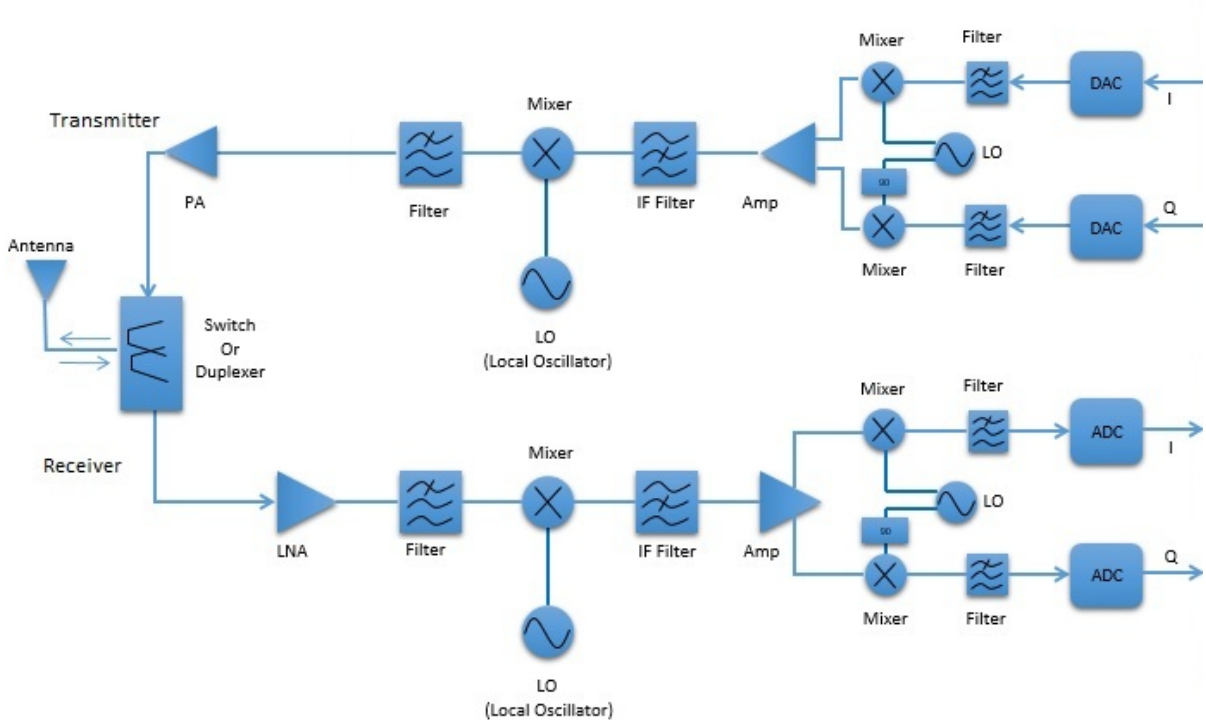

Figure 1.1: General architecture of radio transceiver [3]

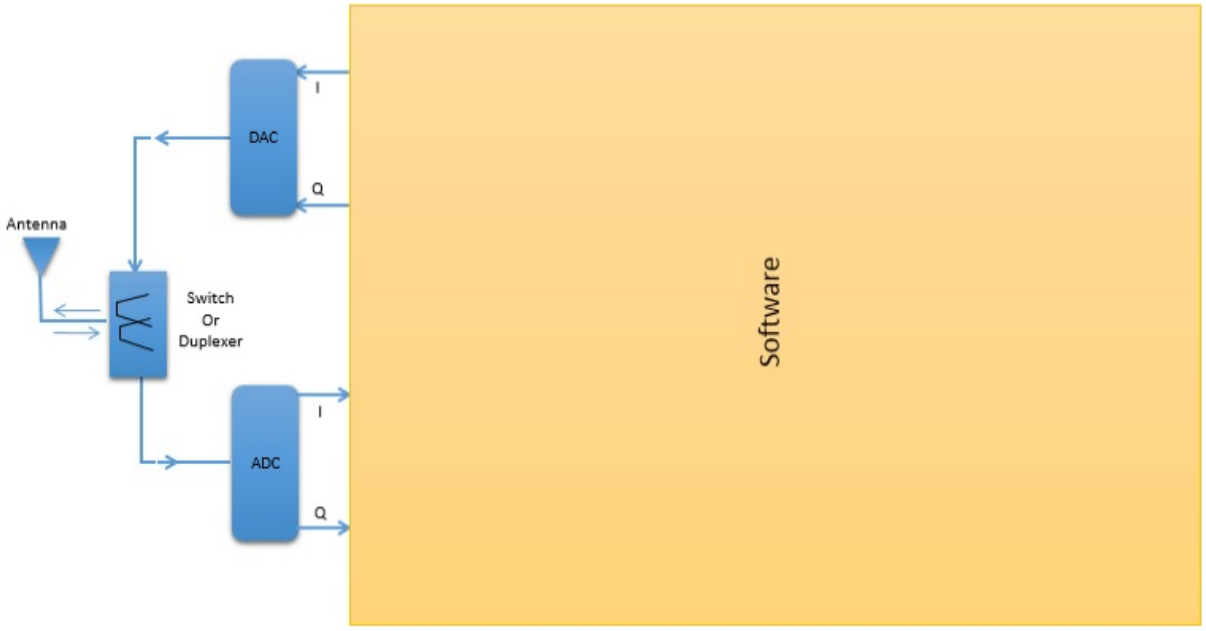

Figure 1.2: Ideal structure of SDR [3]

instead of hardware components increases the hardware lifetime [4]. Software re-usability and portability is also an important benefit as well, since it allows doing tests and simulations of system's behavior before integrating real-time products [5].

Although they are very advantageous, SDR systems have, unfortunately, some few disadvantages, for instance: limitation of the maximum throughput from the USRP to the host device, power consumption, efficiency and speed of hardware since most of the signal processing is being done in the host device. In addition, the use of LNAs, DAC/ADCs limits

the SDR performances since LNAs suffer from bandwidth restrictions [4], and DAC/ADCs are limited in dynamic range, sampling rate and bandwidth requirements [5].

1.2.4 Universal software radio peripheral (USRP)

USRP is a widely used SDR platform. It possess various SDR abilities: wide bandwidth and flexible tunability. USRP connects real-time RF systems to PCs using universal serial bus (USB) or Ethernet connections. USRPs are programmed through different software, such as GNU radio, Labview and Simulink (Figure 1.3). The USRP series under National Instruments' brand are called NI-USRP and are paired with NI-Labview tool boxes.

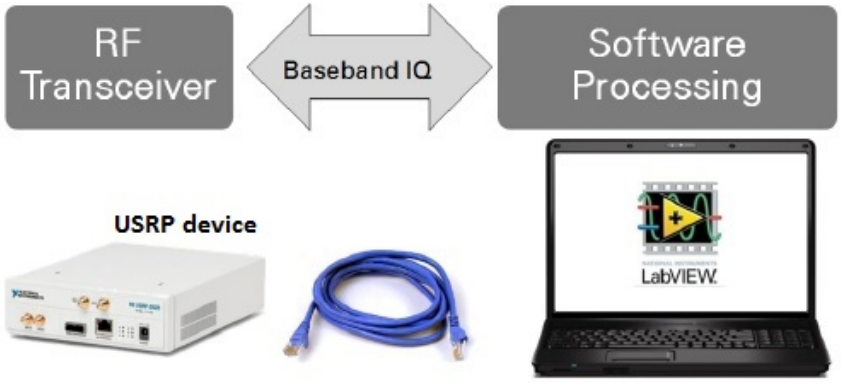

Figure 1.3: Communications system based on USRP device

The USRP contains many different components in the core motherboard: analog-to-digital converters (ADC) and DAC, an FPGA used for decimation, filtering, up/down conversion, and an USB driver for connection with a host device. It provides large bandwidth capability accommodating many different modular RF front-ends. Figure 1.4 depicts a block diagram of the NI USRP2921 architecture [6].

NI USRPs have been upgraded to several modern series. USRP RIO is one of the latest versions of those USRPs. It provides an integrated hardware and software solution for quick prototyping of high-performance wireless communications systems. USRP RIO platform has two RF transceivers with a reconfigurable LabVIEW FPGA target that incorporates DSP coprocessing for high-rate, low-latency applications (Figure 1.5). This design flow is widely used by researchers to prototype a tremendous range of advanced research applications that include multiple-input-multiple-output (MIMO), spectrum sensing, cognitive radio, beamforming, direction finding, and many others [7].

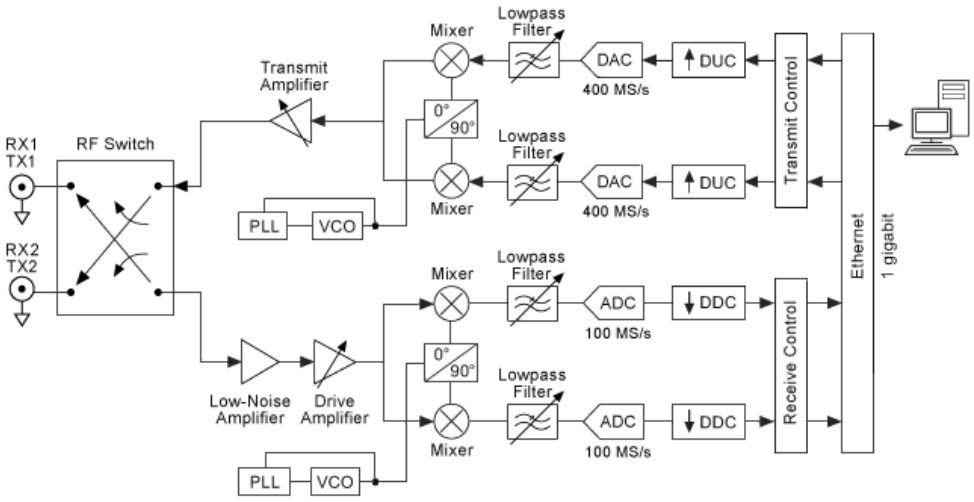

Figure 1.4: USRP2921 Block Diagram [6]

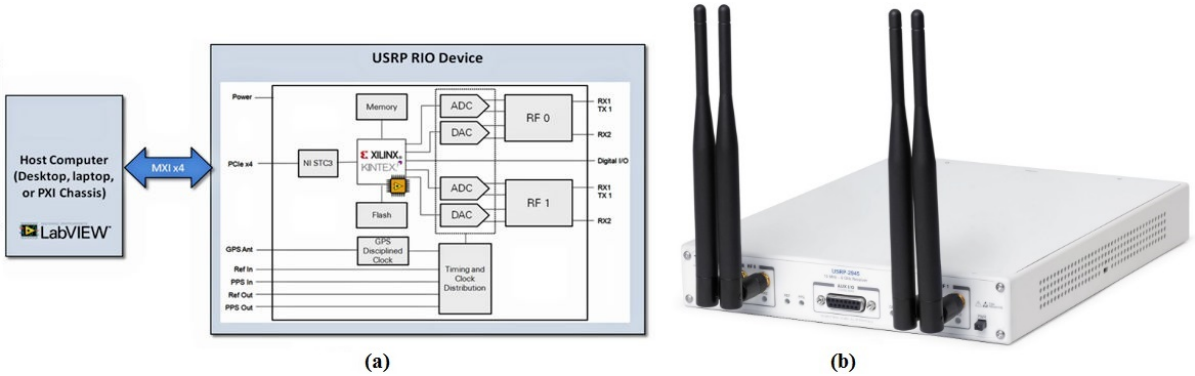

Figure 1.5: USRP RIO (a) Block Diagram (b) Picture [7]

1.3 Antenna pattern reconfiguration

Recently, huge amount of researches were addressed to the reconfigurable antennas. This is motivated by the increasing demand for communications systems which are able to adapt dynamically their parameters to the system requirements and surrounding environment [8]. Being able to control the pattern, the antennas will enhance the flexibility once integrated into SDR front-ends to achieve the aims of future wireless communications.

1.3.1 Pattern reconfigurtion techniques

Three common methods are used, in the literature, for this purpose: parasitic tuning, element phase shifting and co-located radiating aperture [9].

A) ***Parasitic tuning:***

In this technique, elements are electrically switched or tuned. In [10], pattern reconfiguration of Yagi patch antenna is demonstrated (Figure 1.6).

Authors in [11] exploited similar tunning approach to achieve pattern reconfiguration

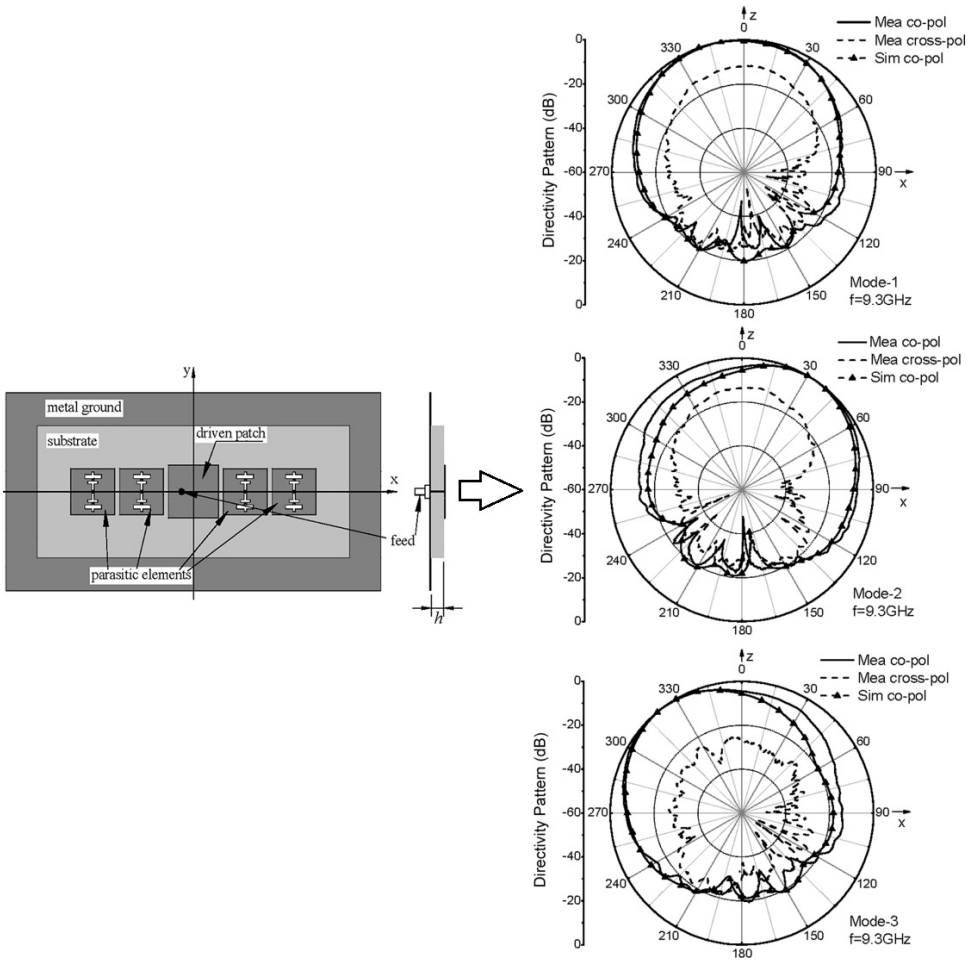

Figure 1.6: Parasitic tuning of Yagi patch antenna pattern [10]

of a disc patch including ring and eight radially symmetrically distributed microstrip monopoles. Eight switches allow providing eight patterns covering the horizontal plane (Figure 1.7).

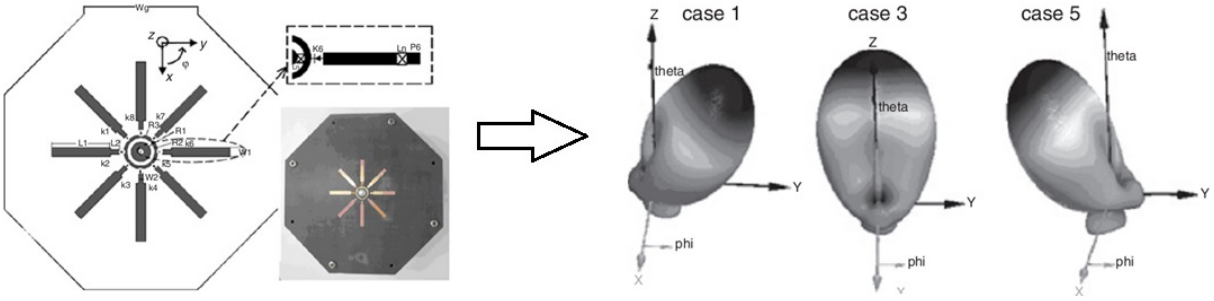

Figure 1.7: Parasitic pattern reconfiguration of ring antenna [11]

B) ***Element phase shifting:***

This second approach is based on the integration of phase shifts into array elements. Hence, a beam steering capability is provided. Various works inspired from this method and succeeded in pattern reconfiguration issue [12]-[13]. In [12], a beam

steerable meander line antenna has been discussed and presented as seen in Figure 1.8. The phase shifting mechanism is widely used in signal processing domain, notably phased arrays and beamforming applications as will be detailed further.

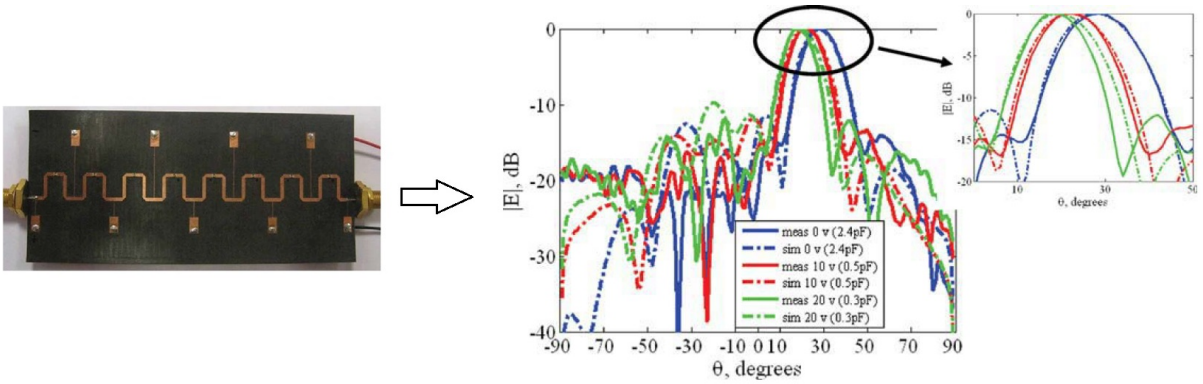

Figure 1.8: Beam steerable meander line antenna [12]

C) *Co-located radiating apertures:*

Different radiators are used to produce different patterns, as conducted in [14], where the pattern reconfiguration is achieved by switching between slotline to CPW feeds using switches (Figure 1.9). Similarly, authors in [15] followed the same approach to provide pattern reconfiguration.

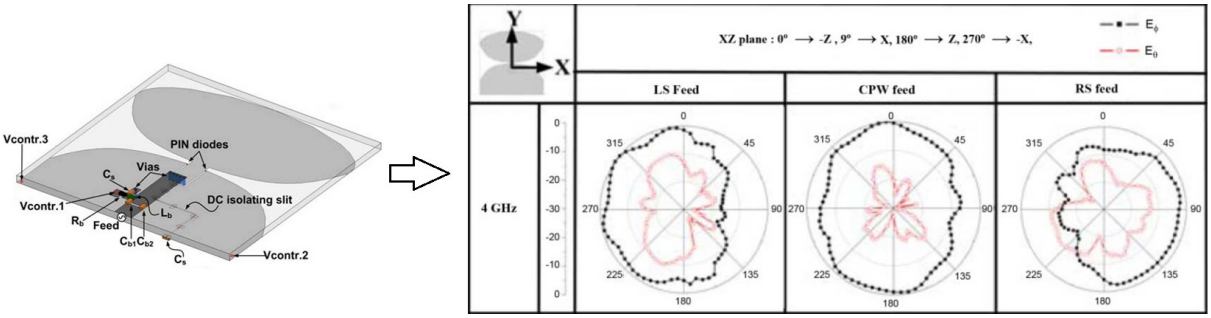

Figure 1.9: Pattern reconfiguration in co-located apertures [14]

1.3.2 Discussion

Although, the reported designs and techniques provide effectively pattern reconfiguration capability, however, they suffer from some drawbacks such as:

- Complexity of structures with requiring extra elements (reflectors and parasitic elements),
- Lot of lumped components (requiring extra connexions which take considerable space with more power losses) [9],
- In most cases, the reconfiguration is obtained around a narrow bandwidth.

1.4 Antenna arrays

1.4.1 Definition

An antenna array is a set of antennas (two or more) used for transmitting or receiving electromagnetic waves (Figure 1.10). The radiating elements are carefully placed in space to form an array with desired characteristics, which can be achieved by varying the feed (amplitude and phase) and position of each element [16]. Signals are then combined to enhance the performance over that of a single antenna [17], [18]. Antenna arrays are used to:

- Increase the overall directivity and gain,
- Provide diversity reception,
- Cancel out interferences from a given direction,
- Steering capability of the array main beam in the direction of interest,
- Maximize the Signal to Interference Noise Ratio (SINR).

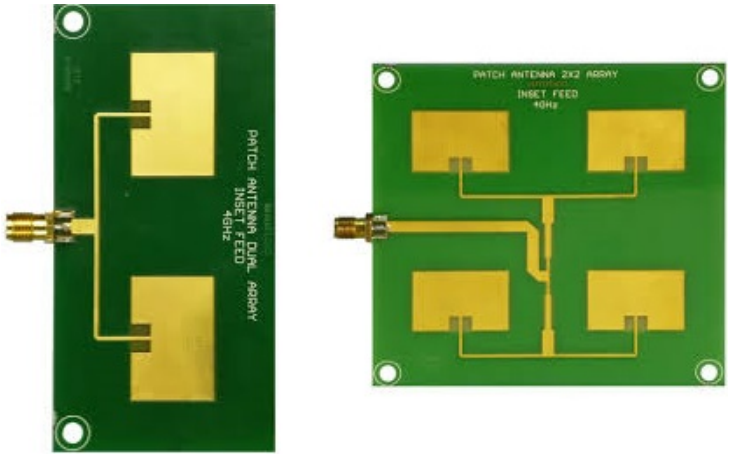

Figure 1.10: Two and four elements patch antenna arrays [19]

1.4.2 Antenna array radiation pattern

In an array of N antenna elements, the phase and amplitude of each element can be adjusted electrically or mechanically using phase shifters and attenuators (Figure 1.11). The total radiated field can be obtained by summing up the radiated field from each element (1.1):

$$E(r, \theta, \phi) = \sum_{1}^{N} E_n(J_n) \tag{1.1}$$

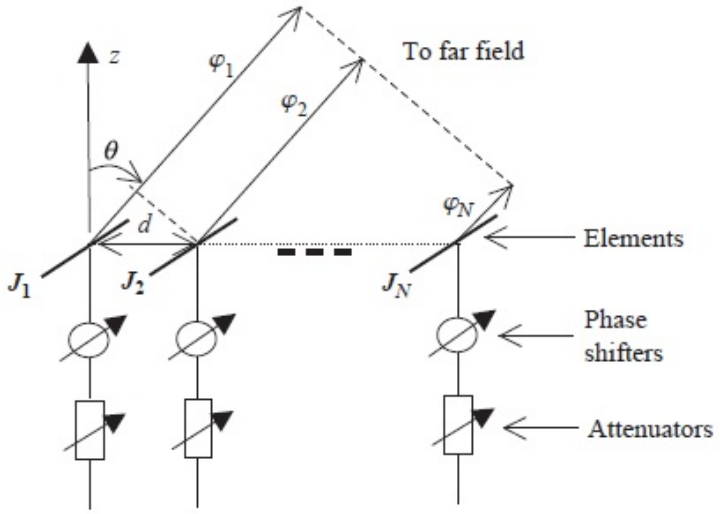

Figure 1.11: N-element antenna array [16]

Since all elements can be individually controlled (amplitude and phase excitation control), the total radiated field is then controlled to achieve the desired radiation characteristics. For more convenience, the elements are placed in a specific geometric configuration to form a well-controlled 1D, 2D or even 3D array (linear, circular, rectangular or elliptical).

1.4.3 Phased (Scanning) Arrays

In antenna array theory, it is demonstrated that the total radiating field can be controlled when varying the element spacing and/or the phase shift between the radiators [20]. Hence the maximum radiation can be oriented in any direction to form a scanning array (Figure 1.12). This concept makes the basic principle of electronic scanning phased array.

Phased arrays are widely used in recent technologies and systems, namely in beam-forming application, since they allow more flexibility and capabilities. Such systems are based on varying phase shifts between elements in feeding network (Figure 1.13), hence the components providing phase shift agility (known as phase shifters) are very crucial. However, design of those phase shifters, in practice, is very challenging. Details of this topic will be discussed later.

1.4.4 Array element mutual coupling

When placing antennas in close proximity, an electromagnetic interaction between them occurs. This phenomenon is known as *mutual coupling*. Consequently, current distribution, input impedance and radiation pattern are seriously affected.

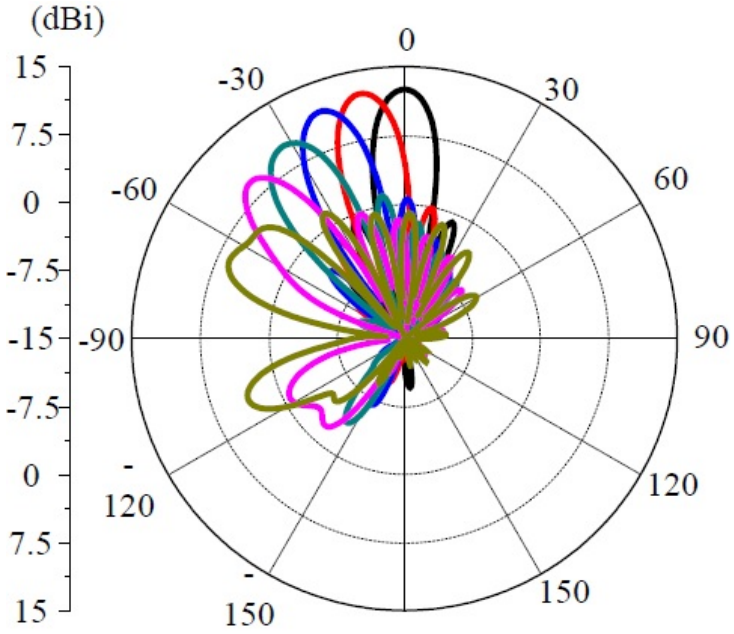

Figure 1.12: Scanning performance of eight-element array [21]

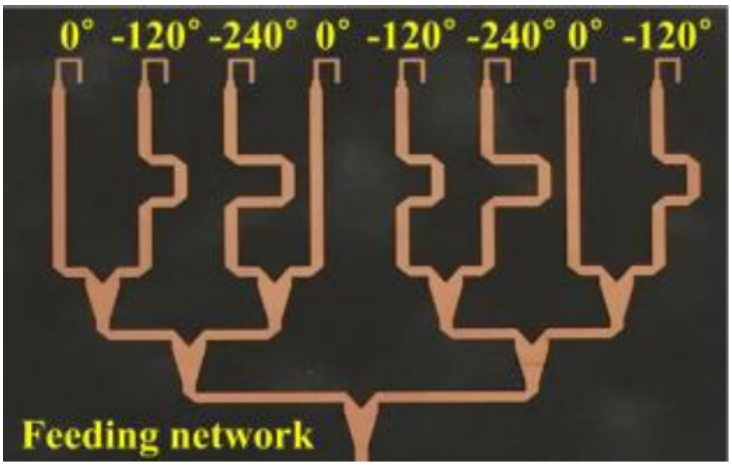

Figure 1.13: Phased feeding network for eight-antenna array [21]

Several studies of the antenna coupling phenomenon [16], [17], [20], [22] reveal that:

- The coupling strength decreases when spacing increases,
- The parallel configuration couples more than the collinear arrangement,
- The coupling becomes stronger when antennas radiate more,
- The coupling is sensitively related to the radiation characteristics of each radiator,
- The coupling effect depends on the feed of each elements of the array.

The energy interchange between neighboring elements is due to various mechanisms and rises either by surface current flowing between excited ports or space radiated fields and surface waves. Indeed, some amount of radiated energy may be received by the adjacent el-

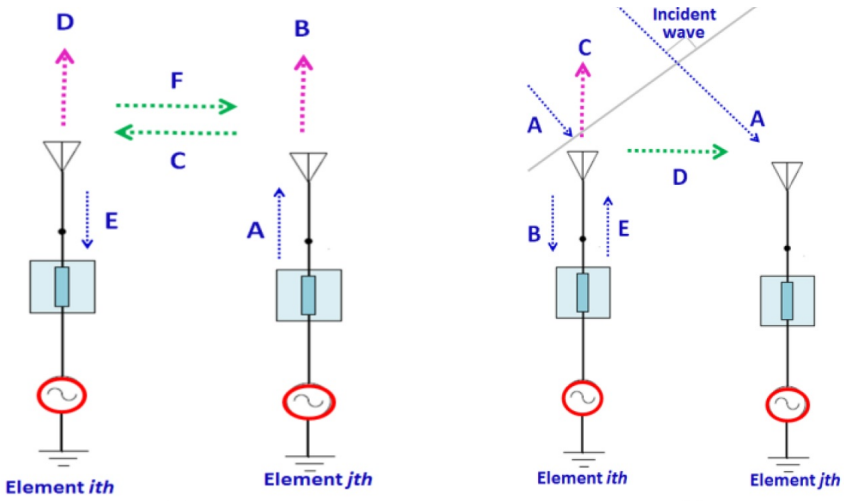

Figure 1.14: Antenna mutual coupling mechanisms (a) Transmitting mode (b) Receiving mode [23]

ement (Figure 1.14(a)). In the receiving side, incident energy can undergo a re-scattering, in all directions, by the array elements (Figure 1.14(b)).

Generally, the coupling phenomenon makes the array design more complex, since it is difficult to be formulated analytically. However, it should be included in multi-antenna system study, because it contributes significantly in the overall performances of such systems.

1.4.5 Applications and challenges of antenna arrays

Antenna arrays are very attractive to several communications systems, radars, mobiles, satellites, base-stations, etc, due to the advantages they offer. Indeed, high date rate is one of the most desired objective of next-generation devices to meet the 5G communications requirements. MIMOs are then attractive candidates to achieve this purpose [24]. However, design of antenna array with desired requirements is still challenging because of the feeding network complexity (impedance matching, phase shifters, excitations) and the bandwidth limitation (mainly due to the feeding network). Further, arrays, in most cases, are subject of electromagnetic mutual coupling which degrades drastically their performances.

In this work, a particular careful is devoted to two particular challenges, often raised in antenna array design:

- Phase shifters design,
- Antenna decoupling issue.

1.5 Phase shifters design

Phase shifters are essential components that are extensively exploited in phased arrays with electronic beam scanning and phase modulators [25]. Many researchers are interested to those components and provide a wide range design techniques with different features.

1.5.1 Definition and principle of operation

A phase shifter is a four-port network. it consists of two different circuits: the main and the reference lines. The phase shift across the main line and the reference lines are assumed to be φ_m and φ_r, respectively (Figure 1.15). The design requirement of such device is to provide a proper (stable) differential phase shift between the two lines, and exhibits small attenuation, over the operating bandwidth [26].
The phase shift value, given by (1.2), depends on the configuration of the phase shifter. Hence, a simple and primitive phase shifter consists of two transmission line sections with different lengths, yet this scheme only provides the required phase difference over a very narrow bandwidth.

$$\Delta\varphi = \varphi_m - \varphi r \tag{1.2}$$

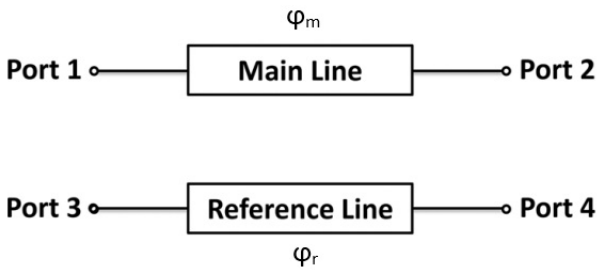

Figure 1.15: General phase shifter configuration

1.5.2 Design techniques

Different techniques were developed in recent years and many schemes and configurations were proposed [27]. Microstrip-coplanar waveguide [28], Schiffman technique [29], loaded transmission line [26], coupled structure [30]–[33], microstrip-slot transitions [34], [35], high/low impedance method [36], and split-ring resonator [37] are some of the methods used in building phase shifters. In the following, selected techniques will be described.

A) ***Schiffman technique:***

Proposed for the first time in 1958 [38], the Schiffman differential phase shifter is the most remarkable configuration. It consists of two transmission lines: simple line which defines the reference and a folded line (symmetrical coupled-line section) with one end connected, called the C-section network (Figure 1.16 (a)-(b)). A careful selection of the length of these lines and the degree of coupling, allows producing an almost constant output phase shift over a broad bandwidth. Figure 1.16 (c) shows one realization of this scheme which provides an output phase shift oscillating around 90° within the band 1.5-3 GHz [29].

The major drawback of this method is that the coupling factor is critically dependent on the gap between the two coupled lines and the dielectric constant of the substrate. Hence, for designs using the printed circuit board (PCB) fabrication technology, it is quit hard to obtain a tight coupling for such phase shifter. Moreover, the measured results of Schiffman's phase shifter reveal an important phase ripple (±10°) [38].

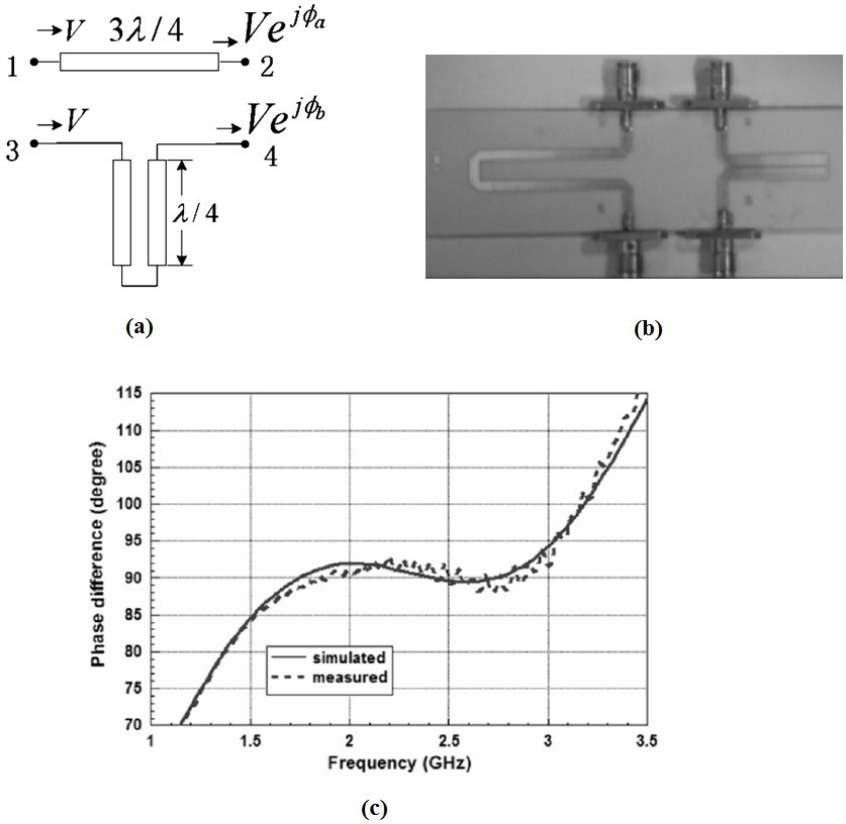

Figure 1.16: Shiffman phase shifter (a) Schematic design (b) Prototype (c) 90° Output phase shift [29]

B) ***Loaded transmission line:***

The basic idea in this configuration is that the main line consists of a transmission

lines (TL) loaded with an open stubs as shown in Figure 1.17. The design can also be achieved using a multi-section TL connected together in the middle and considered as open load (Figure 1.18 (a)). This configuration provides the phase shifting function. When compared with conventional coupled line phase shifter, the structure shows good performance with simplicity of design and fabrication [26]. However, the bandwidth of this type of design decreases with the increasing desired phase shift going with high phase deviation of about 5° (Figure 1.18).

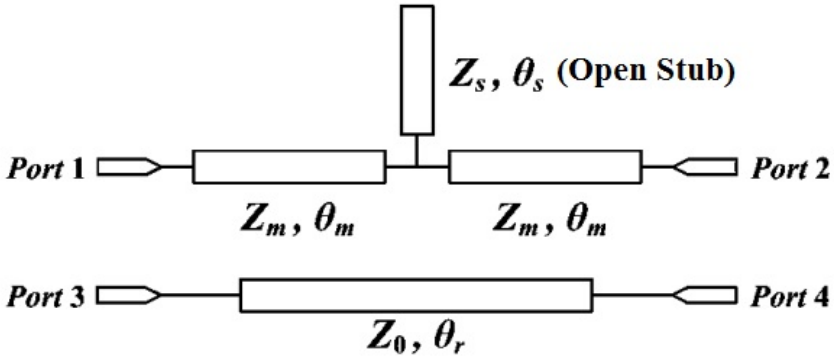

Figure 1.17: Basic architecture of a loaded TL phase shifter [39]

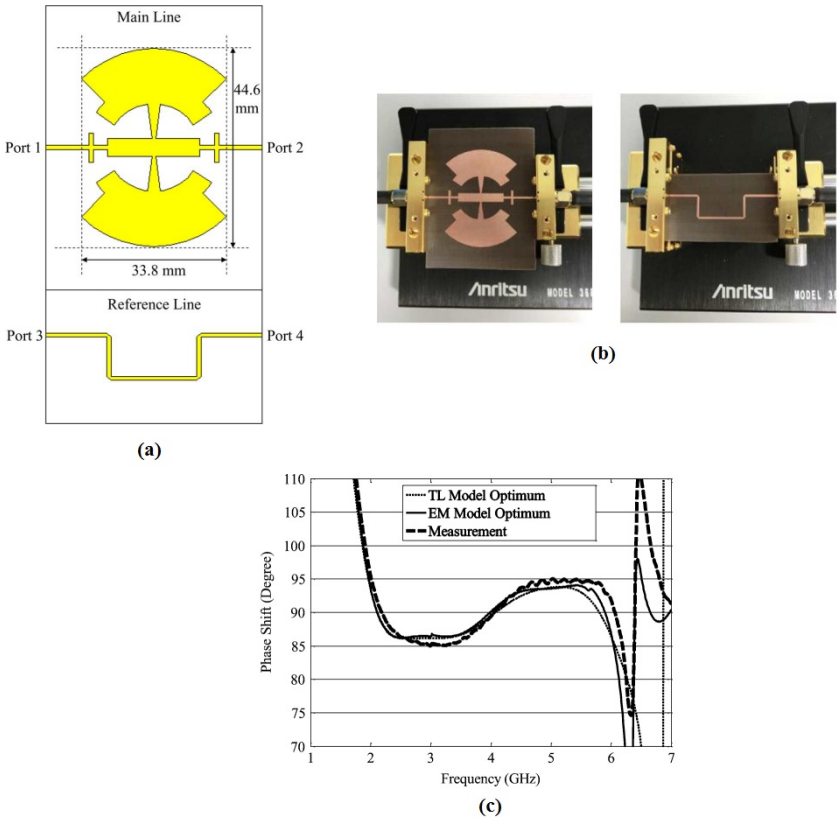

Figure 1.18: Loaded TL based phase shifter (a) Schematic design (b) Prototype (c) 90° Output phase shift [40]

C) *Coupled structure:*

The configuration is based on parallel coupled lines. The design of Figure 1.19 uses the coupling technique combined with short-ended stubs and a section of transmission line as an impedance transformer. The output phase can be adjusted through varying the coupling factor along with the length and impedance of the short-ended stubs and transformer [27].

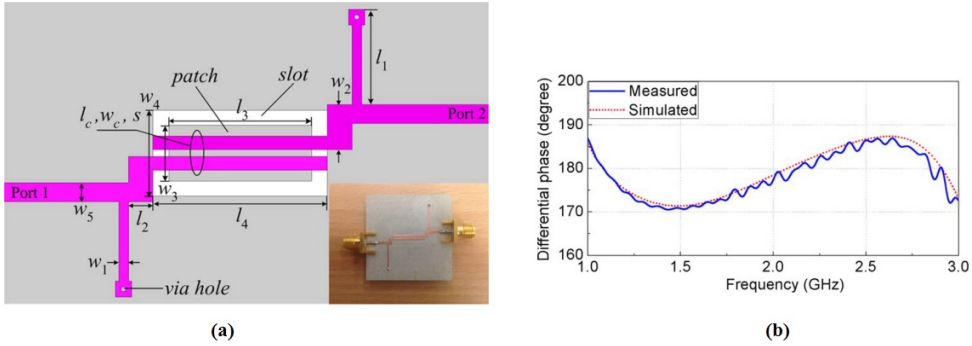

Figure 1.19: Coupled structure based phase shifter (a) Schematic design (b) 180° Output phase shift [27]

Another design is that shown in Figure 1.20, where the coupling principle is exploited as well in both reference and main lines to achieve various differential phases, for instance 45°, 90° and 135° [31].

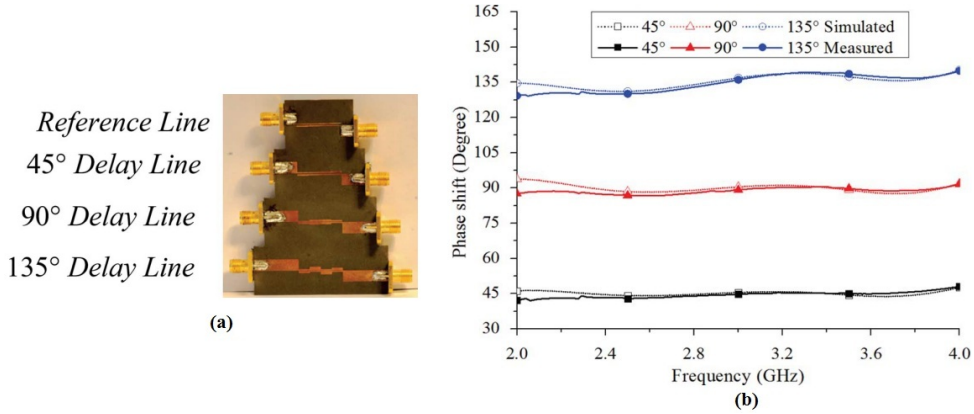

Figure 1.20: Multi-section coupled line phase shifter (a) Configuration design (b) Output phase shifts [31]

Despite the simplicity of the coupling structure technique, it comes out that it suffers from some drawbacks: practical limitation considerations as the desired coupling factor is not certainly realizable, notably when it becomes very tight. In the other hand, differential phase shift may suffer from relative high ripples (around 8°) as in Figure 1.19 (b).

D) ***Split-ring resonator:***

Left-handed (LH) transmission lines are artificial structures. They exhibit special behaviour similar to the medium with negative permittivity and permeability [37]. Consequently, backward-wave propagation with phase delay property is produced. The LH can be realized by transmission line loaded with sub-wavelength resonators (Split-ring resonators) [41].

Figure 1.21 depicts a phase shifter design based on split- ring resonator method. The main line is a transmission line loaded with a split-ring resonator in the ground plane (Figure 1.21 (b)) and the differential phase shift is evaluated by comparison with an ideal transmission line, considered as a reference line (Figure 1.21 (a)) .

Since the LH property is only occurred in a limited frequency band, the phase shifters deploying the discussed technique are roughly narrow-bandwidth (Figure 1.21 (c)).

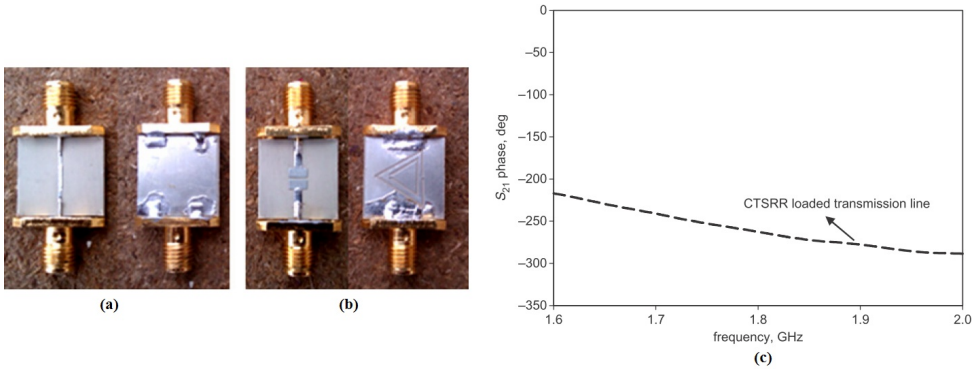

Figure 1.21: Phase shifter based on split-ring resonator (a) Reference line (b) Main line (c) 255° Differential phase shift [41]

E) ***More complex designs (Hybrid designs):***

Another interesting way for phase shifter design is the hybrid technique. With appropriate linking of different methods, it is possible to exploit their advantages and come up with a new phase shifter designs.

Authors in [42] have aspired from this idea and proposed a new design as shown in Figure 1.22. The scheme is based on coupled structures and loaded TL techniques. Indeed, the main line consists of a stepped impedance open stub (a load) and a coupled-Line. The design provided an output phase shift of 90° with ±5°, more than 10 dB return loss and less than 1.1 dB insertion loss, in the frequency band 0.75-2.4GHz (Figure 1.22 (c)).

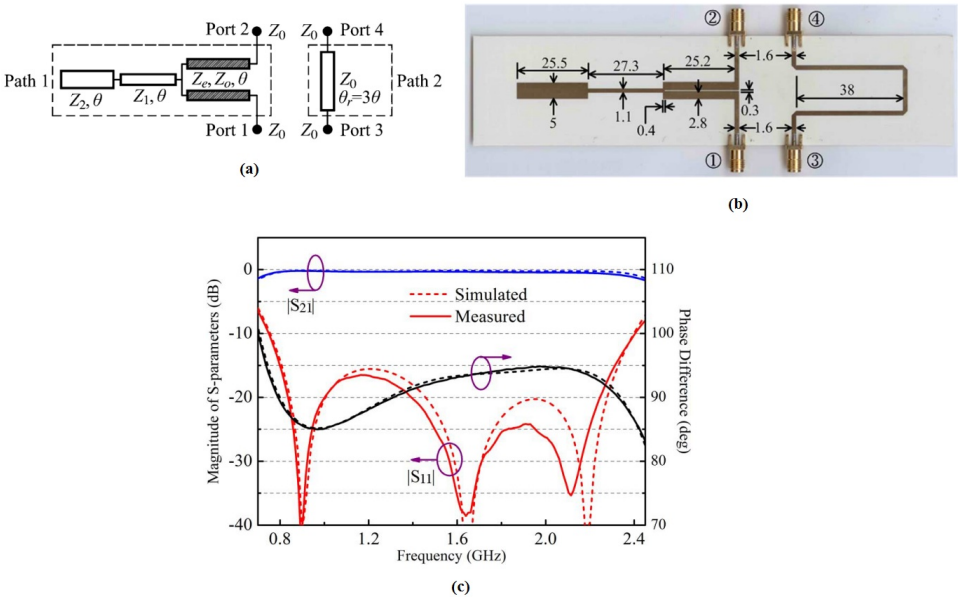

Figure 1.22: Phase shifter based on Hybrid technique (a) Schematic design (b) Prototype (c) 90° Differential phase shift [42]

1.5.3 Discussion

When observing the literature designs, we can conclude that diverse and attractive techniques have been proposed, studied and effectively realized. Moreover, the obtained performances are good and applicable in various domains. Nevertheless, many drawbacks can be outlined:

- Complexity of structures,
- Limited design possibility, notably when using printed circuit board (PCB) technology, due to the extremely small dimensions of some configurations,
- High output phase ripples (more than 8°),
- Narrow bandwidth,
- High insertion loss in some cases (more than 3 dB).

1.6 Antenna decoupling techniques and challenges

1.6.1 Metrics for decoupling performances evaluation

Isolation level is the first metric to evaluate the decoupling between closed antennas. Generally, the isolation is related to the S-parameters of the array (S_{ij}) which quantifies the amount of energy exchanged between the i^{th} and the j^{th} radiators. In addition,

different other metrics may be used to evaluate the coupling effect, such as envelope correlation coefficient (ECC), diversity gain (DG) and TARC.

A) ***Envelope Correlation Coefficient (ECC):***

ECC refers to the relationship between signals at the array antenna ports as it measures the degree of similarity of those signals. It is a necessary metric to evaluate the system performances and channels correlation in MIMOs. High mutual coupling leads to high ECC, hence this parameter is expected to be low for better performances. ECC of less than 0.5 is considered as acceptable value to ensure good diversity [43]. Different methods are developed in the literature to calculate the ECC, using either S-parameters or radiated fields [44] as expressed in (1.3) and (1.4) respectively.

$$ECC = \frac{|S_{11}^{*}S_{12} + S_{21}^{*}S_{22}|^2}{(1-(|S_{11}|^2+|S_{21}|^2))(1-(|S_{22}|^2+|S_{12}|^2))} \tag{1.3}$$

$$ECC = \frac{|\iint\limits_{4\pi} \vec{F_1}(\theta,\varphi) \times \vec{F_2^{*}}(\theta,\varphi) d\Omega|^2}{\iint\limits_{4\pi} |\vec{F_1}(\theta,\varphi)|^2 d\Omega \iint\limits_{4\pi} |\vec{F_2}(\theta,\varphi)|^2 d\Omega} \tag{1.4}$$

Where S_{ij} are the scattering parameters of the elements, $F_i(\theta,\varphi)$ is the field radiation pattern of the i^{th} radiator, and X denotes the Hermitian product.

B) ***Diversity Gain (DG):***

Diversity gain is important parameter in evaluating multi-radiator systems. It provides an idea about the reliability of considered system. In contrast to the ECC, DG is expected to be high for better isolation. DG is directly dependent on the correlation coefficient as described in (1.5) [45].

$$DG = 10 \times \sqrt{1-|ECC|^2} \tag{1.5}$$

C) ***Total Active Reflection Coefficient (TARC):***

TARC is defined as the ratio of the square root of the total reflected power and the total generated power [46]. It is introduced to evaluate the radiation performance and the bandwidth of multi-port antennas. TARC depends on the impedance matching and radiation efficiency as expressed in (1.6). For good performances, this parameter

is desirable to be less than 0dB.

$$TARC = \frac{\sqrt{\sum_{i=1}^{i=N} |b_i|^2}}{\sqrt{\sum_{i=1}^{i=N} |a_i|^2}} \tag{1.6}$$

Where a_i, b_i and N are incident signal, reflected signal and the number of antennas, respectively.

1.6.2 Decoupling techniques

We stated before (section 1.4.4) that mutual coupling has serious effects on MIMO systems, since it changes the antenna characteristics, therefore degrades the whole system performances. The mutual coupling may be partially calibrated out in the digital domain, however the use of decoupling techniques by means of physical implementation is more effective in order to overcome this challenge [47]. Consequently, various methods and mechanisms were developed to achieve the decoupling purpose. Figure 1.23, summarizes some popular decoupling techniques available in the literature, and will be discussed in this section.

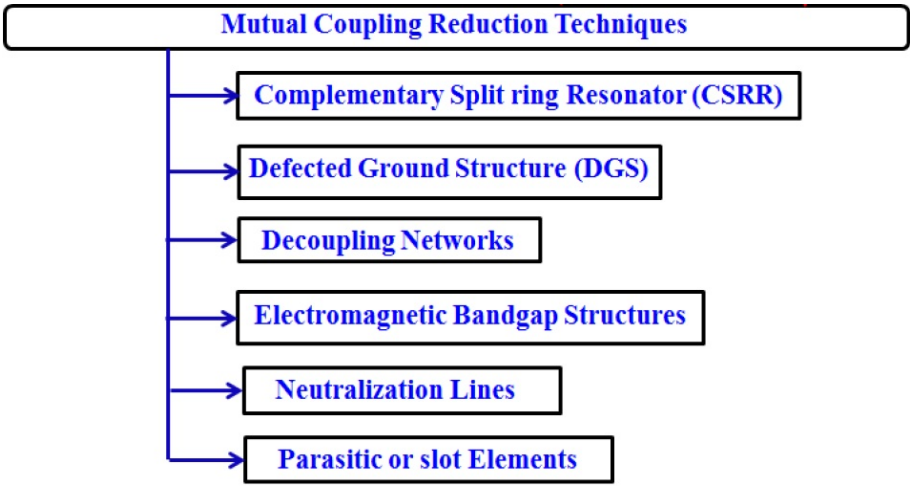

Figure 1.23: Summary of some mutual coupling reduction techniques [23]

A) ***Defected Ground Structure (DGS):***

Defected ground structure (DGS) refers to the defects, slots or other shapes integrated on the ground plane of the array. This emerging technique contributes significantly to reduce mutual coupling and to the improvement of MIMO parameters (bandwidth, polarization and gain) [48],[49].

Some recent works used this method [50]–[52] to overcome the coupling issue. In [50], a periodic S-shaped unit has been placed between two radiating patches to reduce

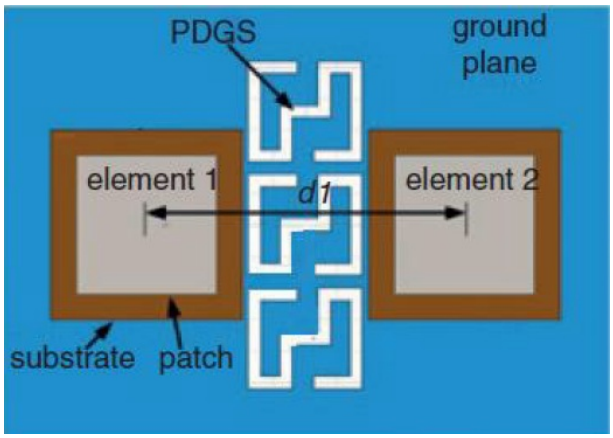

Figure 1.24: Mutual coupling reduction using DGS [50]

mutual coupling (Figure 1.24). The etched unit reduces significantly the amount of current to travel from one port to the other one and confines those currents in limited ground area. Therefore, High port isolation of about 40 dB is achieved.

B) ***Complementary Split-Ring Resonator (CSRR):***

Generally, periodic structures of metallic ring, shunt strip or capacitive gap are known to be complementary split ring resonator (CSRRs). They are often used for filtering and isolation purposes [53], [54].

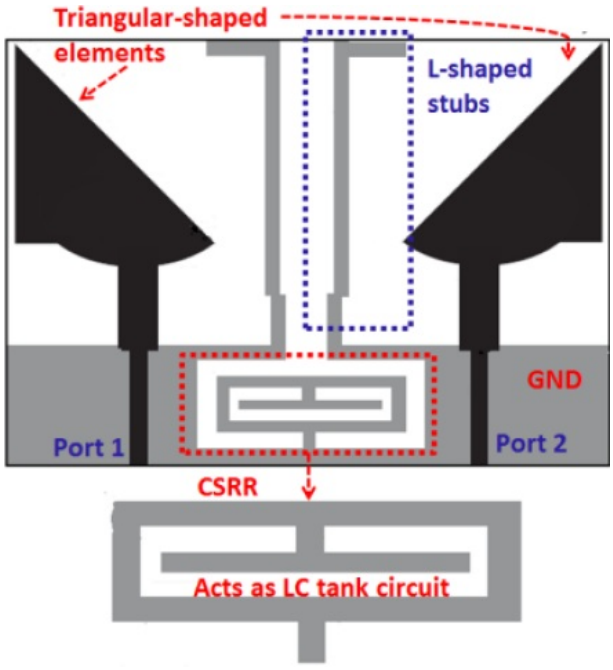

Figure 1.25: Mutual coupling reduction using CSRR [55]

In Figure 1.25 are depicted two triangular radiating elements [55]. A CSRR with L-shaped stubs are introduced in the structure for antenna decoupling. The stubs are considered as reflectors and the CSRR is an LC-circuit which prevents the currents to reach antenna ports, hence a considerable improvement in mutual isolation is noticed.

C) ***Neutralization Lines:***

The principle of this method is based on creating an opposite coupling (at given frequency) through neutralization lines, performed as metallic slit or lumped element, which are used to dispatch waves between antennas [56], [57].

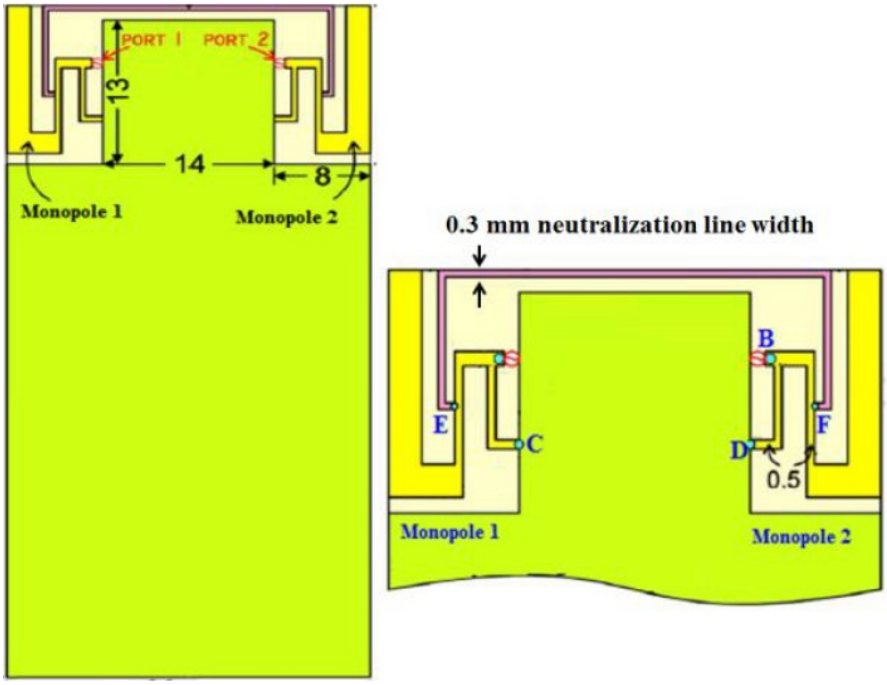

Figure 1.26: Mutual coupling reduction using Neutralization Lines [58]

Authors in [58] inspired from this method to develop a printed neutralization line linking two short-circuited monopoles (Figure 1.26). Hence, the isolation can be controlled by varying the neutralization line length, position and connecting points.

D) ***Parasitic or Slot Elements:***

The mutual coupling is reduced by creating two opposite coupling paths [59], [60]. The advantages of this technique are mainly: simplicity of design, compact size and production flexibility using PCB technology [23].

The example illustrating this concept is depicted in Figure 1.27, where a single radiating patch is shared to form a MIMO antenna [61]. The design comprises two ports fed through perpendicular meandered microstrip lines. Mutual coupling is reduced by an open stub (quarter wavelength), a T-shaped slot etched in the centre of the patch and a small partial ground plane. Furthermore, port currents are driven in orthogonal directions and leading to a weak coupling magnitude. This mechanism provides low mutual coupling (-15 dB) between the two ports.

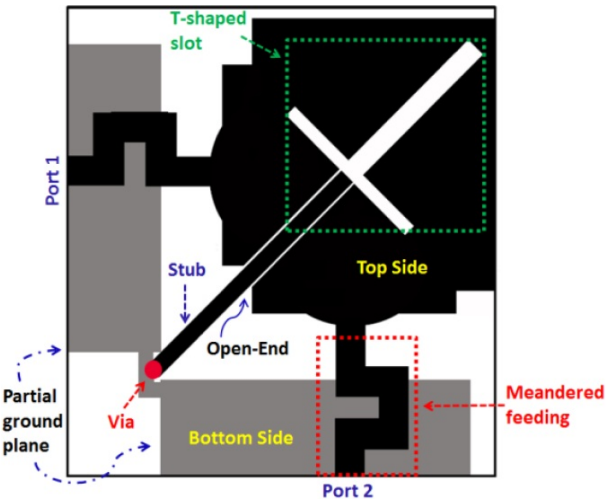

Figure 1.27: Mutual coupling reduction using Parasitic and slot elements [61]

E) ***Electromagnetic Band-Gap Structure (EBG):***

EBG structure is a periodic arrangement of metallic or dielectric material which behaves as a high impedance surface. It can be modeled using lumped elements (capacitors and inductors). Depending on the periodicity of the structure and the element resonances, multiple band-gaps can be generated. This kind of structures are able either to block or transmit electromagnetic waves at desired frequency [62]. Generally, for mutual coupling reduction, radiators are surrounded by EBG elements forming a square ring (called S-EBG configuration). EBG cells may also be arranged between the antennas (called I-EBG configuration) (Figure 1.28). However, the former configuration provides highest isolation as it decreases inter-element coupling. This concept is demonstrated by authors in [63].

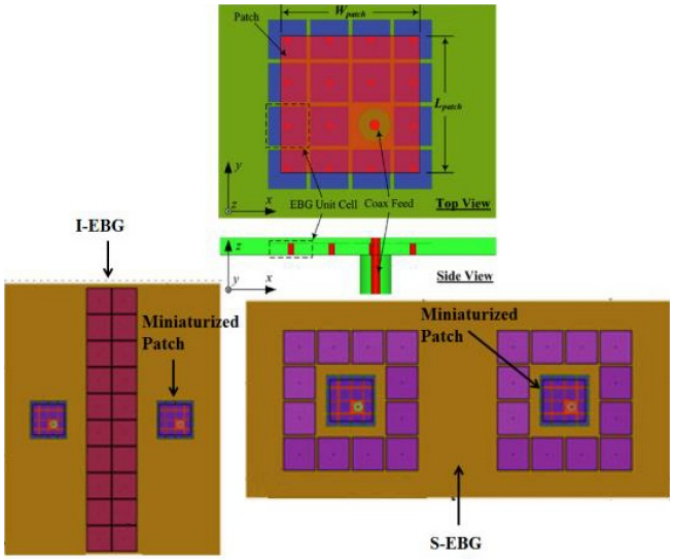

Figure 1.28: EBG meshroom for mutual coupling reduction [63]

F) ***Decoupling and Matching Networks (DMN):***

This technique is extensively exploited in port isolation improvement and antenna matching. It is based on inserting extra-Transmission-Lines to transform the cross admittance to a pure imaginary term. The decoupling is then achieved by reactive lumped components [64].

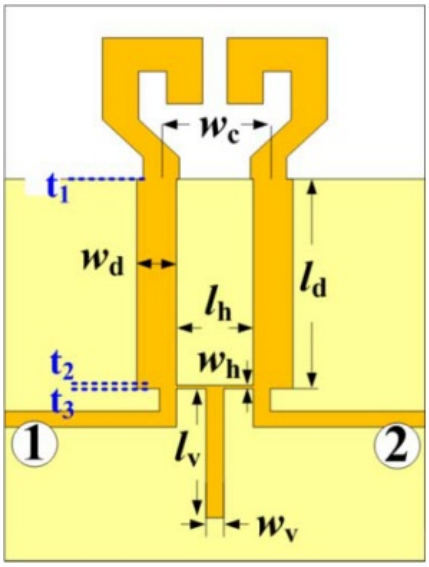

Figure 1.29: Mutual coupling reduction using DMN [65]

Figure 1.29 illustrates this method, and an isolation of about 28.9dB is achieved [65]. Beside the discussed methods, there exist many other techniques used in the decoupling topic, such as Dielectric Resonator Antenna (DRA) [66], reconfigurable antenna [67] and metamaterials antenna [68].

1.6.3 Discussion

Several decoupling techniques have been proposed and discussed in literature. Most of authors adopt 17 dB to 20 dB as a required isolation level (threshold of mutual decoupling).

Depending on the method, different performances can be obtained such as wide bandwidth and low correlation by DGS and CSRR techniques. The neutralization line is also a simple method leading to isolation improvement. Compact size can be achieved by parasitic or slot element technique. EBG structures provide lower bandwidth and good isolation at the cost of complex periodic architectures. Furthermore, decoupling networks are also adopted in decoupling issue, since they are simple and offer acceptable performances. Other methods such as DRA, reconfigurable and metamaterial antennas are

somehow more complex and require expensive manufacturing tools.
Antenna decoupling is a very sensitive field of research since it is directly related to the development of next generation communications systems (5G and beyond, MIMO and massive MIMO). Therefore, a careful study should be devoted to this area in order to enlighten the mutual coupling phenomenon, understand the techniques of port-isolation improvement and mitigating the coupling challenge.

1.7 Conclusion

This chapter was devoted essentially to discuss some challenges in modern wireless communication systems. SDR are found to be very attractive concept in developing such systems, due to the flexibility and reconfigurability they offer. Consequently, some challenges in antenna and front-end designs are raised to achieve recent application requirements such as: antenna pattern reconfiguration and phase shifters design.
Further, multi-antenna systems are discussed as a promising solution for next-generation wireless systems such as 5G and beyond, in which improved performances are desired for higher data rate and more compactness. Hence, the implication of MIMO antenna design is presented and the mutual coupling problem is then deeply investigated.

Chapter 2

Chapter 2

Antenna Pattern Reconfiguration

2.1 Introduction

With the rapid development of the advanced and miniaturized wireless communications systems, need of the dynamic reconfiguration even in frequency or in pattern has become of important priority. The main reason of this challenge is providing compact wireless systems capable of adapting their behavior with respect to the environment to ensure best performances. This is well known in case of cognitive radio applications where the frequency reconfigurability is the main challenge.

Pattern reconfiguration is another important area of research which allows higher diversity, increases channel capacity, mitigates multi-path fading and noisy environments, improves radiation coverage and saves energy by directing signals towards the desired direction, notably in MIMO systems. A lot of researchers are interested in this idea and resulting to many different designs providing possibility of pattern reconfiguration [8], [11], [69]–[82]. Three common methods are used for this purpose: parasitic tuning, element phase shifting and co-located radiating aperture [9]. However, all the designs reported in these references suffer from complexity, requiring extra structures, lot of lumped components and phase shifters which occupy considerable space [14]. In addition, the reconfiguration is narrow band.

In this chapter, a simple approach is proposed to achieve pattern reconfiguration of UWB CPW-Fed monopole antenna. The antenna, as designed, is capable of switching between three different states of its pattern in a wide reconfiguration band without changing size or form of the monopole. The design is therefore suitable in diversity applications and may allow enhancing channel capacity.

2.2 Pattern reconfigurable antenna classification

2.2.1 Shifting the main beam while keeping the pattern shape

Several designs available in the literature about pattern reconfiguration concern the main beam shift and maintain the initial pattern shape [83]–[85].

Authors in [84] present a reconfigurable parasitic array as seen in Figure 2.1. Switched parasitic elements are used in each side of the central radiator. Controlling the switch state allows shifting the maximum radiation into three different directions: -35°, 0°, +35° (Figure 2.2). The beam steering does not alter the original pattern shape.

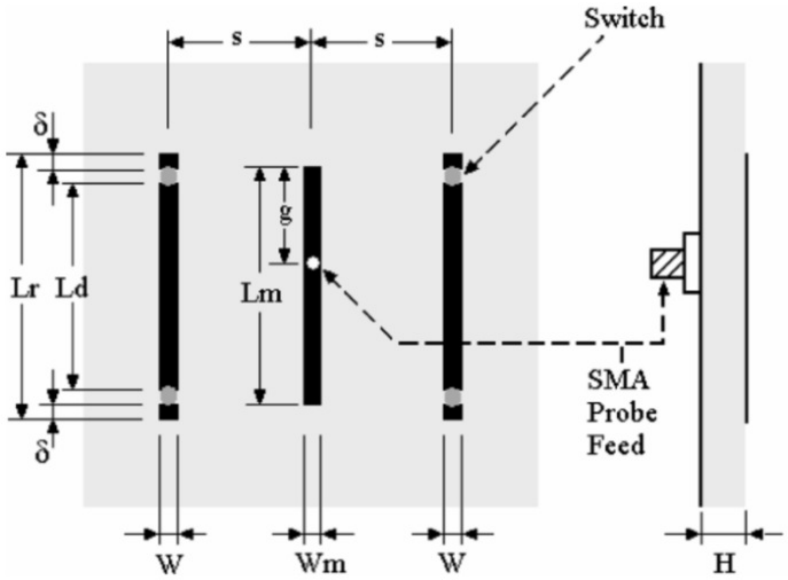

Figure 2.1: Reconfigurable microstrip parasitic array [84]

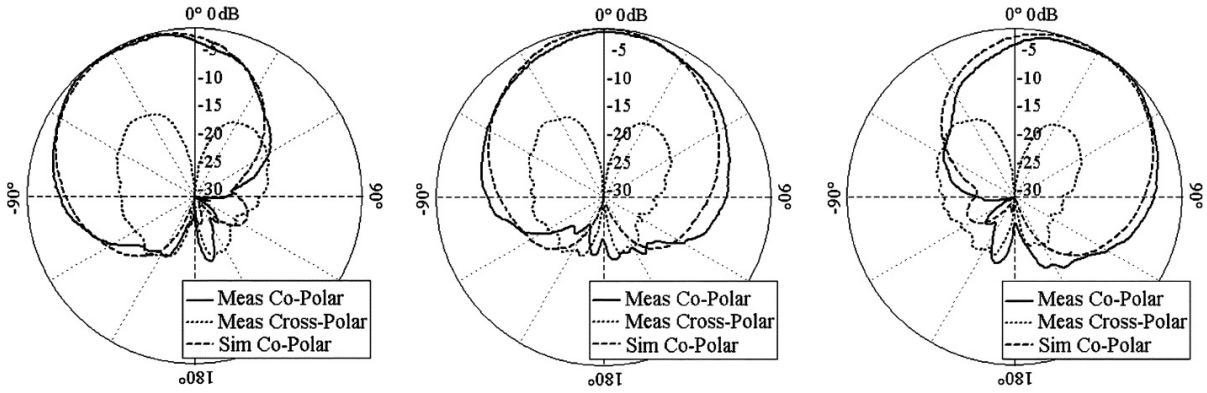

Figure 2.2: Radiation pattern of the reconfigurable microstrip parasitic array [84]

Another design providing pattern reconfiguration is that of [85]. The pattern of a rectangular patch is tuned by combination with two folded dipoles inserted in left and right side of the central radiator (rectangular patch) (Figure 2.3). Hence, four beam directions

(Figure 2.4) can be obtained by judicious setting of four switches (A, B, C, D) used as alternate connection or disconnection between the patch, folded dipoles and the ground.

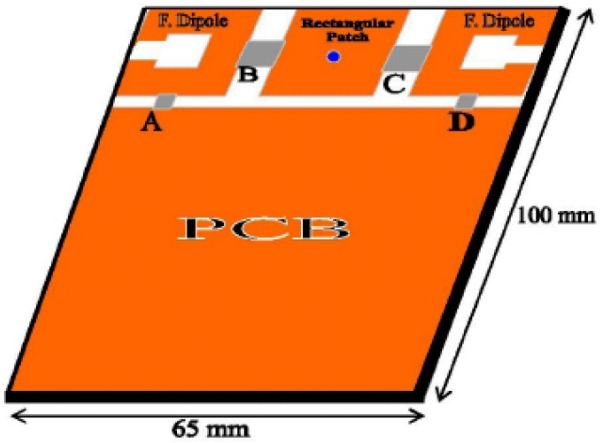

Figure 2.3: Rectangular patch antenna with parasitic folded dipoles [85]

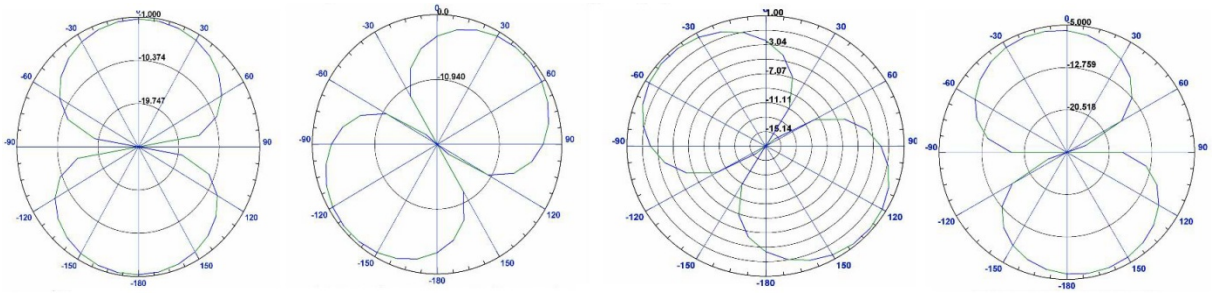

Figure 2.4: Radiation pattern of the reconfigurable patch antenna [85]

2.2.2 Shifting the main beam and changing the beam shape

In this category of reconfigurable antennas, the main beam can be steered to different directions, however the pattern shape may be changed [86]–[88].

In [86], monopole antenna is combined with dipole antenna and reflector to provide beam steering capability (Figure 2.5). Depending on the switch states, the proposed antenna may operate as monopole (omnidirectional pattern) or directional antenna obtained by combining dipole and reflector (Figure 2.6).

Parasitic microstrip architecture is also proposed in [88] in order to achieve beam steering. Active and passive elements compose the antenna (Figure 2.7). Switches are used to activate or deactivate a given parasitic part in order to obtain desired pattern. Thus, the antenna may radiate omnidirectional or directional patterns (Figure 2.8) with pattern shape changing. This kind of designs may be interesting in signal detection, positioning and direction of arrival applications.

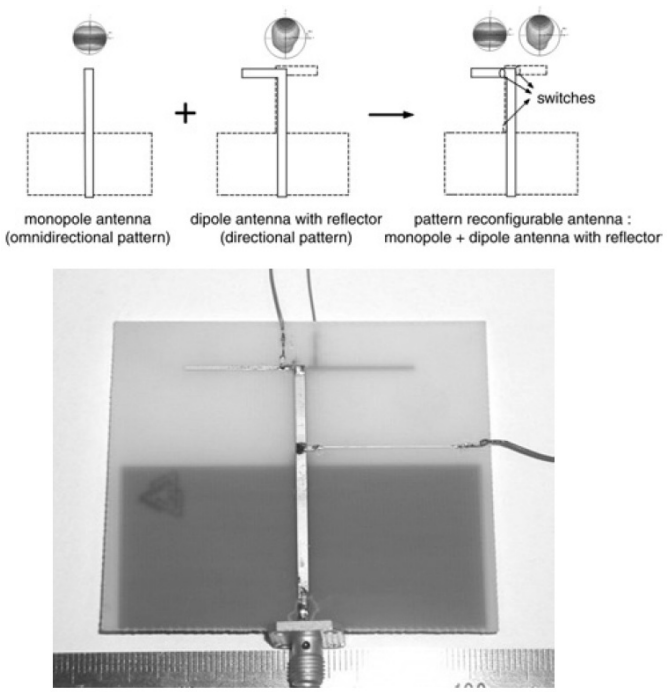

Figure 2.5: Reconfiguration principle and prototype [86]

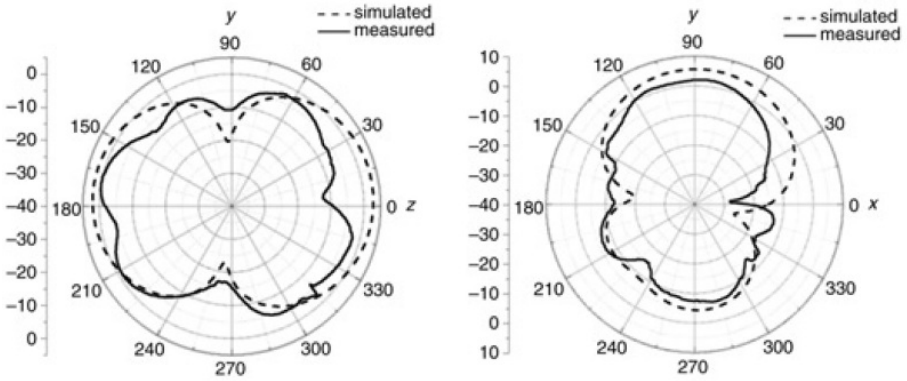

Figure 2.6: Radiation pattern of the reconfigurable monopole antenna [86]

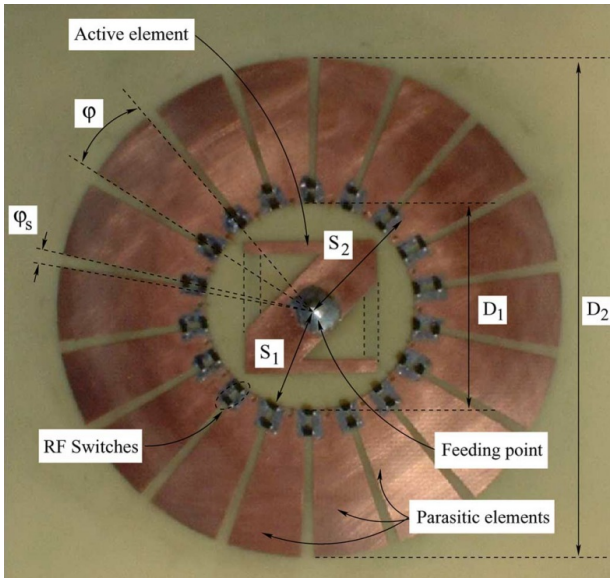

Figure 2.7: Prototype of the parasitic antenna[88]

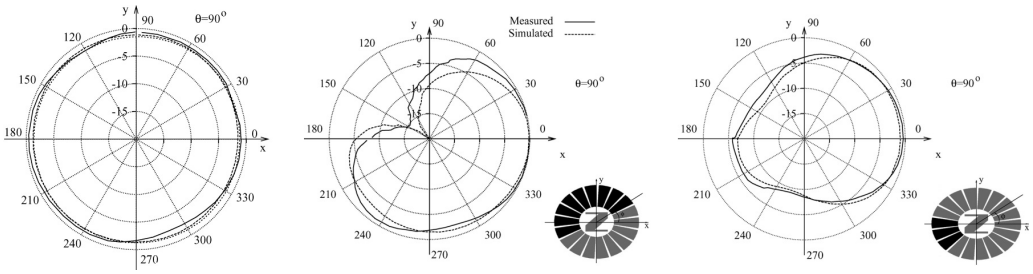

Figure 2.8: Radiation pattern of the reconfigurable parasitic antenna [88]

2.2.3 Multiple reconfigurable antenna features

In such antennas, different characteristics may be tuned. Generally, reconfiguration includes: operating frequency, radiation pattern and polarization. The reconfiguration can also be individual (one parameter at a time) or multiple (several parameters are tuned at a time). The choice is basically related to the application requirements such as diversity in MIMO systems, channel capacity improvement, mitigating interferences, spectrum opportunity and so on.

Several examples are proposed in the literature. In [89], frequency and pattern reconfigurable slot antenna is designed (Figure 2.9). The slot is controlled by two switches to produce three reconfigurable bands: 1.82 GHz, 1.93 GHz and 2.10 GHz (Figure 2.10). Further, the antenna is capable of controlling the pattern direction by using slits introduced in the ground plane, hence three main beam angle are obtained (-15°, 0°, +15°) as depicted in Figure 2.11.

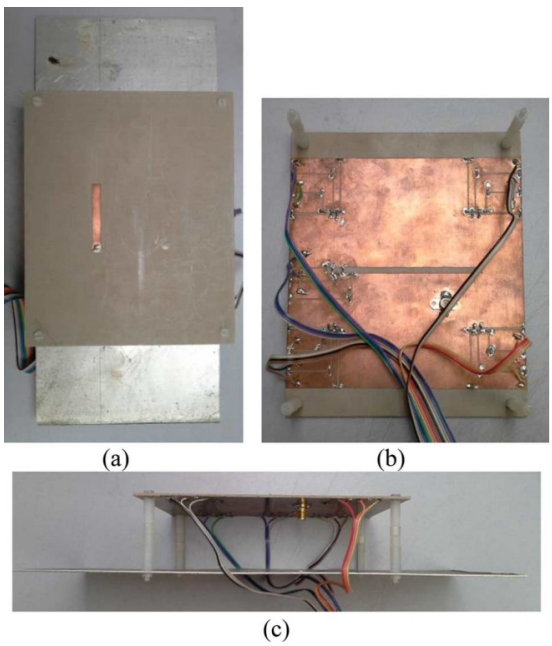

Figure 2.9: Frequency and pattern slot reconfigurable antenna[89]

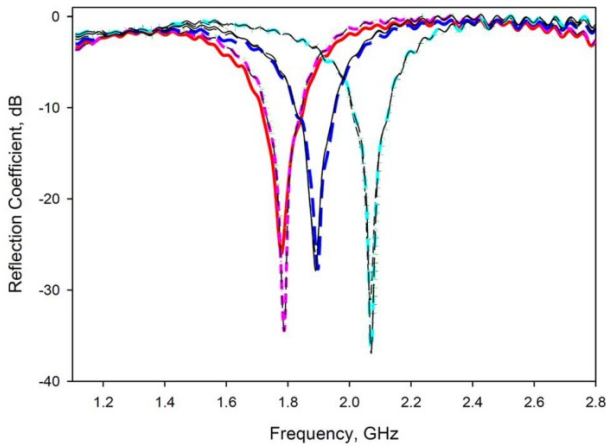

Figure 2.10: Frequency bands of the slot reconfigurable antenna[89]

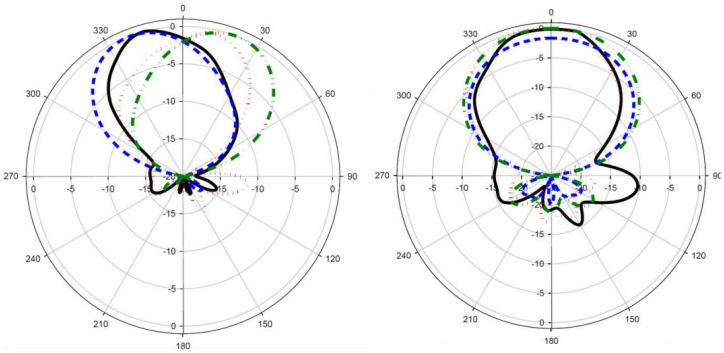

Figure 2.11: Pattern of the slot reconfigurable antenna[89]

Truncated monopole antenna is proposed in [90] to achieve pattern and polarization reconfiguration. The antenna is fed through microstrip line and presents compact structure (Figure 2.12). Two meander lines are excited alternatively by two switches, thus polarization diversity is achieved. Depending on the excited meander line, different radiation patterns can be obtained (when vertical line is excited, maximum radiation is in $x-z$ plane. The horizontal line provides maximum radiation in $y-z$ plane) (Figure 2.13). The design is suitable in channel capacity improvement of communications systems.

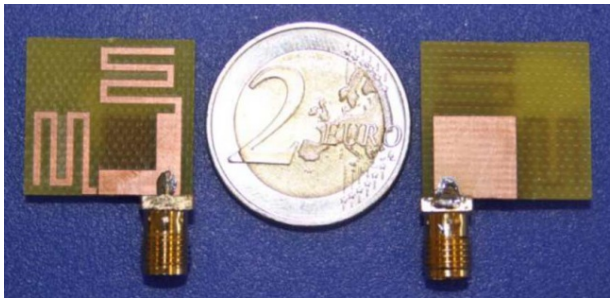

Figure 2.12: Pattern and polarization reconfigurable antenna[90]

In addition to the previous examples, authors in [91] proposed a Rhombic patch antenna reconfigurable in frequency, pattern and polarization. The architecture is composed of a rhombus radiator with three excitation lines (Figure 2.14). The antenna operates in

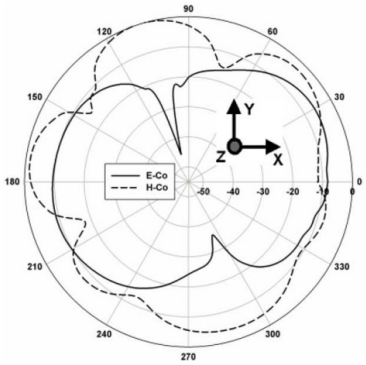

Figure 2.13: Radiation pattern of the meander antenna[90]

two bands: 5.2 GHz and 5.8 GHz (Figure 2.15) with linear, circular and ± 45° slant polarization. Switches are used to provide reconfiguration and pattern can be steered toward ± 30° (Figure 2.16).

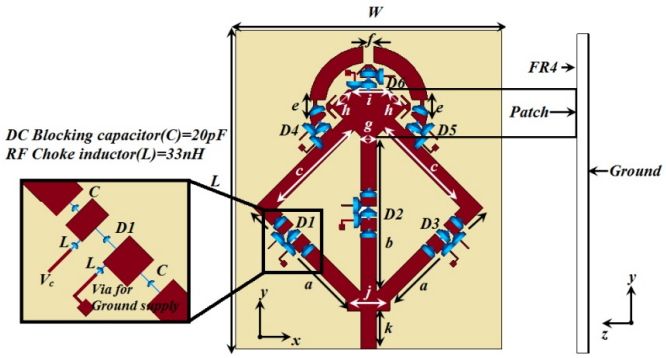

Figure 2.14: Rhombic patch reconfigurable antenna[91]

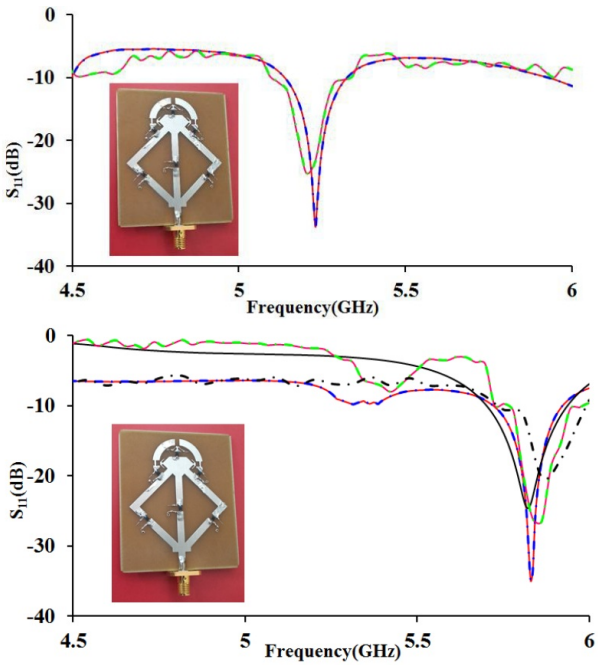

Figure 2.15: Frequency reconfigurtion of the Rhombic antenna[91]

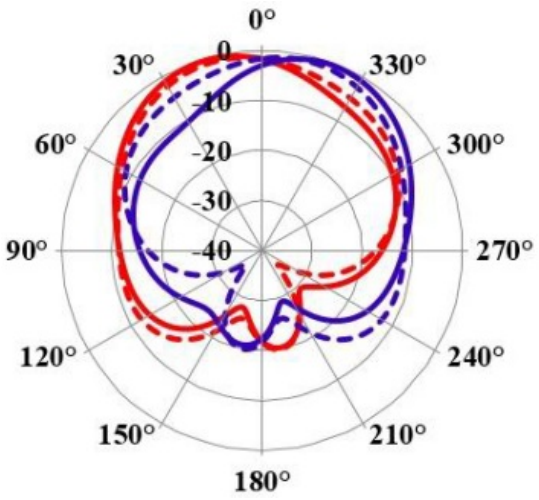

Figure 2.16: Pattern reconfigurtion of the Rhombic antenna[91]

2.3 Reconfiguration task implementation

Antenna pattern reconfiguration may be obtained in various possibilities. Changing path current by switches, insertion of parasitic elements and affecting current behaviour by different loading are some of those possibilities [92]. The question is then, how to implement practically these methods?

PIN diodes and MEMS are the most used components in reconfiguration task. They are known to be electronic switches. Many designs use PIN diodes [85], [93], [94] or MEMS [95], [96] to achieve reconfiguration.

PIN diodes require relatively high voltage (some volts) and they are somewhat power consuming (can reach 50 mW). Figure 2.17 illustrates an example of PIN diodes (Skyworks SMP1320-011LF) in two states "ON state" and "OFF state". One can notice that even the diode is ON, it still presents a small resistor effect.

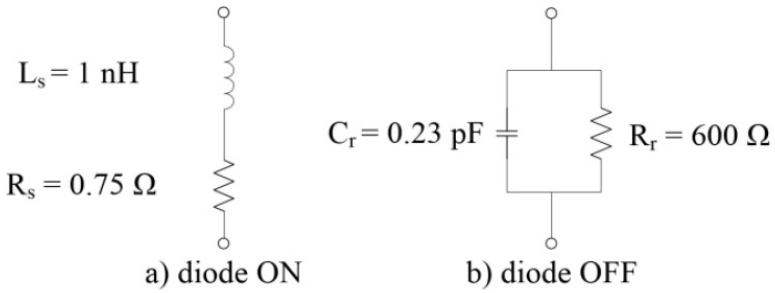

Figure 2.17: PIN diode model [97]

MEMS switches, however are advantageous. They present lower resistance in ON state, negligible capacitance, low insertion loss and high isolation with small dimensions. They are also low power consumption.

2.4 Proposed approach for reconfiguring the pattern of an UWB CPW-Fed monopole antenna

2.4.1 Antenna design and configuration

A) ***Introduced reconfiguration shape and principle of operation***

By analyzing the current distribution of a CPW-Fed monopole, we can notice that this distribution is in its maximum value in areas near the ground plane (Figure 2.18), this behaviour is owing to the coupling currents between the radiator and the ground plane. Furthermore, the symmetrical current distribution provides symmetrical pattern of the monopole hence the omnidirectional behavior.

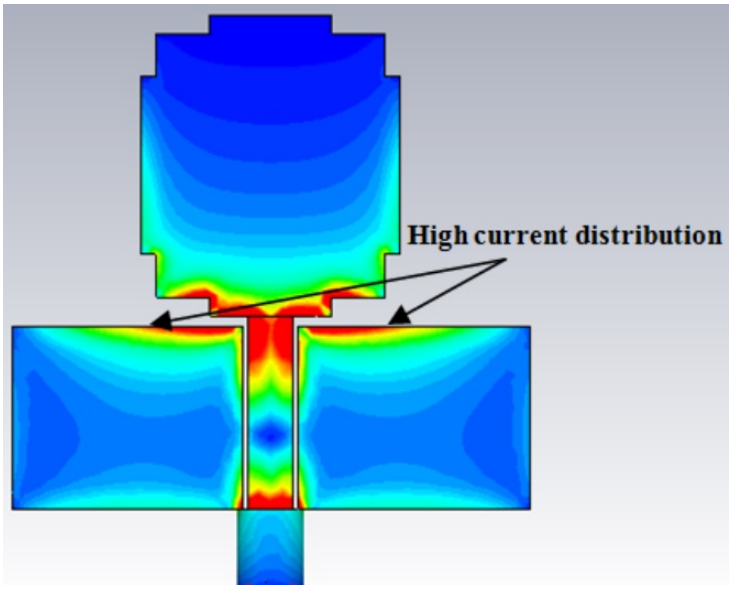

Figure 2.18: Current distribution in the ground plane of a CPW-Fed monopole antenna

To redirect the main beam to one side instead of the two sides, a dis-symmetry of the radiator current distribution has to be performed; this is done by introducing a VIVALDI shape (slot) in the ground plane as seen in Figure 2.19. The slot can be designed by following equations (3.13) while the flare opening rate r is a crucial parameter which should be carefully studied in order to maintain UWB feature. Since this shape is UWB, its flare reduces significantly the currents to distribute symmetrically in the radiator, then the modified side (open side) contributes weakly in the far-field radiation. Furthermore, a switch is introduced to allow opening and/or closing the flare, thus the reconfiguration can be achieved. The proposed approach may be applicable for different CPW monopoles as will be detailed next.

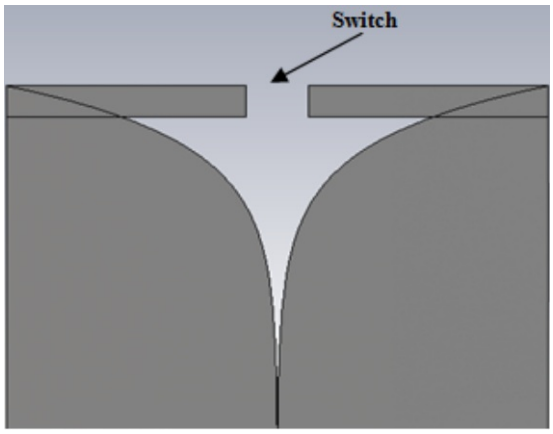

Figure 2.19: VIVALDI shape introduced in the ground plane of the monopole antenna

B) ***First application: Printed stepped rectangular monopole antenna***

The first application of our proposition is the stepped rectangular coplanar waveguide fed monopole (CPW). The antenna is designed on FR-4 substrate of thickness 1.6 mm, dielectric constant of 4.3 and loss tangent of 0.025. Dimensions of the antenna are depicted in Figure 2.20, and more details can be found in [98]. The monopole is UWB as the operating frequency extends from 3 GHz to more than 11 GHz (Figure 2.21), with omnidirectional radiation (Figure 2.22).

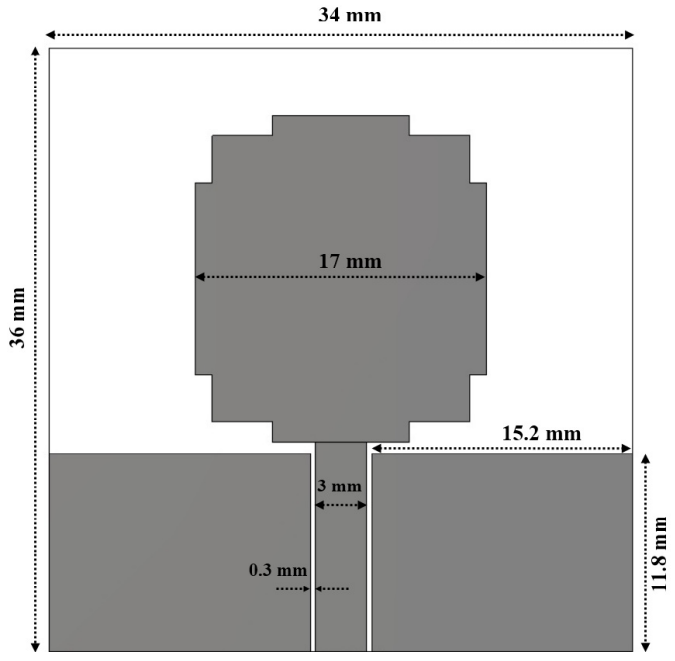

Figure 2.20: Printed stepped rectangular monopole antenna

The reconfiguration approach is applied to this antenna and the new shape is depicted in Figure 2.23, where r is set to 0.8 after being optimized by CST Software. Depending on the presence or absence of conductor, the switches are considered as close or open respectively.

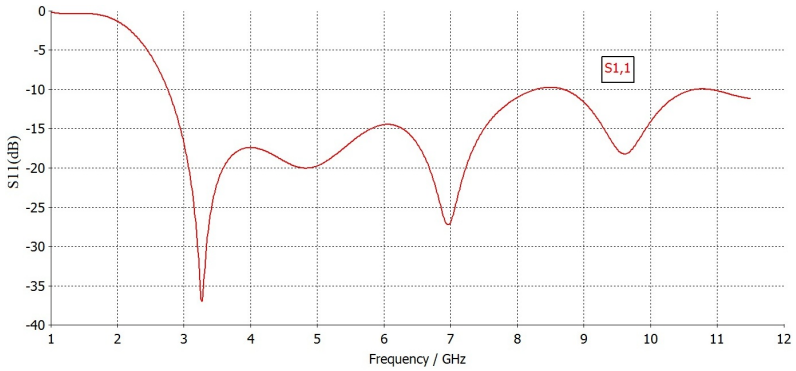

Figure 2.21: Reflexion coefficient S_{11} of the printed stepped rectangular monopole antenna

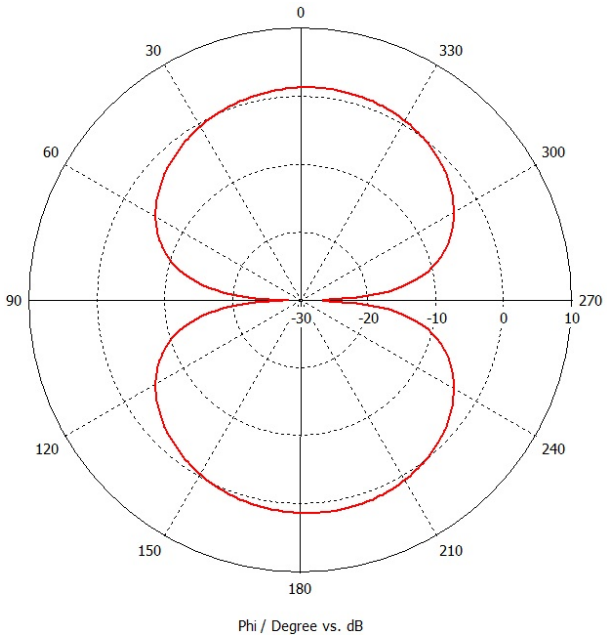

Figure 2.22: Radiation pattern of the printed stepped rectangular monopole antenna

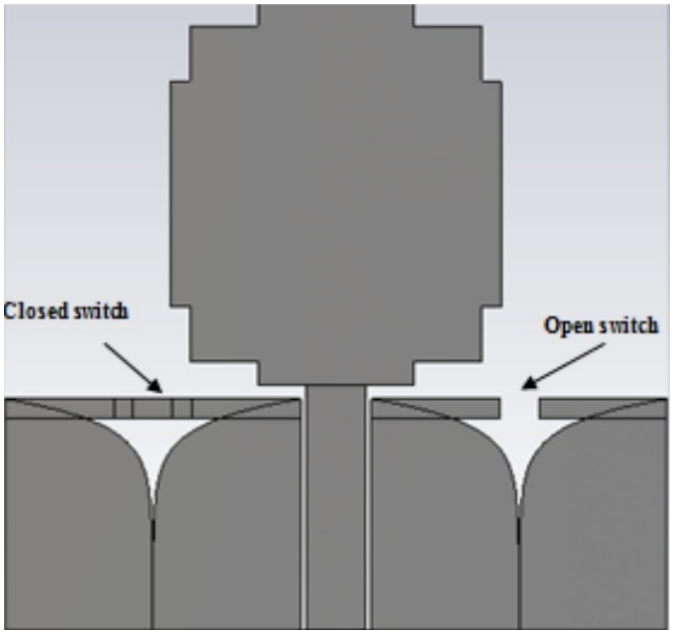

Figure 2.23: Printed stepped rectangular monopole antenna with switched VIVALDI ground plane shape

C) ***Second application: Printed circular disc monopole antenna***

This second application concerns a printed circular disc CPW-Fed monopole, designed on FR-4 substrate of thickness 1.6 mm, dielectric constant of 4.3 and loss tangent of 0.025. Design guidelines follow those reported in [99], with disc radius of 12.5 mm. The introduced slot is characterized by a flare opening rate r of 0.55. Figure 2.24 depicts the proposed antenna. UWB and omnidirectional radiation are the main features of the disc monopole as well (Figure 2.25 and Figure 2.26 , respectively).

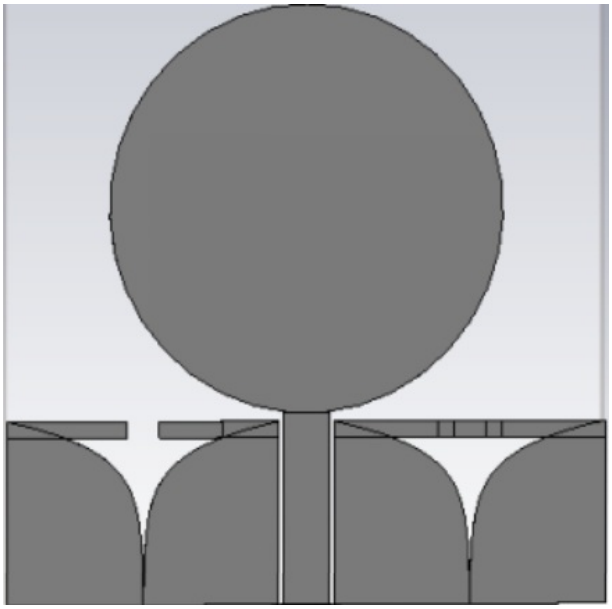

Figure 2.24: Printed circular disc monopole antenna with switched VIVALDI ground plane shape

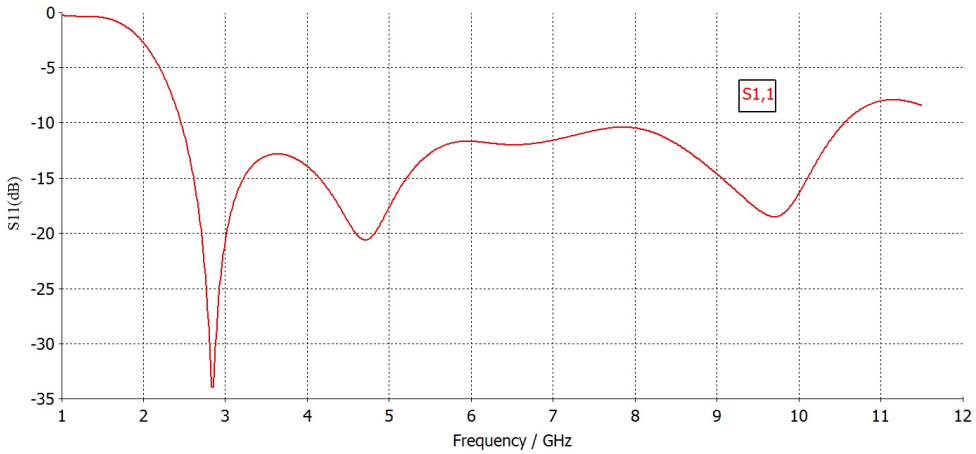

Figure 2.25: Reflexion coefficient S_{11} of the disc monopole antenna

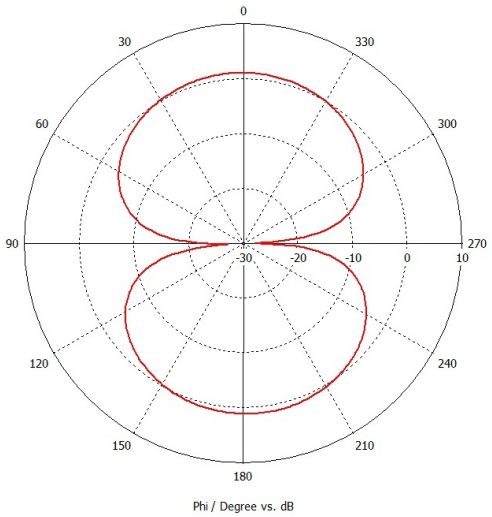

Figure 2.26: Radiation pattern of the disc monopole antenna

2.4.2 Results and discussions

A) ***Case 1: Printed stepped rectangular monopole antenna***

All simulations are carried out using CST Microwave Studio Software. Switches (PIN diodes) are supposed to be ideal in first time; this means that the presence (or absence) of conductor indicates closed/opened state respectively (Figure 2.23).

Figure 2.27 depicts the reflection coefficient S_{11} of the antenna in its initial form and with VIVALDI ground plane. It is obvious that the introduced shape does not affect the impedance matching of the antenna from 2.7 GHz to 7 GHz, hence its wide band characteristic is still valid.

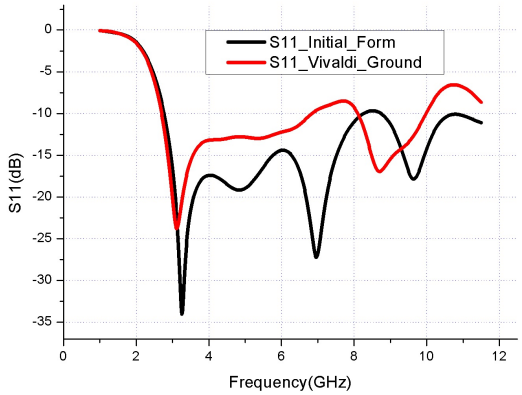

Figure 2.27: Reflection coefficient S_{11} of the printed stepped rectangular monopole antenna with and without switched VIVALDI ground plane

Further, symmetrical/asymmetrical current distributions in the initial/modified form of the antenna can be easily distinguished from Figures 2.18 and 2.28, respectively, as discussed in section (2.4.1).

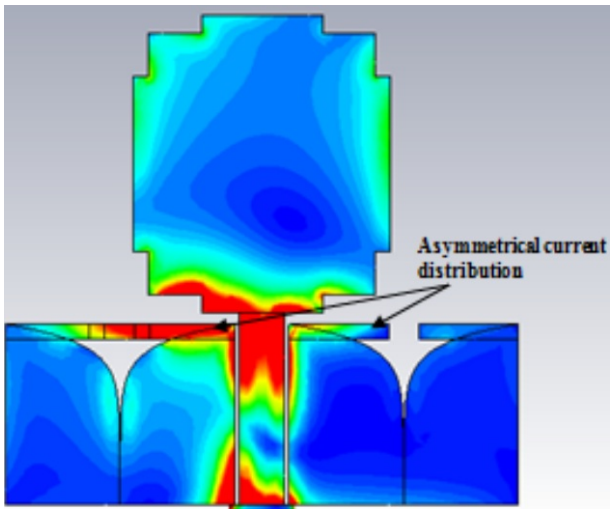

Figure 2.28: Asymmetrical current distribution in the modified antenna

Table 2.1: Reconfigured radiation pattern of the stepped rectangular monopole

F GHz	Initial form	Left switch open	Right switch open	XY plane
5.5	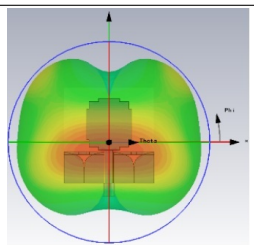	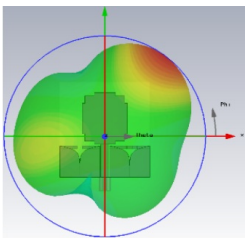	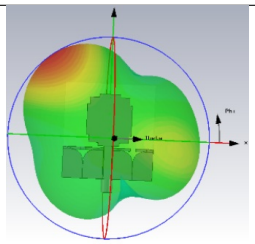	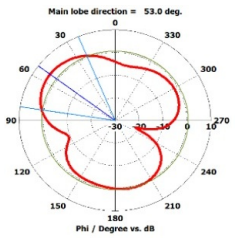
6	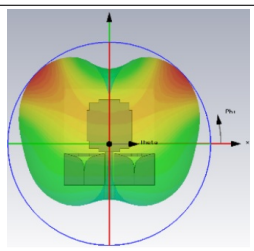	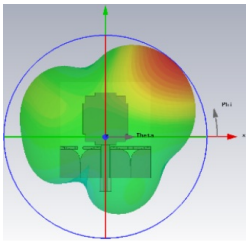	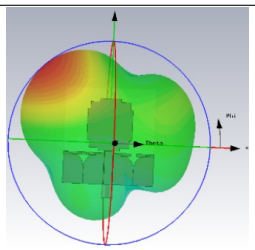	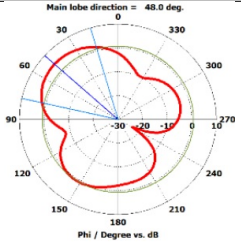
6.5	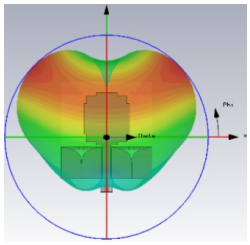	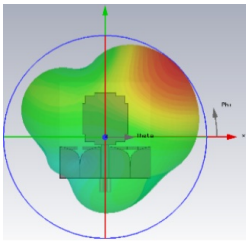	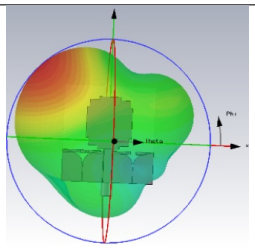	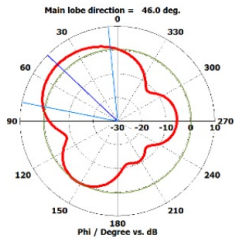
7	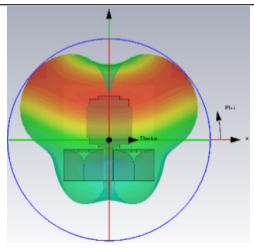	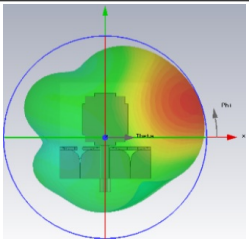	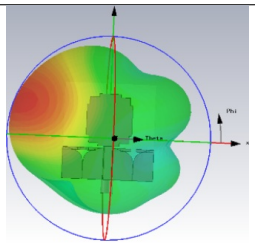	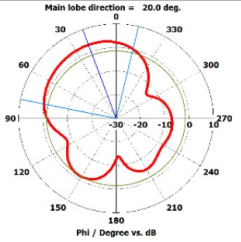

In Table 2.1 are compared the radiation patterns of the proposed antennas with the initial ones in the band of reconfiguration. Moreover, 3D pattern and different plane cuts are shown. We observe that opening a switch in one side shifts the main beam into

the opposite side, thus we can distinguish three states of the pattern: left side (right switch open, left one closed), right side and both sides (both switches are closed). From this, we conclude that effectively, the introduced approach allows shifting the main beam with respect to the state of the switches.

B) ***Case 2: Printed circular disc monopole antenna***

The same methodology is followed in this second application, and all the results are depicted in Figure 2.29 and Table 2.2.

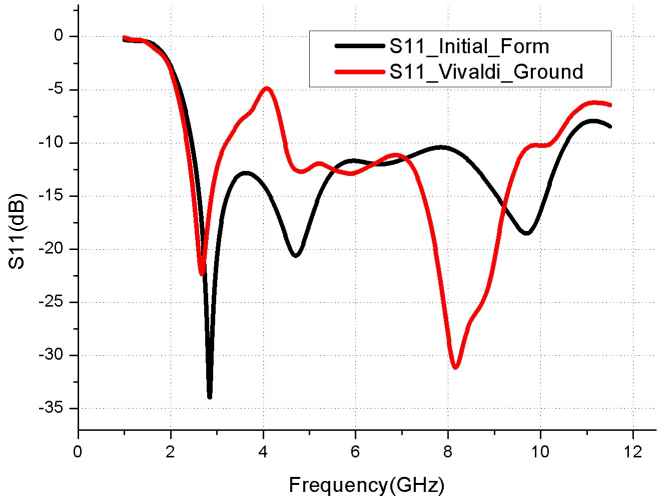

Figure 2.29: Reflection coefficient S_{11} of the printed circular disc monopole antenna with and without switched VIVALDI ground plane

The difference noticed in this case is that the impedance matching is altered in the lower band: 3.2 GHz-4.5 GHz (Figure 2.29). This may be explained by the fact that the ground plane contributes significantly in the matching of the radiator (Disc) in this band. Hence, slotting the ground provides the noticed mismatching.

2.4.3 Experimental considerations

The practical design of such reconfigurable antennas needs a special care since external components are used (PIN diodes are used as switches). First, 0.3mm-width slots are introduced in the ground plane to separate the two ports of the switches and to ensure a voltage difference in between (DC isolation), however RF continuity of the ground plane has to be guaranteed, hence 100-pF surface-mount RF capacitors are used to bridge the slots and nearly providing a short circuit (0.6 Ohm). BAR50-02V PIN diodes are used in this design and their effect is taken into account in the simulations by inserting their

Table 2.2: Reconfigured radiation pattern of the circular disc monopole

F GHz	Initial form	Left switch open	Right switch open	XY plane
4.5	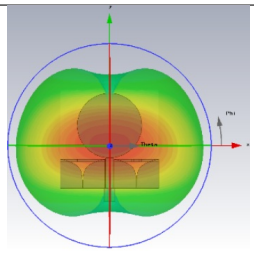	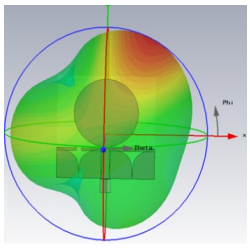	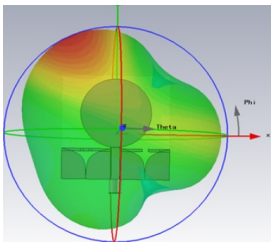	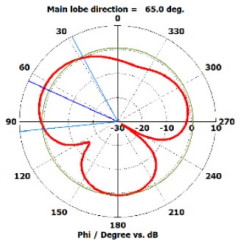
5	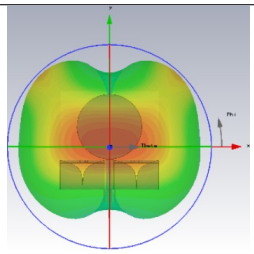	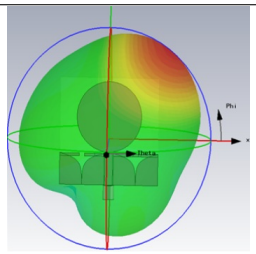	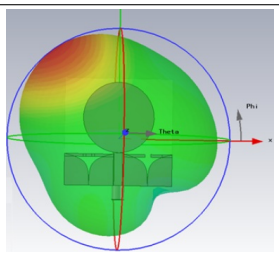	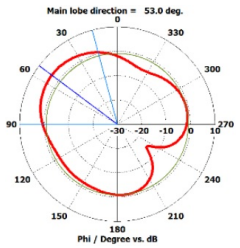
5.5	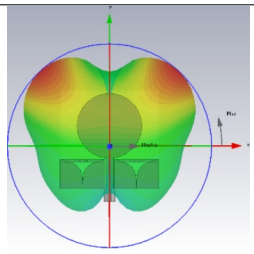	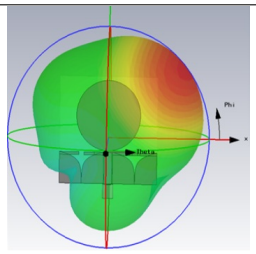	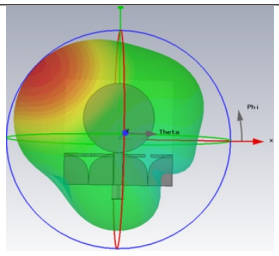	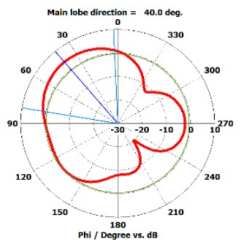
6	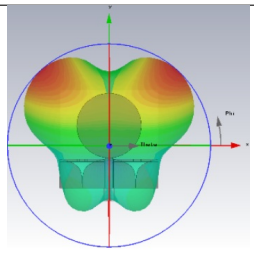	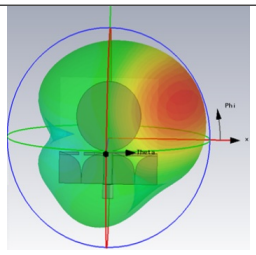	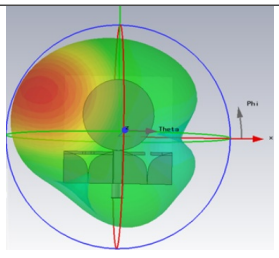	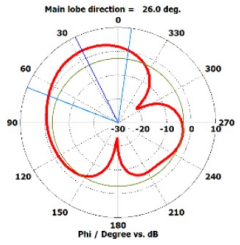

S-parameters provided by the constructor. Figure 2.30 depicts the new practical design in which slots, capacitors and PIN diodes are clearly shown. Furthermore, the manufactured prototype is shown in Figure 2.31.

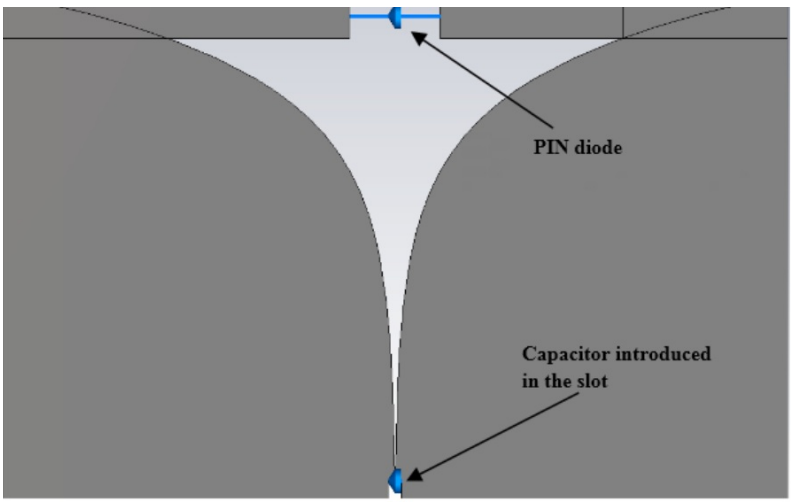

Figure 2.30: Practical considerations in the proposed design

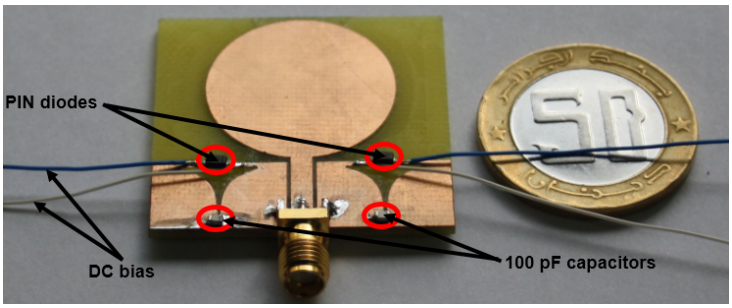

Figure 2.31: Fabricated prototype

The equipment in-availability constraint allowed us to measure only the reflection parameter S_{11} by the Network Analyzer at CDTA (Centre de Développement des Technologies Avancées). The radiation pattern measurements need anechoic chamber which is not in our possession. Figure 2.32 shows the simulated and measured S_{11}, taking into account PIN diodes S-parameters. Since maximum operation frequency of BAR50-02V PIN diodes is 6 GHz, the measurements are carried out until this maximum frequency.

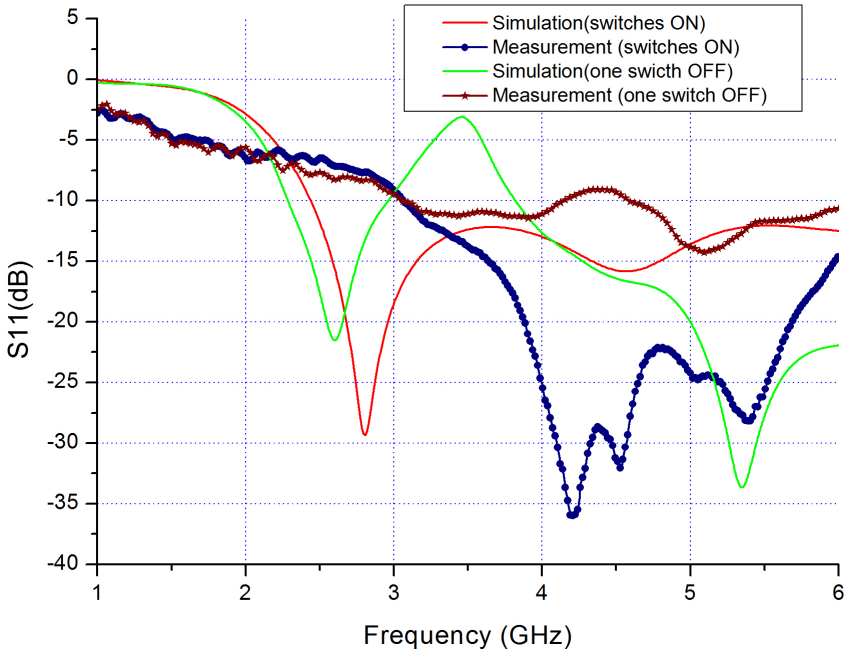

Figure 2.32: S_{11} simulations and measurements

A small disagreement in simulated S_{11} parameter is noticed, particularly in case of OFF switches, this occurs because the impedance matching of a CPW-Fed antenna is tightly dependent on the shape of the ground plane and its distance to the radiator. To overcome this difficulty, a careful study of the flare opening rate and switch position need to be performed. A good selection of switches with suitable S parameters is another concerned component.

In this work, our optimization study with using available BAR50-02V PIN diodes lead

to the results of Figure 2.32. One can notice that measurements are somehow shifted to higher frequency since -10 dB measured bandwidth, in case of ON switches (Blue line), starts from 3GHz instead of 2.5GHz of simulated one (Red line). The same remark is noticed as well in case of OFF switches as the measured notch is found around 4.2GHz (Crimson line) and the simulated one is around 3.5GHz (Green line). In addition to the fabrication process uncertainties, the noticed issues may be explained by the integration of the PIN diodes with soldered feeding cables in the ground plane, also the permittivity instability of the cheap substrate (FR-4) may be another important tender of this disagreement. Albeit those discrepancies in the lower band, we can conclude that acceptable agreement between simulations and measurements is obtained in the reconfiguration band (4.5 GHz-6 GHz).

2.4.4 Conclusion

A simple pattern reconfiguration approach is presented. It is based on introducing VIVALDI shape in the ground plane of CPW-Fed antennas. This idea comes from the UWB (theoretically infinite bandwidth) principle characteristic of the VIVALDI shape. Therefore, we believe that this UWB feature allows modifying the radiator current distribution. Hence, the ability to control the antenna pattern is allowed around a wide band frequency. This is an advantage when comparing to the literature techniques which, in most cases, lead to narrow band reconfiguration.

In this chapter, two examples are used to validate our approach; CPW-Fed stepped rectangular and CPW-Fed disc monopole antennas. The pattern reconfiguration is achieved by switching. Furthermore, a prototype is realized and measurements are performed. Despite some noticed discrepancies, a reasonable agreement between simulations and measurements has been achieved.

The proposed approach has been published in The 7^{th} Seminar On Detection Systems: Architectures and Technologies (DAT 2017, IEEE indexed).

Chapter 3

Chapter 3

Microwave Phase Shifters

3.1 Introduction

Microwave components have become of important priority in diverse modern radiofrequency (RF) systems. Antennas, filters, couplers are some examples of those crucial devices. Phase shifters are also key components in recent technologies dealing with RF challenges, hence various applications motivate the use of phase shifters as driver devices, for instance: phased array antennas, beamforming networks, modulators, radars, measurement systems and many other industrial applications.

Design a wideband phase shifter with high performances including: low insertion loss and stable output phase shift is a very challenging issue. In addition to these requirements, the device should be compact and easily manufacturable, as the need for different types of miniaturized structures is growing up as well in order to provide compact and efficient devices.

Many designs available in the literature [25], [27], [42], [100]–[103] suffer from three main drawbacks: narrow bandwidth, high phase ripple and complexity of the structure. However, in some recent works, UWB and low phase ripple are achieved [30], [33], [34]. In [37], a planar dual frequency phase shifter is described. It exploits the phase-delay characteristics of complementary split-ring resonator to provide 180° phase shift at 2.4 GHz and 90° phase shift at 5.4 GHz, however the proposed scheme is frequency limited as it operates only at 2.4 GHz and 5.4 GHz.

In this chapter, new alternatives for phase shifters design are demonstrated. The first design is based on UWB coupled sections settled to provide 180° output phase shift, the second one consists of comparing two inverted transitions which leads to frequency independent 180° phase shift between them, and the third design is an UWB 45° phase shifter

based on tapered coupled transitions. All measurements were carried out at CDTA.

3.2 Frequency Independent 180° Phase Shifter Based on UWB Coupled Sections

A novel Ultra-Wideband (UWB) 180° planar phase shifter is proposed in this first contribution. The design is mainly based on coupled sections which are realized by inserting slots into the common ground plane of the multilayer circuit. Further, the structure is theoretically analyzed as a four port network to explain the main characteristics.

3.2.1 Analysis and formulation

The proposed schematic design is depicted in Figure 3.1. It is a multilayer structure in which two UWB slot-coupled transitions are etched as in [33], and [104]. Input ports (ports 1, 1') and output ports (ports 2, 2') are connected through 50 Ohm Microstrip lines.

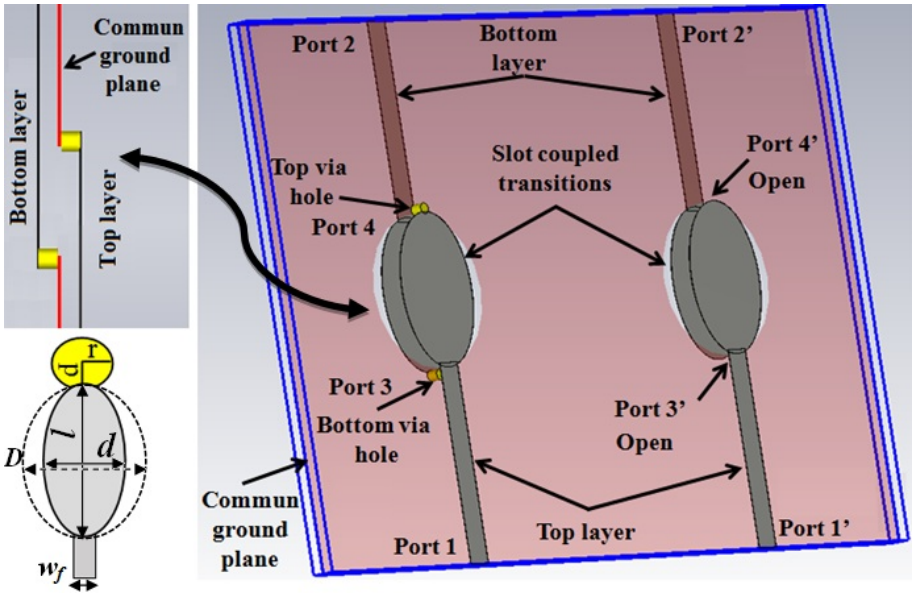

Figure 3.1: Schematic design of the proposed phase shifter

Analysis of this structure can be done by considering the circuit as a juxtaposition of two four-port devices (two ports in each layer). One of them is taken as a main line in which two ports (3 and 4) are short-circuited, the other four-port circuit is the reference line with ports 3', and 4' are open-circuit (Figure 3.2).

Let us note K as a coupling factor of the elliptical slot transition and a_i, b_i are input, output signals at port i respectively. As in [33], [105] and [106]:

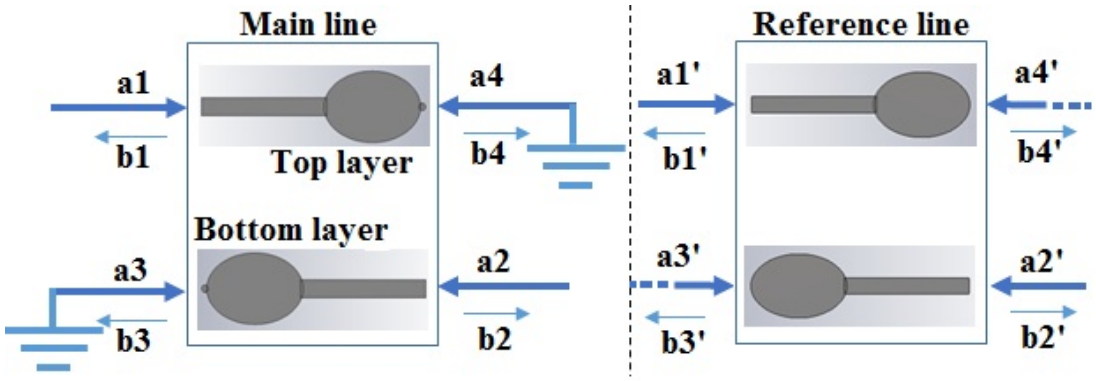

Figure 3.2: Four-Port Network analysis of the proposed design

$$b_1 = \frac{jKsin(\beta_e l)a_3 + (\sqrt{1-K^2})a_4}{(\sqrt{1-K^2})cos(\beta_e l) + jsin(\beta_e l)} \tag{3.1}$$

$$b_2 = \frac{jKsin(\beta_e l)a_4 + (\sqrt{1-K^2})a_3}{(\sqrt{1-K^2})cos(\beta_e l) + jsin(\beta_e l)} \tag{3.2}$$

$$b_3 = \frac{jKsin(\beta_e l)a_1}{(\sqrt{1-K^2})cos(\beta_e l) + jsin(\beta_e l)} \tag{3.3}$$

$$b_4 = \frac{(\sqrt{1-K^2})a_1}{(\sqrt{1-K^2})cos(\beta_e l) + jsin(\beta_e l)} \tag{3.4}$$

Where l is the physical length of the coupled structure and β_e is the effective phase constant in the medium of the coupled structure.

Since ports 3 and 4 are short-circuited, the reflection coefficient $b_3/a_3 = b_4/a_4 = -1$, thus:

$$S_{11} = \frac{b_1}{a_1} = \frac{-[1-K^2(1+sin^2(\beta_e l))]}{[(\sqrt{1-K^2})cos(\beta_e l) + jsin(\beta_e l)]^2} \tag{3.5}$$

$$S_{21} = \frac{b_2}{a_1} = \frac{-2jK(\sqrt{1-K^2})sin(\beta_e l)}{[(\sqrt{1-K^2})cos(\beta_e l) + jsin(\beta_e l)]^2} \tag{3.6}$$

Output phase shift of the transmitted signal (from port 1 to port 2) is given by S_{21} argument in (3.6), as:

$$\begin{aligned} \varphi_{main_{cc}} &= Arg(S_{21}) \\ &= -90° - 2arctang\left\{\frac{sin(\beta_e l)}{(\sqrt{1-K^2})cos(\beta_e l)}\right\} \end{aligned} \tag{3.7}$$

Same analysis is done to the reference line in which the ports 3' and 4' are open-circuit

(reflection equal to 1). Hence the phase shift is:

$$\varphi_{ref_{open}} = +90° - 2arctang\left\{\frac{sin(\beta_e l)}{(\sqrt{1-K^2})cos(\beta_e l)}\right\} \tag{3.8}$$

Comparing the phase of reference and main lines (Figure 3.1, Figure 3.2) leads to the differential phase shift as follows (taken between ports 2 and 2'):

$$\Delta\varphi = \varphi_{main_{cc}} - \varphi_{ref_{open}} \tag{3.9}$$

From (3.7), (3.8) and (3.9), we get $\Delta\varphi = -180°$. This phase difference is theoretically frequency independent.

3.2.2 Phase shifter design and results discussion

In this section, we tend to prove that the proposed idea of 180° phase shifter is applicable. To achieve this purpose, real measurements have to be performed.

Short-circuited ports in the main line allowing a pure reflection of almost (-1), as discussed previously, are realized using via holes [107]–[109]. Optimization of dimensions; radius r and position p of the via hole in the structure (Figure 3.1), is studied using CST Microwave Studio as a simulation tool.

Figure 3.3 shows the variation of the phase shift ($\Delta\varphi$) for different values of the radius r and the position p. It is observed that the phase shift is considerably affected by the variation of r and p. Hence, to avoid high $\Delta\varphi$ ripples, the radius r and the position p need to be carefully chosen. Details of optimized dimensions are depicted in Figure 3.4.

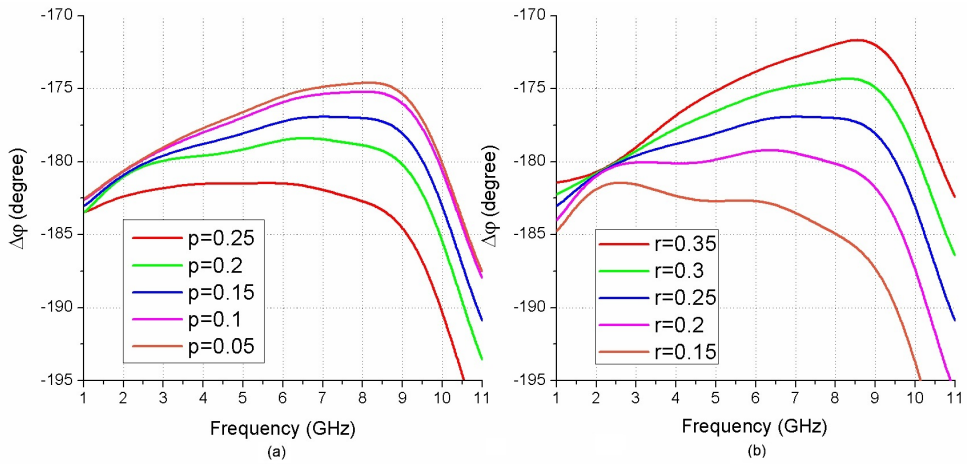

Figure 3.3: Parametric study of the via hole dimensions (a) Output phase shift for different p (b) Output phase shift for different r

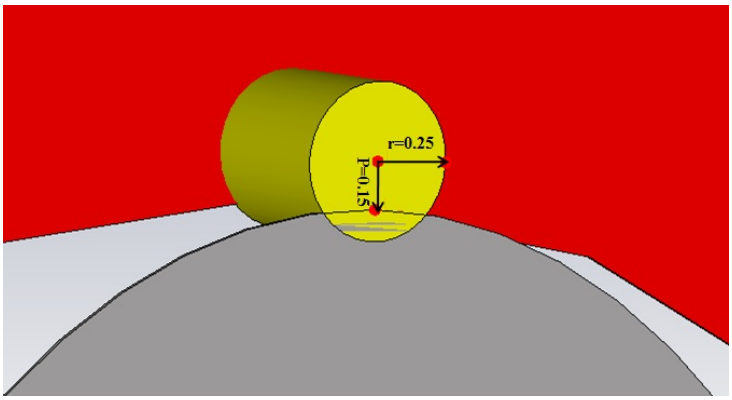

Figure 3.4: Optimized dimensions r, p in (mm) of the via hole

The manufactured prototype, as shown in Figure 3.5, consists of two coupled-microstrip elliptical transitions etched on Rogers *RO4003C* ($\varepsilon_r = 3.38$, *h=0.508 mm and loss tangent=0.0027)* substrate. The dimensions of the design are initially based on the procedure reported in [33], then optimized by CST Microwave Studio software. The ports are connected to 50 Ohm Microstrip transmission lines of width w_f obtained using standard formulas presented in [110], [20]. The final design dimensions (Figure 3.1) are: $w_f = 1.2mm, l = 7.1mm, d = 4.75mm$, and $D = 7.3mm$. One can notice the compactness of the structure, since its total size is $25 \times 30 \times 1mm^3$.

Figure 3.6 presents the simulated and experimental amplitude characteristics of the design (main line). It is noticed that simulations and measurements are in good agreement. Moreover, return loss is more than 10 dB and insertion loss is better than 0.95 dB for both simulation and measurement results in the frequency band 3-10.2 GHz.

Output phase simulation and measurement results are depicted in Figure 3.7. The simulated differential phase shift is around 180° ± 3° and the measured one is 180° ± 6° in the frequency band 1-10.2 GHz. The measured and simulated output phase shift are in line. Small discrepancies are noticed mainly due to the fabrication process tolerances and the alignment of the two layers forming the structure.

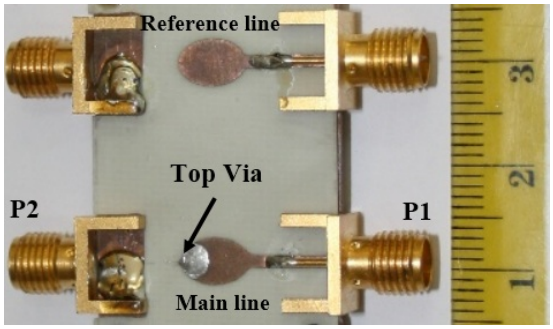

Figure 3.5: Photograph of the manufactured phase shifter

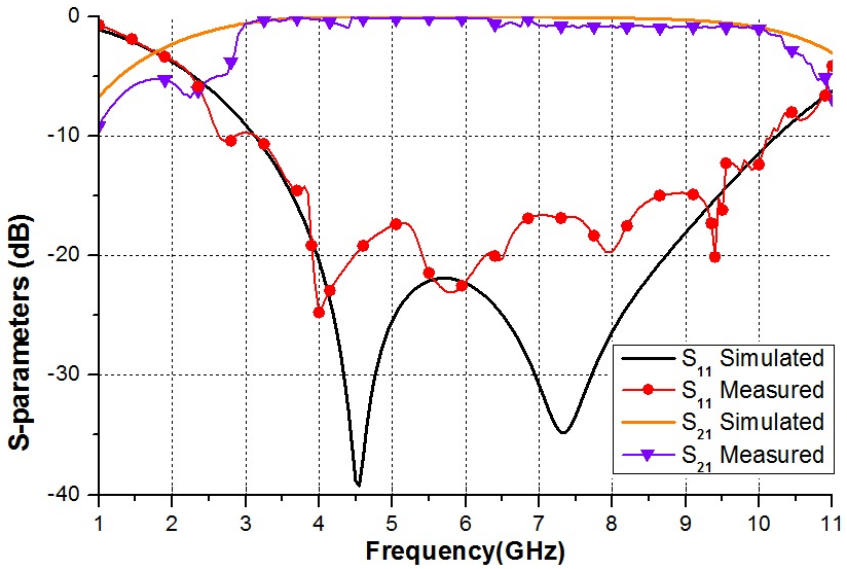

Figure 3.6: Simulated and measured S parameters of the designed phase shifter

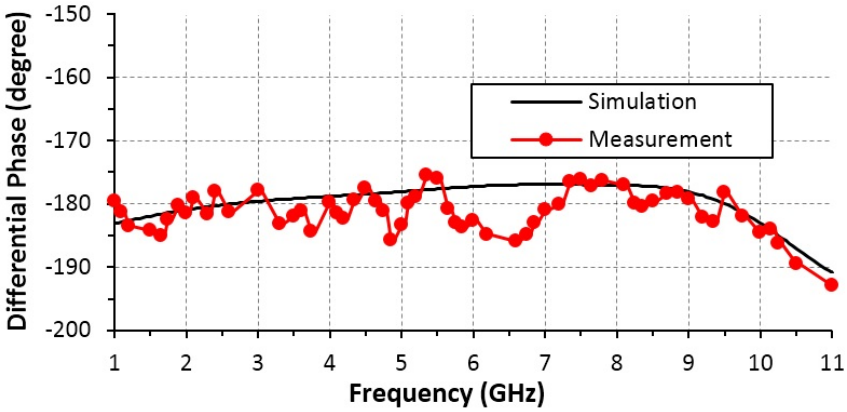

Figure 3.7: Simulated and measured output differential phase shift

Therefore, to get frequency independent 180° phase shifter as explained in the theoretical formulation, we need to guarantee the following three basic conditions: perfect matched ports (50 Ohm), pure short-circuited ports in the main line, and identical main and reference lines. All these previous requirements must be valid at any frequency, which is not easily achievable. We not that the bandwidth achieved by our design meets most of practical applications requirement, as it extends from 3 to 10.2 GHz.

3.2.3 Summary of the first achievement

An UWB phase shifter is presented. The main idea revealed in this work consists of comparing two identical structures with short-circuited ports in the main line. This method provides frequency independent 180° phase shifter. The design is a multilayer structure which uses slot-coupled transitions leading to the UWB characteristics. Theoretical formulations explaining the frequency independence behavior are presented as well.

The proposed approach is validated after comparing the simulated and measured results. Measurements reveal that the proposed design achieves a compact 180° phase shifter with better than 6° phase stability, less than 1dB insertion loss, and better than 10 dB return loss within the band 3-10.2 GHz.

Compactness, multilayer structure and stable output phase shift across an UWB allow the proposed device to be a suitable candidate in several modern applications. For instance, multilayer integrated circuits.

3.3 Novel Flowchart Design of Frequency Independent 180° Phase Shifters

This second contribution describes the design guidelines for frequency independent 180° phase shifters. The proposed configuration is based on microstrip slot transition technique. The frequency independence feature is due to comparing two quasi-identical structures and the phase inversion (180°) is related to the chosen inverted orientation of the main line compared to the reference one. The design is very simple, free from via-holes, frequency independent and highly stable.

3.3.1 Design and analysis

A) *Phase shifter architecture*

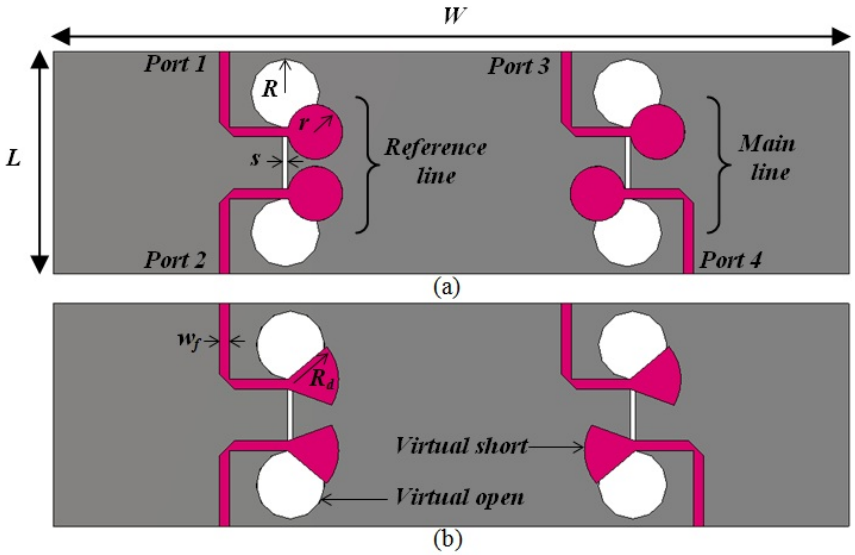

Figure 3.8: Schematic design of the proposed phase shifters (a) Circular terminated configuration (b) Radial terminated configuration

The schematic design of the proposed phase shifter is depicted in Figure 3.8. It is a

fully planar device in which the main and reference lines are microstrip slot transition based technique [35]. The reference line is a direct transition; it consists of two parallel microstrip lines coupled through the dumbbell slots etched on the ground plane. The main line however, is an inverted transition; it is identical to the reference line with inverted orientation of the coupled microstrip lines. For good power transmission, the microstrip and slotline sections have to be ended with suitable reactive loads, hence they are virtually short and open circuits terminated (Figure 3.8). Circular, radial, and rectangular/uniform line or multi-arm lines (stubs) are common used configurations for such terminations [35], [111].

B) ***Principle of operation***

The input signals are guided to the output ports through the narrow slot in the common ground plane. Beside the phase shift introduced by the physical length of the direct/inverted microstrip slot transition, additional 180° is inserted in the signal main path due to the chosen orientation of the inverted transition (back-to-back connection) which allows E-field lines propagate regularly in opposite direction as depicted in Figure 3.9.

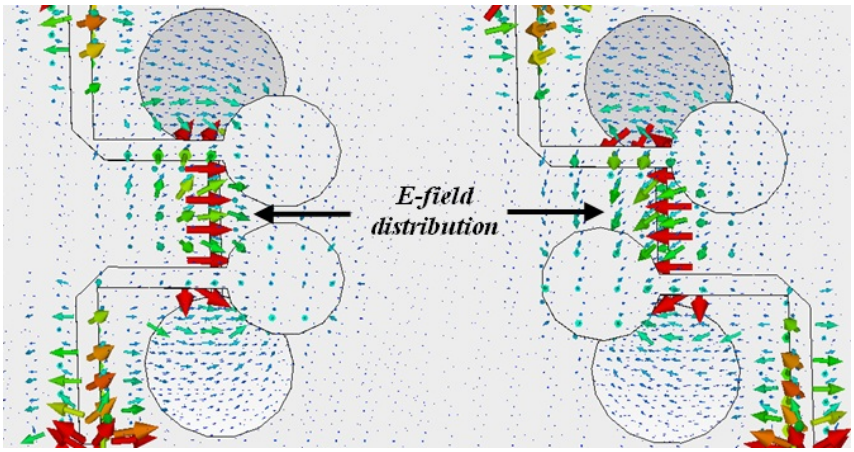

Figure 3.9: Simulated E-field distribution in the direct/inverted microstrip-slot transition

Moreover, the mechanism of E-field inversion in the main line is detailed as follows: referring to Figure 3.10 and considering E-field distribution associated with the coupled transition; the input E-field (near the transition) which is in the –y direction leads to a slotline wave with E-field in the x direction. In the second side (output), the x-directed E provides an output microstrip E-field lying in +y direction. Thus, the E-field is inverted from –y to +y, which amounts to 180° inserted phase [112]. Hence a simple comparison between the main and reference lines cancels the intro-

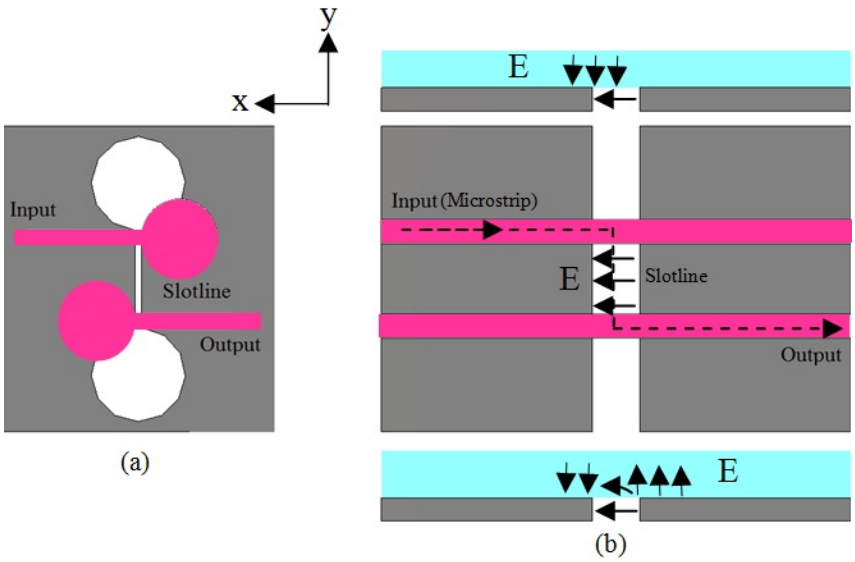

Figure 3.10: Mechanism of the E-field inversion (a) Inverted transition view (b) E-field evolution in the slotline [112]

duced common phase shift (due to line length transitions) and only 180° is left as output differential phase which is frequency independent. This can be formulated mathematically as follows:

$$\Delta\varphi = Phase(S_{43}) - Phase(S_{21}) \tag{3.10}$$

$$Phase(S_{43}) = Phase(S_{21}) + 180^{\circ} \tag{3.11}$$

Where S_{ij} indicates the scattering parameters of the four port device and $Phase(S_{43}) - Phase(S_{21})$ denotes the phase difference between the main line (port 3 and port 4) and the reference line (port 1 and port 2). Thus from (3.10), and (3.11) we find:

$$\Delta\varphi = 180^{\circ} \tag{3.12}$$

3.3.2 Results and discussion

To validate the proposed approach, two prototypes were manufactured. One of them is microstrip circular terminated and the other is radial ended (Figure 3.8). The designs follow the guidelines reported in [35], [112], and the final dimensions given in Table 3.1 are optimized using CST Microwave Studio as a simulation tool. Input/output ports are connected through 50 Ohm microstrip lines of width w_f calculated using standard formulas as in [110]. Rogers *RT6010 (thickness =0.64 mm,* $\varepsilon_r = 10.2$*, and tangent loss=0.0023)* is used as substrate and a photograph of the final prototypes is shown in Figure 3.11. The

Table 3.1: Proposed phase shifter parameters

Parameters	Signification	Value (mm)
R	Dumbbell slot radius	2
r	Circular short-circuit radius	1.6
R_d	Radial short-circuit radius	2.97
s	Dumbbell slot width	0.3
w_f	50 Ohm feeding line width	0.58
W	Width of the device	46.5
L	Length of the device	13

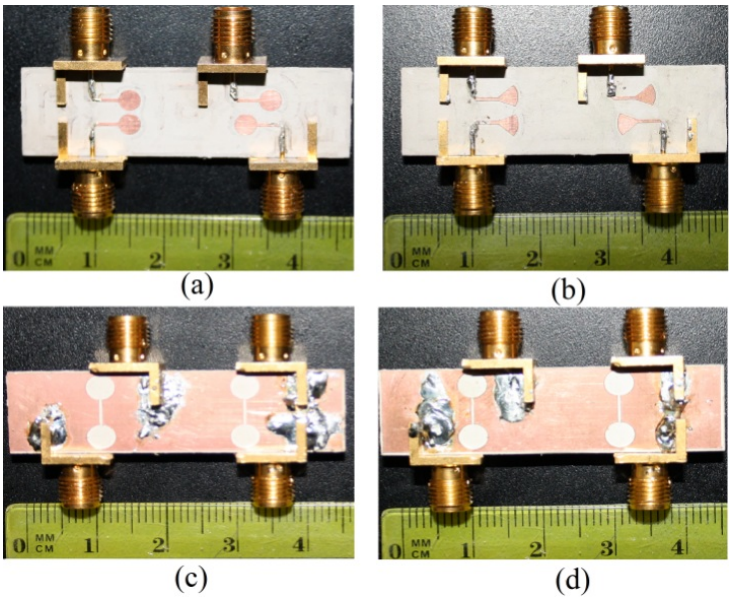

Figure 3.11: Manufactured prototypes (a) Top view (circular terminated) (b) Top view (radial terminated) (c) Bottom view (circular terminated) (d) Bottom view (radial terminated)

total size of $46.5 \times 13 \times 0.64mm^3$ reveals compactness of the proposed device.

Figure 3.12 depicts the amplitude characteristics of the proposed phase shifters. In the two varieties, it is observed that return losses are not less than 10 dB in both simulations and measurements within the band 2 GHz to more than 12 GHz. The insertion losses, however vary from 0.36 dB to 2 dB in simulation and from 0.5 dB to 2.1 dB in measurements. Hence, small discrepancies between simulations and measurements are revealed. Manufacturing tolerances and alignment mismatching are some main reasons of those disagreement. Moreover, residual radiations are directly involved in the insertion losses increase which can be minimized by introducing a conducting enclosure [29].

Figure 3.13 exposes the simulated and measured output phase shift of the two manufactured devices. Simulations reveal 180° ± 3° differential phase shifts and measured ones oscillate smoothly around 180° with less than ±3.6° phase deviation for both prototypes over the band 2 GHz to more than 12 GHz. Thus, observed results are very close and highly stable.

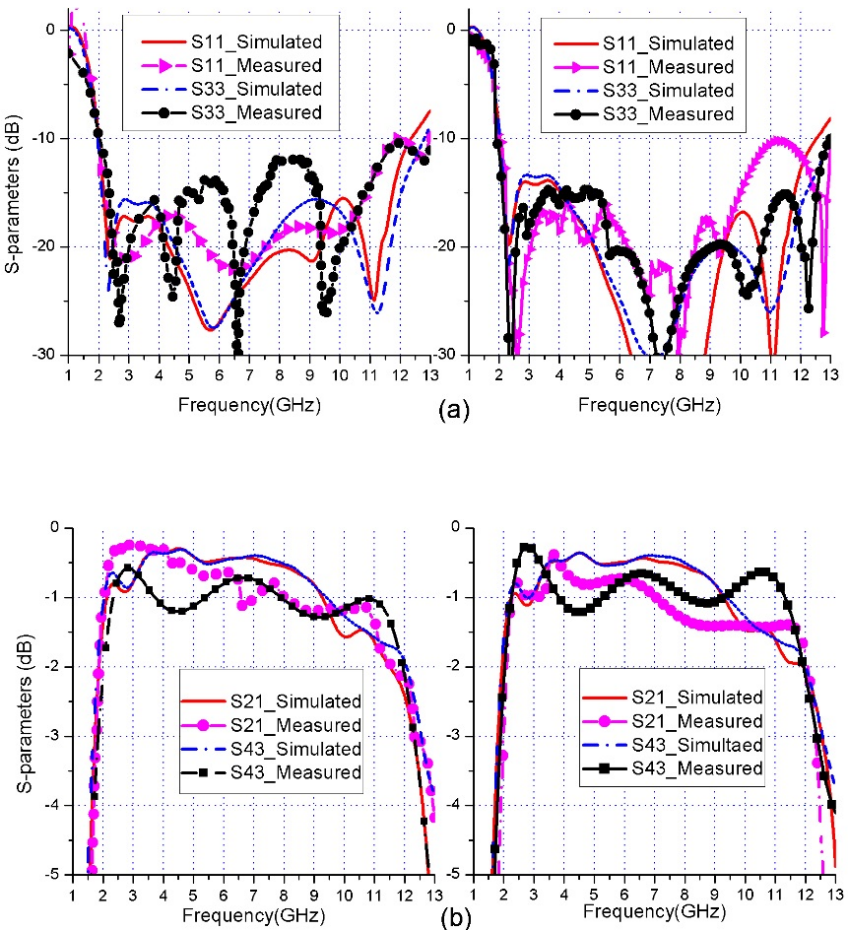

Figure 3.12: Simulated and measured S-parameters of the circular (left) and radial (right) phase shifters (a) Reflection coefficient (b) Transmission coefficient

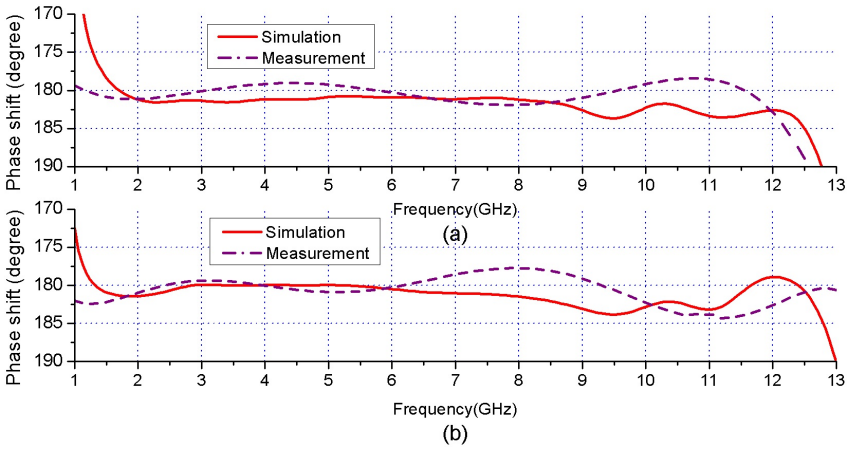

Figure 3.13: Simulated and measured differential phase shift (a) Phase shift of circular configuration (b) Phase shift of radial configuration

Besides the good obtained performances, and in order to get the frequency independent behavior (as expected in theory), we need to guarantee two basic conditions: pure matched ports (50 Ohm) and perfect inversion of the main line compared to the reference one. These requirements must be satisfied at any frequency, which is not easily reachable.

We note that the obtained bandwidth extending from 2 GHz to more than 12 GHz is

widely satisfactory as it exceeds the UWB (3.1-10.6 GHz) and meets most of practical applications.

A comparison between the proposed design and some recent phase shifters is shown in Table 3.2 (λ_g refers to the guided wavelength evaluated in the central frequency of the operating bandwidth). Our design demonstrates some advantages as the widest operating band, simplicity and stability with low phase deviation.

Table 3.2: Comparative study between some recent phase shifters

Reference	**Phase(°)**	**Phase drift(°)**	**Bandwidth (%)**	**Insertion loss(dB)**	**Size (λ_g)**
[27]	$45 \sim 180$	± 8	100	≤ 0.6	0.5×0.3
[26]	90	± 9	114	≤ 1.2	0.81×0.54
[30]	90	± 4	80	≤ 2.3	0.75×0.15
This work	**180**	**$\pm$3.6**	**144**	**$\leq$2.1**	**0.89x0.53**

3.3.3 Summary of the second achievement

This work is a flowchart for designing highly stable 180° phase shifters in a simple manner. The proposed methodology is based on comparing two direct and inverted microstrip slot-transitions considered as reference and main lines respectively. Two configurations were manufactured and tested. The obtained results demonstrate very high performances as they provide 180° differential phase with less than ±3.6° phase deviation, more than 10 dB return loss and less than 2.1 dB insertion loss in the frequency band extending from 2 GHz to more than 12 GHz which widely exceeds the UWB (3.1 GHz-10.6 GHz). In addition to the achieved good performances, the device is planar, compact and features low cost. Moreover, the proposed design is frequency and substrate independent which allow the device to be very attractive to many and diverse modern applications, such as multilayer integrated circuits and laminated multichip modules.

3.4 Compact 45° Phase Shifter Based on Coupled Tapered Transition for UWB Applications

In this section, an UWB phase shifter is proposed, it exploits the double microstrip-slot transition technique. In addition, wide band transition feature is achieved by using a new proposed shape which is a tapered stripline since these tapered shapes are well known to be UWB. The designed phase shifter is a multilayer structure composed of a reference

line (simple transmission line) and a main line (double tapered microstrip-slot transition). The device provides 45° stable output phase shift across a wide bandwidth.

3.4.1 Proposed structure and analysis

The schematic design of the proposed structure is shown in Figure 3.14. It consists of two layers (top and bottom) and a common ground plane in between. The reference line (transmission line) is etched on the top layer and the main line (double microstrip-slot transition) is a coupled section realized by inserting a rectangular slot in the common ground plane of the two layers. The tapered shapes are designed using the following formulas (3.13)[113]:

$$\begin{aligned} y &= C_1 e^{rx} + C_2 \\ C_1 &= \frac{x_2 - x_1}{e^{ry_2} - e^{ry_1}} \\ C_2 &= \frac{x_1 e^{ry_2} - x_2 e^{ry_1}}{e^{ry_2} - e^{ry_1}} \end{aligned} \tag{3.13}$$

Where r is the flare opening rate and (x_i, y_i) are start and end points of the flare in (x, y, z) system coordinates (Figure 3.14 (d)).

To ensure a good transition coupling, a careful study of the flare opening rate r is carried out. Optimization of the design is performed by CST Microwave Studio used as a simulation tool. Input/output ports are connected through 50 Ohm microstrip lines obtained using formulas presented in [110].

The final selected dimensions (Figure 3.14) are: *W=40 mm, L= 20 mm, W_f=1.3 mm, W_t=3.7 mm, W_s=6.5 mm, L_s=7.7 mm, the length of the reference line l_{ref} =29.1 mm and r=0.8.*

The output phase shift is the difference between the reference line and the main line phases:

$$\Delta\varphi = \varphi_{main} - \varphi_{ref} \tag{3.14}$$

Signal transmission between ports 1 and 2 through the coupled transition is evaluated using S_{21} parameter given by the following formula [33]:

$$S_{21} = \frac{2jK(\sqrt{1-K^2})sin(\beta_e l)}{[(\sqrt{1-K^2})cos(\beta_e l) + jsin(\beta_e l)]^2} \tag{3.15}$$

Hence, the phase shift of the output signal compared to the input signal can be calculated

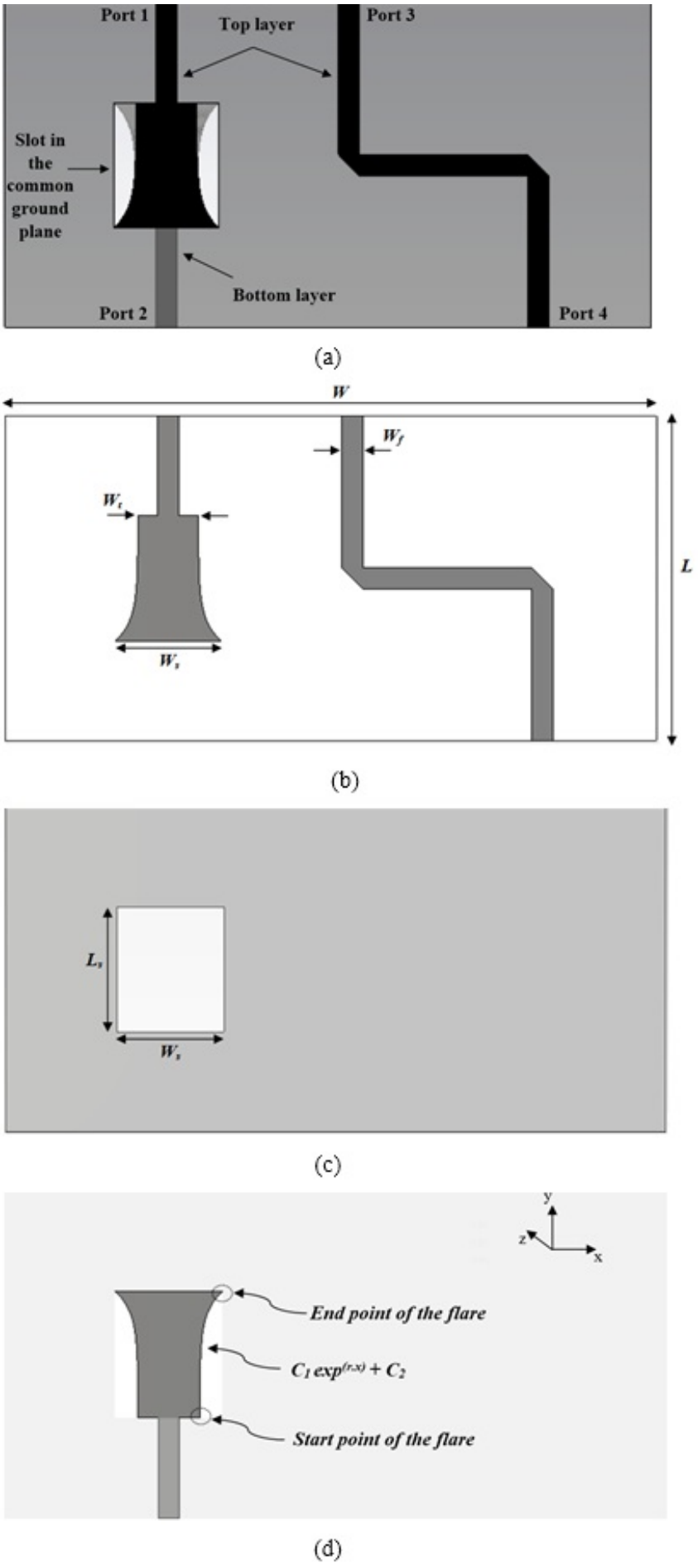

Figure 3.14: Schematic design of the proposed phase shifter (a) Front view of the whole structure (b) Top layer (c) Common ground plane (Middle layer) (d) Bottom layer

from (3.15) as follows:

$$\varphi_{main} = 90^\circ - 2arctang\left\{\frac{sin(\beta_e l)}{(\sqrt{1-K^2})cos(\beta_e l)}\right\} \tag{3.16}$$

Where K is the coupling factor between the top and bottom patches, l is the physical length of the coupled structure and β_e is the effective phase constant in the medium of the coupled structure.

A 50 Ohm microstrip line is assumed as a reference line. The phase shift inserted by a section of microstrip line of physical length l_{ref} is:

$$\begin{aligned} \varphi_{ref} &= -\beta_{ref} l_{ref} \\ &= -360^\circ \frac{\sqrt{\varepsilon_{ref}}}{\lambda} l_{ref} \end{aligned} \tag{3.17}$$

Where λ, ε_{ref} and β_{ref} are the wavelength, effective dielectric constant and phase constant of the microstrip transmission line, respectively.

The differential phase shift $\Delta\varphi$ from (3.15), (3.16) and (3.17) is:

$$\Delta\varphi = 90^\circ - 2arctang\left\{\frac{sin(\beta_e l)}{(\sqrt{1-K^2})cos(\beta_e l)}\right\} + \beta_{ref} l_{ref} \tag{3.18}$$

3.4.2 Results and discussion

The proposed phase shifter is designed and fabricated on Rogers *RT5880* substrate of thickness $h = 0.51mm$, $\varepsilon_r = 2.2$ and *loss tangent* $= 0.0027$. Figure 3.15 depicts the manufactured prototype. Measurements are carried out by a four port Network Analyzer. The simulated and measured amplitude characteristics of the device are presented in Figure 3.16. It is observed that simulations and measurements are in good agreement, return loss (Figure 3.16 (a)) is more than 10 dB and insertion loss (Figure 3.16 (b)) is

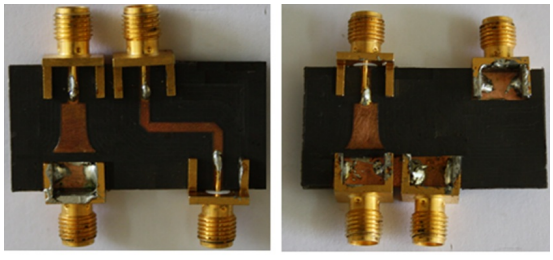

Figure 3.15: Manufactured prototype (a) Top view (b) Bottom view

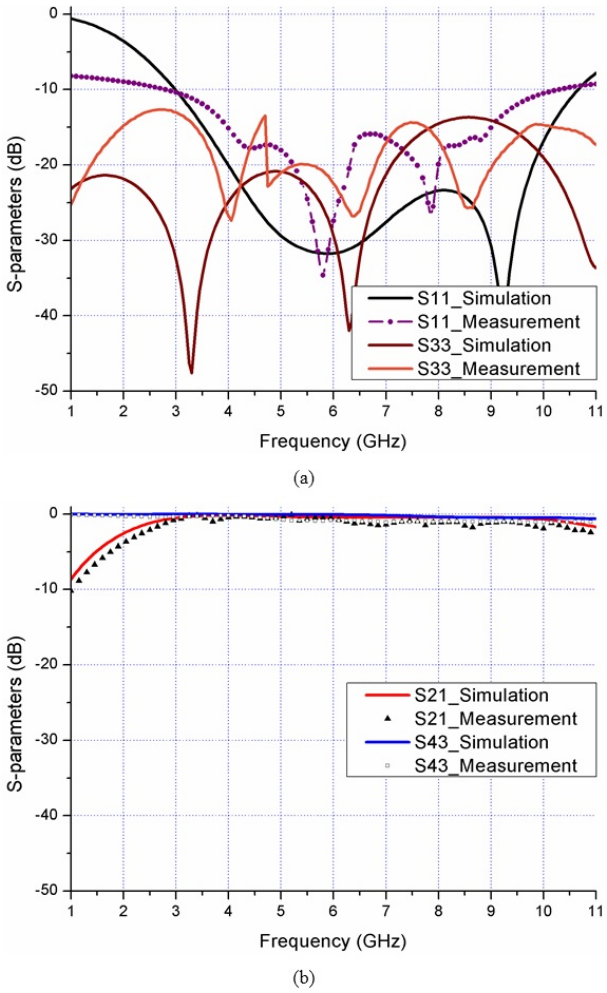

Figure 3.16: Simulated and measured S parameters of the designed phase shifter (a) Reflexion coefficient (b) Transmission coefficient

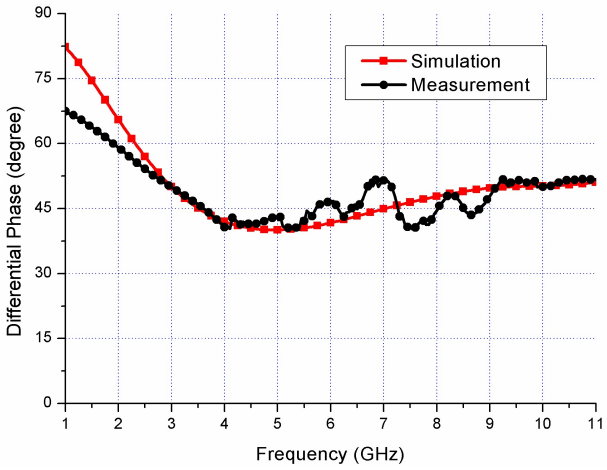

Figure 3.17: Simulated and measured differential output phase shift

better than 1 dB for both simulations and measurements in the frequency band 3-10.6 GHz.

The simulated and measured output differential phase shift is reported in Figure 3.17. By observing this result, we can conclude that simulation and measurement are very close

and provide a quasi-stable phase shift of 45°±5° in the frequency band extending from 3 GHz to more than 11 GHz.

Despite the observed good agreement, it is worthwhile to point out that some discrepancies between simulations and measurements are noticed. This disagreement is basically due to some common factors: fabrication process tolerance, difficulty related to the superposition of top and bottom layers and material characteristics dependent on frequency, notably in the upper band.

3.4.3 Summary of the third achievement

An UWB phase shifter is presented in this section. By exploiting the principle feature of tapered shapes, a new UWB coupled transition is designed and integrated to provide a stable phase shifter. The proposed device is compact and efficient since it allows quasi-stable output phase shift of 45° with low ripples (less than 5°), return loss of more than 10 dB and less than 1 dB insertion loss across the frequency band 3-10.6 GHz.

Beside its good performances, the component is cheap and easily manufacturable. Moreover, the multilayer characteristic allows the device to be attractive to many and diverse modern applications as: integrated circuits, butler matrix, beamforming networks, laminated multichip modules (MCMs-L) and many others.

3.5 Conclusion

This chapter was devoted to microwave phase shifters. Due to their importance in several applications, a deep study was conducted in order to understand and contribute to this interesting field of research. Consequently, we proposed two novel designs providing frequency independent 180° stable output phase shift. The developed designs are published in Microwave and Optical Technology Letters (MOTL) Journal. The third contribution concerns a phase shifter providing 45° phase shift with low insertion loss and relatively simple architecture. The work is published in The 5^{th} International Conference on Electrical Engineering-Boumerdes (ICEE 2017, IEEE indexed).

We believe that the proposed configurations lead to enhance the design of such components and contribute to improve several applications notably in phased arrays challenges.

Chapter 4

Chapter 4

Decoupling Mechanism for Strongly Coupled Antenna Arrays

4.1 Introduction

Miniaturization of systems is still one of the most challenging issues notably in recent wireless devices (e.g., smartphones). Reaching compactness is being a common point of interest for researchers and industrials as well. Multiple-input-multiple-output (MIMO) systems which promise high channel-capacity are extremely concerned with miniaturization in current and future technologies, for instance long term evolution (LTE) standard, 5G and beyond [114]–[116]. However, integrating a couple of closely spaced antennas (less than half wavelength spacing) in a compact device provides high mutual coupling and leads to a drastic performance degradation of MIMO systems: high information correlation, low data rate, and decrease of radiation efficiency due to the power loss in the coupled antenna ports [117]–[120].

To tackle this challenge, tremendous efforts were devoted to mitigate the antenna coupling issue, hence various decoupling techniques were developed over the past decade [121]–[134]. Most of the proposed methods succeeded in the port isolation improvement at the expense of adding extra-elements which yield to bulky circuits, increase of power losses and impairment of radiation efficiency [135]. In [56] a suspended line linking two inverted F antennas (PIFAs) is used to neutralize the electromagnetic coupling between the elements. The same approach is applied to a monopole array [58], however, the technique is still based on tuning process due to the lack of straight design procedure. Forbidding surface wave propagation is the main feature of electromagnetic band gap (EBG) structures which are exploited to come up with another method for enhancing the port

isolation of nearby antennas [136], [137], nevertheless more occupied area is needed to apply this method in practical applications. Authors in [138] and [139] demonstrate another decoupling configuration based on defected ground structure (DGS) to tackle the isolation matter of two single-frequency elements (monopoles and patches) and two dual-frequency patches respectively. Impedance transformation through connecting transmission lines is also developed and analytical formulas for decoupling two nearby antennas are reported in [64]. The isolation is achieved by a reactive shunt component which cancels the coupling signal between elements. The idea is also extended to three element antenna arrays in [140].

Further, different networks are extensively used to achieve high isolation purpose [65], [141]–[149]. Among the above, the decoupling and matching networks (DMNs) designed as lumped-element circuits and even-odd mode analysis is exploited to prove the feasibility of the technique [141], [142]. Moreover, closed form equations are derived and presented. The aforementioned idea is an extension of the stub-loaded reactive decoupling network [65] in which the DMN is fully based on transmission lines (stubs) configuration. Although the good obtained isolation, the reactive elements require additional power consumption and lead to more power dissipation caused by their parasitic resistance which is not suitable for higher frequency applications as well [118]. Besides, the all-transmission line scheme provides large size and voluminous circuit.

Many other decoupling networks are presented in the literature. In [149], a dual band decoupling of two antennas is achieved. The topology is a combination of the reactive element decoupling method and the eigenmode feed network consisting of a dual-mode 180° hybrid coupler. In [150], a four element dipole array is decoupled by inserting a 3 dB 90° branch-line and rate-race 180° hybrid couplers. However, the practical application of these techniques is not easy, since it is contradictory with the most important purpose of the future systems still looking for more and more miniaturization with less complexity.

Most recently, a new decoupling concept is introduced [145]. Mutual coupling of two L-shaped antennas is canceled by reproducing an opposite coupling to the unwanted one (superposition of original coupling and designed one which is identical to the original mutual coupling with opposite phase). The above architecture consists of directional couplers, transmission line, and parallel resonant circuit. In [151], authors revealed, for the first time, an innovative decoupling concept called array-antenna decoupling surface

(ADS) applicable for large-scale array antennas. This method is based on controlling and canceling the undesirable coupled waves diffracted from a thin surface composed of a number of small patches located in front of the array. Despite the good obtained results, the method is still bulky and requires added volume and space. Therefore, its implementation in the future systems is not quite conceivable.

In this chapter, we investigate a new approach easily and simply applicable for port isolation improvement of two closely spaced and strongly coupled antennas. The developed mechanism is integrated to a monopole-array of two elements. Further, the feasibility of this novel architecture is demonstrated through practical application in which 50 Ohm antenna matching and high port isolation are achieved. In addition to its good performances, the proposed concept contributes significantly in the development of miniaturized devices since it does not require extra reactive components or transmission lines.

4.2 Description of the practical challenge

A general and basic architecture of wireless communicating devices with more than one radiator is the mutli-antenna system of two monopoles as depicted in Figure 4.1. This configuration is used as illustrative example in this work, to tackle the mutual coupling issue.

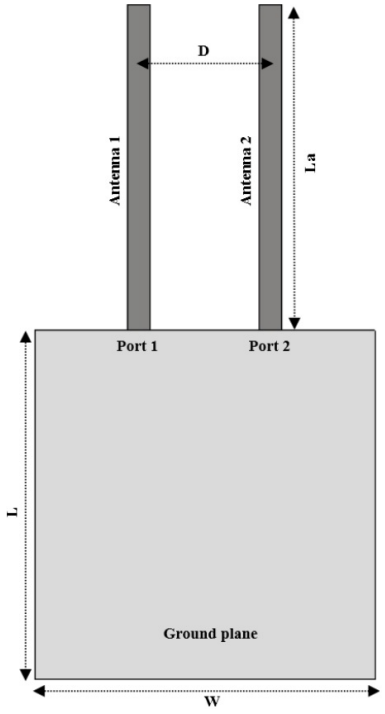

Figure 4.1: Configuration of the two closely spaced monopoles

The elements are identical and symmetrically printed on the top layer of a cheap FR-4 substrate *(thickness =1 mm,* $\varepsilon_r = 4.5$*, and tangent loss=0.02)* and closely spaced ($0.069\lambda_0$ center to center spacing), where λ_0 indicates the free space wavelength evaluated at the operating frequency of 2.45 GHz. The ground plane is located in the bottom layer of the substrate. Optimization of the design is carried out by using CST Microwave Studio as a simulation tool and the final dimensions of the two monopole array are listed in Table 4.1. Antennas are fed from 50 Ohm input ports behind the ground plane.

Table 4.1: Antenna array parameters

Symbol	Signification	Value (mm)
L_a	Length of the monopole	21
D	Center to center antenna spacing	8.5
W	Width of the ground plane	22
L	Length of the ground plane	22.5

Before integrating our decoupling mechanism, it is crucial to analyze the general behavior of the array. Figure 4.2 depicts the simulated and measured reflection coefficients (S_{11}, S_{22}) and the transmission coefficient (S_{21}) of the coupled antennas. Measurements were carried out at CDTA. It is noticed that the two monopoles are well matched (less than -18dB reflection coefficient) and strongly coupled (about -4 dB measured transmission coefficient) around the operating frequency of 2.45 GHz.

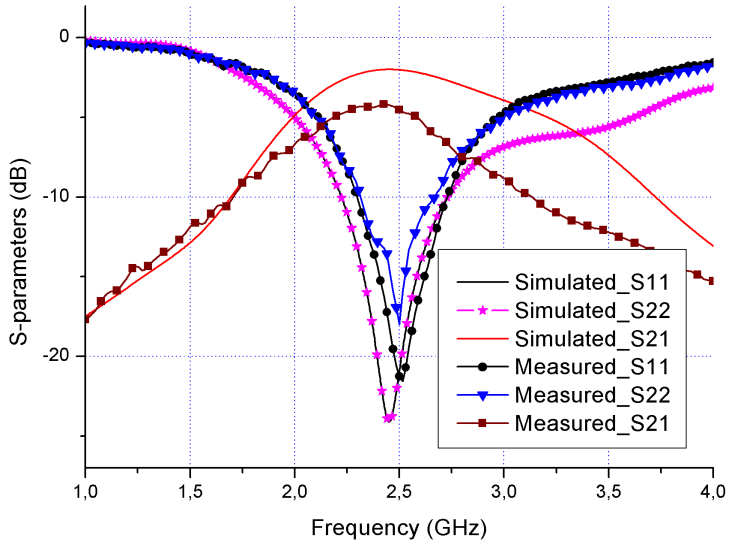

Figure 4.2: Simulated and measured S-parameters of the coupled antenna array

Further, current distribution at 2.45 GHz is shown in Figure 4.3 as well. It is found that a considerable amount of current is flowing between the two antenna ports. This rolling current favors extensively the creation of high mutual coupling between the radiators. From the above considerations, an important question naturally arises: how is possible

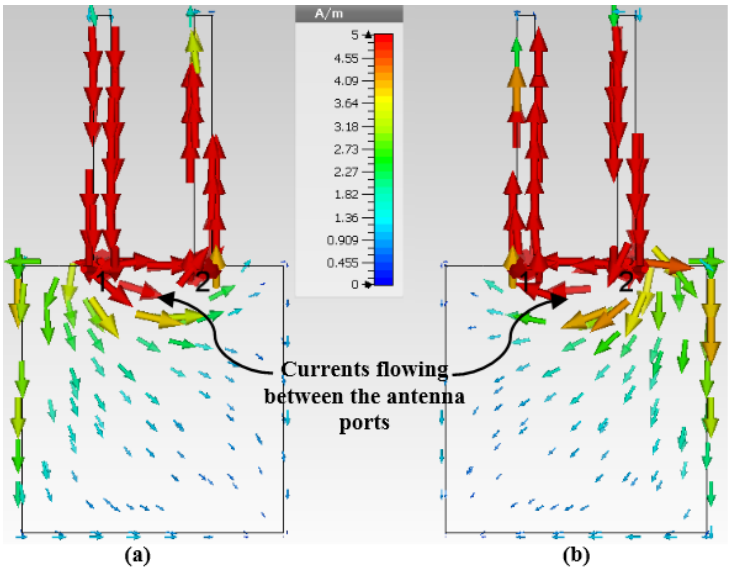

Figure 4.3: Current distribution of the two coupled monopoles at 2.45 GHz (a) port 1 excited (b) port 2 excited

to improve the port isolation between the nearby strongly coupled antennas in this kind of most used architectures, under constraints of keeping the compactness and avoiding complexity and bulk?

In the next section, we investigate, in details, the proposed decoupling concept as an answer to the raised question.

4.3 Decoupling concept

The proposed decoupling concept is based on expelling the flowing currents between the two antennas. To achieve this purpose, a tapered slot is etched on the ground plane of the array as seen in Figure 4.4. The tapered slot allows extracting currents and ejects them outside similarly to the VIVALDI antenna operation principle (traveling wave) [152], [153]. Consequently, ground-currents are forbidden from flowing transversally (from one antenna to the other), thus the currents follow the tapered slot in the longitudinal direction.

The design of those tapered slots is conducted by the exponential equations (3.13) presented in [113].

For good current extraction, a careful study of r (flare opening rate), R (radius of the circular slotline cavity), and s (position of the circular slotline in the ground plane) is required. The tapered slot design follows the guidelines reported in [113] and optimization is performed by CST Microwave Studio (Figure 4.8(b)). The final slot-parameters are depicted in Table 4.2.

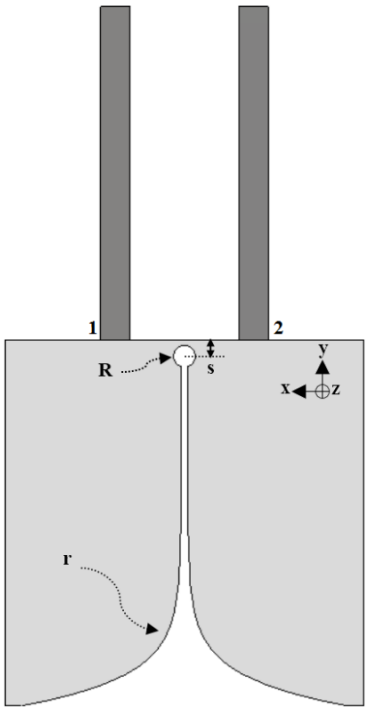

Figure 4.4: Tapered slot etched on the array ground plane

Table 4.2: Tapered slot parameters

Symbol	Signification	Value
R	Radius of the circular slotline cavity	0.7 mm
r	Flare opening rate	0.55
s	Circular slotline cavity position	1 mm

Beside the simplicity of the proposed mechanism, one can notice that the developed architecture is highly suitable to be integrated in compact devices where the allocated volume for antennas is strictly limited.

4.4 Results and discussion

The validation of the proposed decoupling mechanism is tackled in this current section. Further, practical study is conducted and compared to theory in order to find out adjustments if required.

The practical example mentioned above (monopole array of two elements) is prototyped and tested (Figure 4.5). We note that slotting the ground plane of the array provides a small shift in the center frequency, hence antenna impedance matching can be readjusted by a simple L-section network, with a series inductor of 3.74 nH and a shunt capacitor of 1.5 pF (Figure 4.5(a)). This matching network allows pulling back the matched frequency to 2.45 GHz as required.

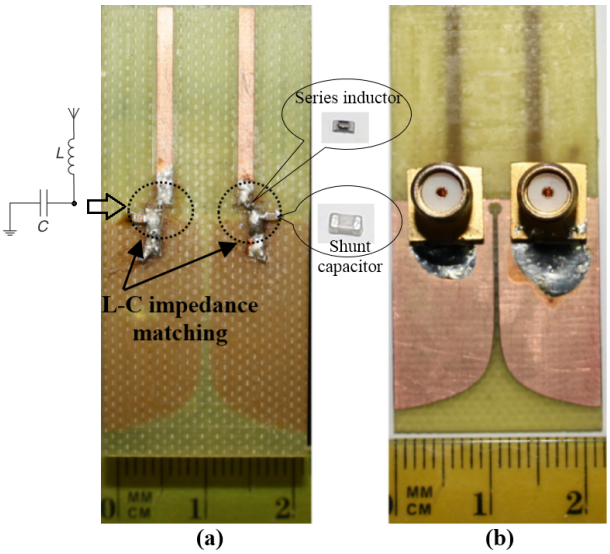

Figure 4.5: Photograph of the prototyped design (a) top view with L-C impedance matching (b) bottom view

4.4.1 S-parameters analysis

Figure 4.6 depicts the simulated and measured S-parameters of the decoupled antenna array (simulations are carried out by CST Microwave Studio).

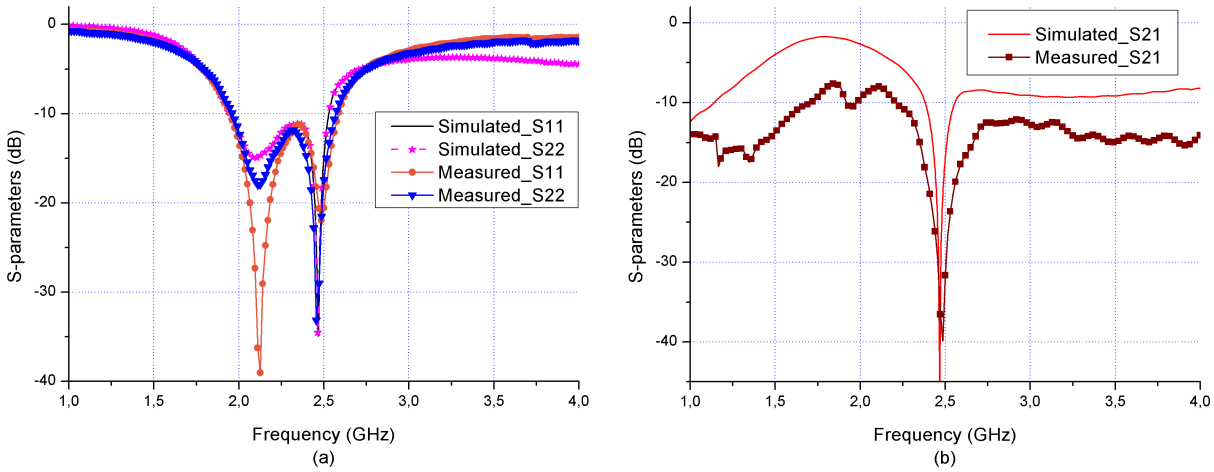

Figure 4.6: Simulated and measured S-parameters of the decoupled antenna array (a) reflection coefficients (b) transmission coefficients

From Figure 4.6(a), it can be observed that a good impedance matching for both monopoles is achieved at 2.45 GHz (less than -20 dB reflection coefficient). Simultaneously, high port isolation is noticed at the same operating frequency with measured peak of around 40 dB (Figure 4.6(b)). Hence, an isolation improvement of about 36 dB is achieved (difference between S_{21} of decoupled monopoles (Figure 4.6(b)) and S_{21} of coupled ones (Figure 4.2)). Furthermore, simulations and measurements agree quite well in matching-decoupling process with small discrepancies, mainly frequency shift, due to hand-manufacturing and

measurement setup tolerances.

In order to check and confirm the operation principle of our mechanism, current distribution of decoupled monopole array is simulated (at 2.45 GHz) and presented in Figure 4.7. After comparison between current distributions of coupled and decoupled arrays shown in Figure 4.3 and Figure 4.7, respectively, it is obvious that currents are effectively expelled and forbidden from transition between the two antennas as expected. Thus, decoupling concept is well validated.

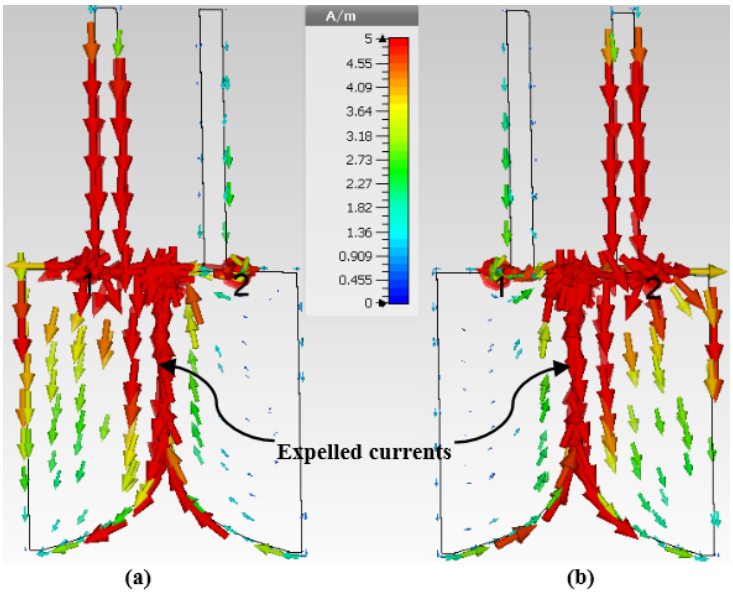

Figure 4.7: Current distribution of the decoupled monopoles at 2.45 GHz (a) port 1 excited (b) port 2 excited

4.4.2 Equivalent circuit analysis

The decoupling mechanism can be also enlightened on the base of equivalent circuits. Indeed, a parallel LC band stop behavior (S_{21} response) is quite close to the response of our proposed decoupling structure. Further, the similarities are demonstrated through comparative study conducted between the band stop filter and our structure. Figure 4.8 shows the behavior of both circuits after parametric study; tuning of r, R and s of our design and L tuning of the resonator (for 2.45 GHz operating frequency, $L = 10nH$, and $C = 0.422pF$, calculated using standard equation of filters). When analyzing the results (for example, tuning of r), the operating frequency of the design (S_{21} response) shifts to lower frequencies similarly when increasing L of the parallel resonator (Figure 4.8(a)). Hence, the proposed decoupling technique exhibits a band stop effect as the electrical circuit detailed above.

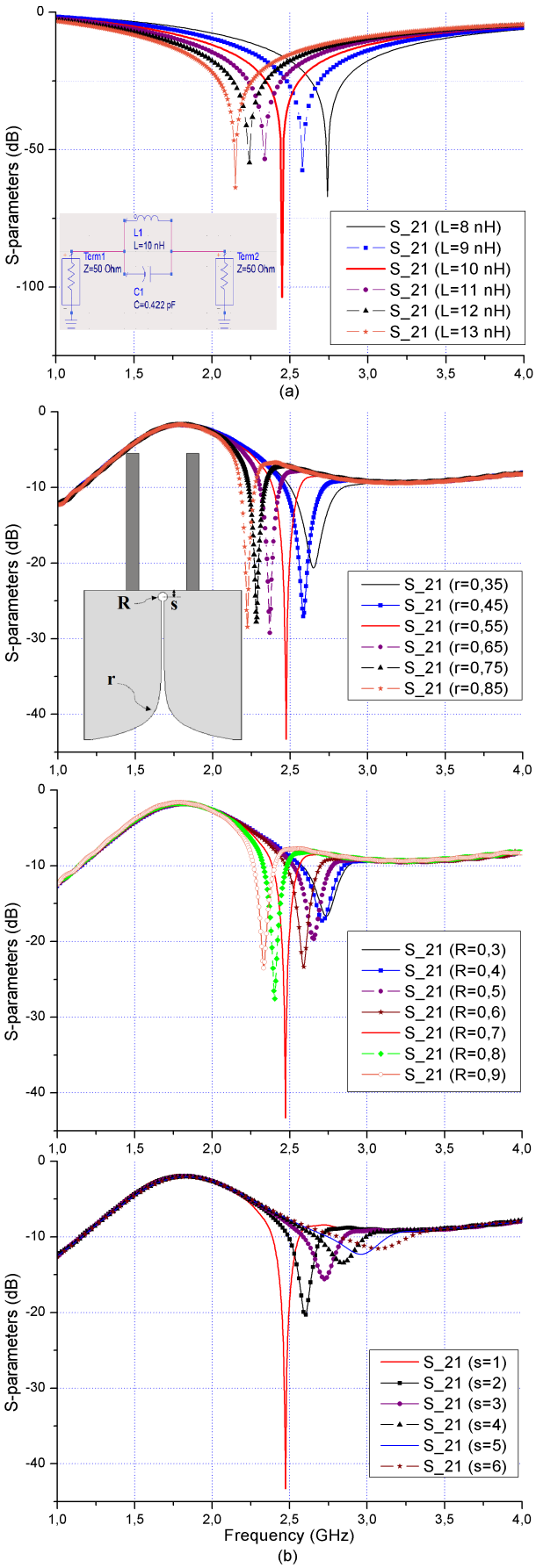

Figure 4.8: Parametric study (a) behavior of parallel LC band stop circuit with L tuning (b) behavior of the proposed design with r, R and s tuning

4.4.3 Radiation pattern analysis

The radiation patterns of both coupled and decoupled arrays are carefully investigated and evaluated by simulation and measurement at 2.45 GHz, as illustrated in Figure 4.9 and Figure 4.10 respectively, where the *2-D* figures are the simulated and measured normalized far-field radiation patterns.

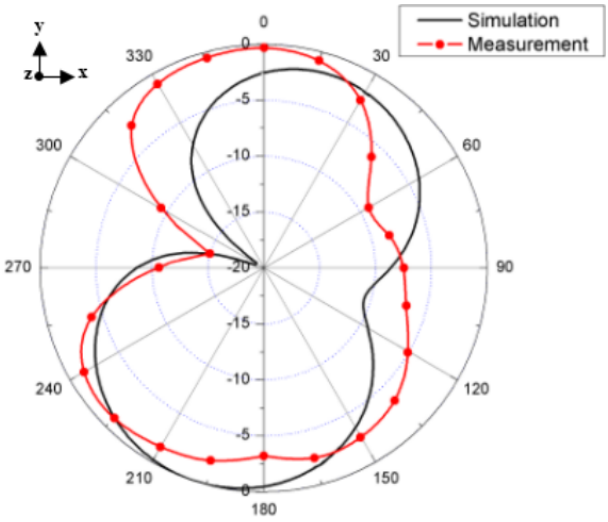

Figure 4.9: Simulated and measured 2-D radiation patterns of the coupled antenna array (one port is excited) at 2.45 GHz in xy-plane

Measurements are carried out in anechoic chamber of USTHB University (Figure 4.11) with alternate excitation of the antenna ports (i.e., as one port is excited the second one is 50 Ohm load terminated) (Figure 4.11(b)).

Before decoupling (Figure 4.9), it is seen that radiation pattern is similar to that of the traditional monopole with some deteriorations and tilt of the main beam owing to the coupling introduced by the closely spaced antennas. After decoupling (Figure 4.10), it is observed that radiation patterns are symmetrical with respect to the array-center plane (yz). Moreover, patterns become more directional and point either in $+x$ or $-x$ direction according to the excitation port. Hence, complementary diversity radiation is obtained, which is fairly suitable in MIMO applications to mitigate the multipath effects, this because the null of one antenna is covered by the radiation pattern of the second one. Further, acceptable agreement between simulations and measurements is noticed.

Moreover, it is to be highlighted that after decoupling, a significant improvement is obtained as the total efficiency of the monopole array jumps from 49.3% (before decoupling) to 81.7% as the decoupled mechanism is introduced and the peak gain of the decoupled array is 1.9 dBi.

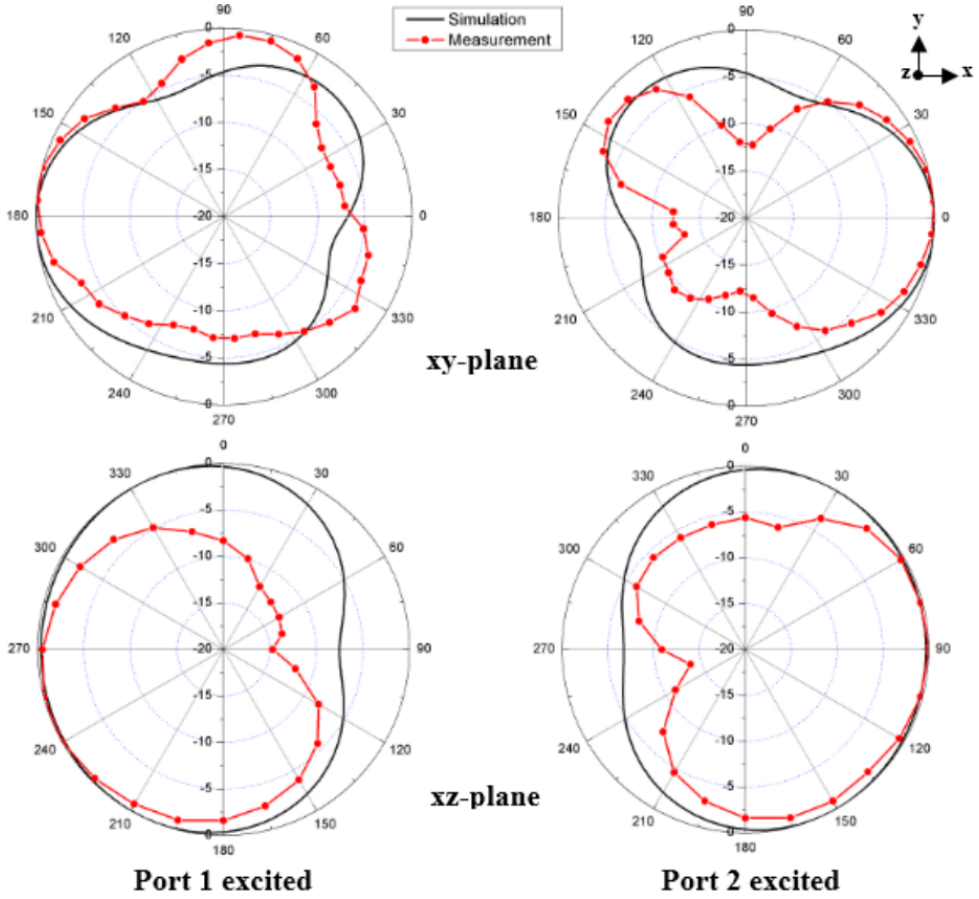

Figure 4.10: Simulated and measured radiation pattern of the decoupled antenna array at 2.45 GHz, in the xy-plane (top) and xz-plane (bottom)

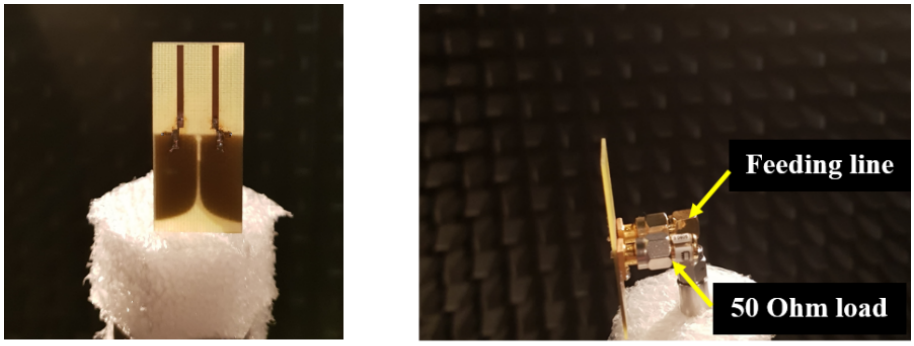

Figure 4.11: Setup of antenna pattern measurements (a) front view (b) side view

4.4.4 Envelope Correlation Coefficient (ECC)

Envelope Correlation Coefficient (ECC) is another key parameter for evaluating the diversity performance of MIMO systems, since the diversity cannot be effectively reached unless the radiation patterns are uncorrelated. An ECC of less than 0.5 can be a rule of thumb for MIMO antenna design [154].

Either S-parameters [44] or radiation patterns [155] can be used to derive this factor as reported in equations (1.3), and (1.4), respectively.

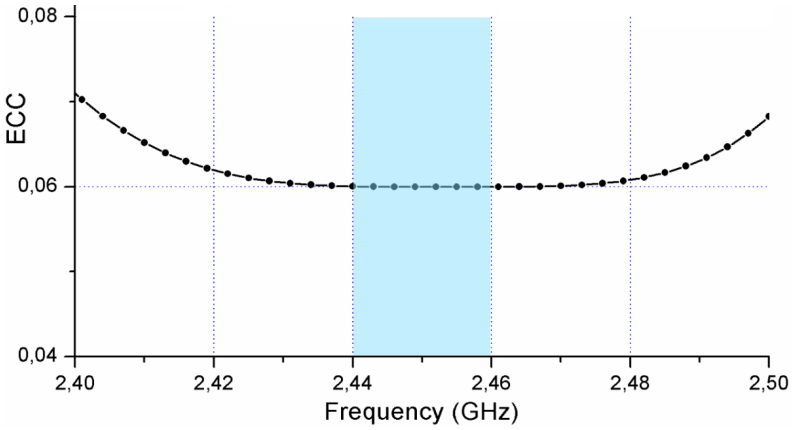

Figure 4.12: Envelope Correlation Coefficient (ECC) evaluated from S-parameters

The ECC of the decoupled monopole array is evaluated using S-parameters (Figure 4.12). It is noticed that the introduced decoupling approach reduces significantly the correlation of the monopole array since the ECC drops to the around of 0.06 at 2.45 GHz. This ECC decrease outcomes to higher channel capacity and demonstrates the good diversity performance of the array.

4.4.5 Comparative study

The advantages of the proposed approach are demonstrated through comparative study with recent works as detailed in Table 4.3.

Although good performances are obtained in considered references, however to the detriment of size (more antenna spacing) and adding external devices (transmission lines, metamaterial resonators and lumped reactive networks) which critically limit their applications, notably when the occupied area is considerable. Hence, one can notice the superiority of the proposed design on the other works since high isolation and low ECC are obtained by using a simple tunable design integrated easily and directly between extremely closed antennas ($0.069\lambda_0$ center to center antenna spacing) while keeping compact size of the scheme.

We note that the developed design exhibits low profile with miniaturized overall size of $0.18\lambda_0 \times 0.35\lambda_0 \times 0.008\lambda_0$. Further, our approach has also the added merit of low complexity with clear design guidelines.

Table 4.3: Comparative study

References	**[138]**	**[123]**	**[144]**	**[127]**	**Proposed**
Overall size (mm)	$25 \times 40 \times 32.5$	$50 \times 100 \times 0.8$	$80 \times 120 \times 0.8$	$50 \times 100 \times 1$	$\mathbf{22 \times 43.5 \times 1}$
Antenna spacing (λ_0)	0.093	0.18	0.11	0.32	**0.069**
Operating frequency (GHz)	2.53	2.64	0.74	2.42	**2.45**
Isolation (dB)	21.8	37.6	25	37	**40**
Isolation improvement (dB)	15.9	16	19	27	**36**
Max ECC	-	-	0.05	0.3	**0.06**
Approach	DGS	Metamaterial resonators+ T-shaped branch	Transmission line + LC network	DGS+ lumped R,L, C	**DGS (tapered slot)**

4.5 Evaluation of the proposed decoupling mechanism through array signal processing

In this section, the decoupling capability of the proposed antenna design is demonstrated through an array signal processing application. For this purpose, the decoupled monopole array is integrated in a two antenna receiver testbed (USRP RIO2942R of NI, available at CDTA) as seen in Figure 4.13. This system is practically evaluated by quantifying the mutual coupling matrix (MCM) through correlation measurement of transmitted and received signals at 2.45 GHz.

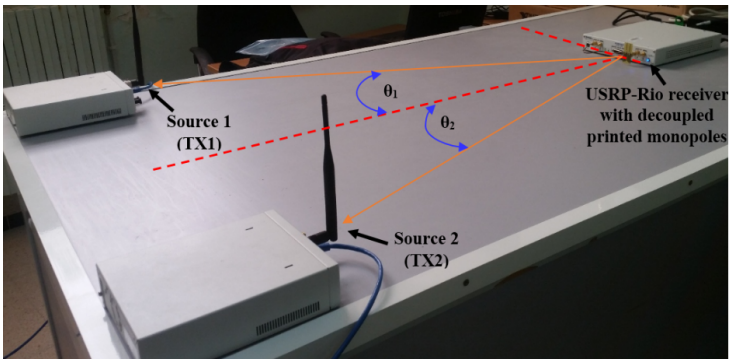

Figure 4.13: Testbed of two transmitters (located in known positions: θ_1 and θ_2) and USRP-RIO receiver with decoupled printed monopoles

Considering the direction of arrival (DOA) application in which the narrowband baseband model of signals is given by:

$$X(t) = A(\theta)S(t) + N(t) \tag{4.1}$$

Where $X(t)$ is the received signal vector, $S(t)$ is transmitted signals, $N(t)$ is an Additive White Gaussian Noise (AWGN) vector, and $A(\theta)$ is a matrix defining the impact of the receiving array (array response) on the incoming signal. Hence, the matrix $A(\theta)$ comprises the angles of arrival (source location).

The signal model given by (4.1) is an ideal model in which receiving antennas are considered perfectly decoupled. However, when considering the case of coupled array which often happens in practice, the matrix A can be written as follows:

$$A(\theta) = CD(\theta) \tag{4.2}$$

Where C is the MCM matrix, and $D(\theta)$ is the decoupled array matrix which defines the angle location of each source, hence columns of $D(\theta)$ are directly related to source angles as written in (4.3) and (4.4). If the antenna mutual coupling is negligible, then the matrix C is diagonal and indicates the gain and phase of the receiving array elements [156].

$$D(\theta) = \begin{pmatrix} 1 & 1 & \dots & 1 \\ e^{-i\varphi_1} & e^{-i\varphi_2} & \dots & e^{-i\varphi_p} \\ \vdots & \vdots & \dots & \vdots \\ e^{-i(M-1)\varphi_1} & e^{-i(M-1)\varphi_2} & \dots & e^{-i(M-1)\varphi_p} \end{pmatrix} \tag{4.3}$$

with:

$$\varphi_k = 2\pi\frac{d}{\lambda}sin(\theta_k) \tag{4.4}$$

Where, P and M are the number of sources and receivers, respectively. λ is the free space wavelength, d is the antenna spacing, and θ_k is the position (angle) of the k^{th} source.

We used a 2×2 MIMO testbed of two different sources (transmitters) located in known positions (angles θ_1, θ_2) and a receiving array with our decoupled monopoles (Figure 4.13). We note that, since source positions are known, $D(\theta)$ is then a well-defined 2×2 matrix and we tend to evaluate the MCM matrix C.

The correlation matrix is defined as:

$$R_{xs} = E[x(t)s(t)^H] \tag{4.5}$$

With $E(.)$ is the expectation operator and $(.)^H$ is the conjugate transpose.

Under suitable assumption (transmitted signals S and noise N are independent and uncorrelated), it can be demonstrated, from (4.1), (4.2) and (4.5), that:

$$C = R_{xs}R_{ss}^{-1}D^{-1} \tag{4.6}$$

Where R_{xs} is the correlation matrix of received and transmitted signals and R_{ss} is the covariance matrix of transmitted signal S.

The testbed depicted in Figure 4.13 allows measuring transmitted and received signals which are processed through computer codes developed with LABVIEW software. Then, covariance matrices can be estimated with the following equations:

$$\begin{aligned} \hat{R}_{xs} &= \frac{1}{n}\sum_{i=1}^{i=n} x_i s_i^* \\ \hat{R}_{ss} &= \frac{1}{n}\sum_{i=1}^{i=n} s_i s_i^* \end{aligned} \tag{4.7}$$

Where n refers to the number of samples and $(.)^*$ is the conjugate operator.

In order to get reliable and comparative results, first we used two standard decoupled monopoles (more than half wavelength spacing between monopoles) (Figure 4.14). In the second time, we integrated our decoupled monopoles in the same test-bed.

The evaluation of the decoupling mechanism can be achieved through comparing the off-diagonal entries and the diagonal ones of the MCM matrix (C). As explained before, a

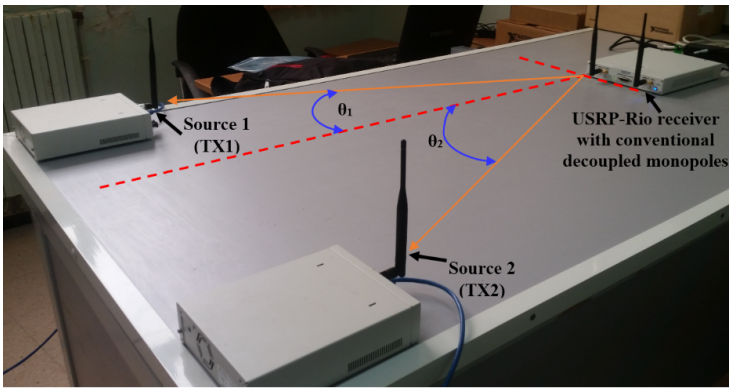

Figure 4.14: Testbed of two transmitters (located in known positions: θ_1 and θ_2) and USRP-RIO receiver with conventional decoupled monopoles

diagonal MCM means perfect decoupling array. Hence, a simple criterion of validation can be formulated as follows:

$$Criterion = \frac{\sum_{i \neq j} |c_{ij}^2|}{\sum_i |c_{ii}^2|} \tag{4.8}$$

Where C_{ij} are the entries of the MCM matrix.

Three decoupling criteria were evaluated for three different arrays: two conventional decoupled monopoles, two closely spaced printed monopoles without decoupling mechanism, and our proposed decoupled array. The obtained results are depicted in Table 4.4. It is worthwhile to point out that this criterion is a relative evaluation depending on the signal to noise ratio, test conditions, type of the array and other phenomenons which may arise, hence the procedure may provide only a hint in decoupling study.

Table 4.4: Isolation criterion of three different monopole arrays

Array	**Criterion (dB)**
Two printed monopoles without decoupling mechanism	-5.3
Conventional decoupled monopoles	-21.6
Proposed decoupled array	-17.9

From Table 4.4, it is noticed that the isolation criterion of our proposed array is close to that of the conventional decoupled monopoles. On the other hand, both criteria are much smaller than that of the printed monopoles without decoupling mechanism. The small value of the criterion means that off-diagonal entries of the MCM matrix are negligible compared to the diagonal ones, hence the MCM matrix can be considered quasi-diagonal and the antenna array is decoupled. Consequently, we can conclude on the effectiveness of the proposed decoupling technique which contributes significantly in MIMO performance enhancement notably in signal processing applications, for instance: direction of arrivals and source separation.

4.6 Conclusion

In this chapter, we propose a novel decoupling mechanism of closely spaced antennas. The concept is based on extracting coupled currents through a tapered slot. The principle of operation is validated through simulations and measurements applied to a monopole array of two strongly coupled elements, used as proof of concept. Hence a set of parameters confirm the effectiveness of the proposed method, for instance: an isolation of about 40 dB is achieved, a radiation pattern diversity is demonstrated as well, and the ECC drops

significantly to 0.06 which is highly suitable for MIMO applications. The decoupling method is further checked through signal measurement realized with a 2×2 MIMO system. The testbed comprises two transmitters and an USRP-RIO receiver which integrates the proposed decoupled array. Achieved results are consistent with aforementioned electromagnetic conclusions and the decoupling concept is effective.

In addition to the good obtained performances, the proposed technique is highly compact, simple and easily integrated into closely spaced antennas, since it does not require any extra-reactive components, no additional space, and no direct-contact between the antennas is needed as well. Moreover, the proposed decoupling concept may be extensible to large arrays of more than two elements, this hypothesis will be a subject of investigation in further works.

This decoupling mechanism is very motivating to diverse mutli-element communicating systems requiring miniaturization, such as MIMO and massive MIMO architectures, notably for current and future advances as the case of LTE standard, five generation (5G) technology and beyond.

The present contribution is published in IEEE Transactions on Antennas and Propagation (TAP) journal.

General Conclusion

"The brain imagination is an infinite set of darkrooms, more one lightens rooms more he is visionary in the life"

General Conclusion

During this research work, different aspects of wireless communications systems have been discussed. Modern challenges are then introduced and some solutions are proposed as well.

The thesis starts with SDR as important concept promising more radio flexibility and higher performances. However, achieving desired requirements needs to overcome several technical difficulties and challenges in system design, particularly antenna and some microwave devices.

Hence, antenna pattern reconfiguration is exposed. The topic is highly interesting in fading and interference combat since it allows steering the main beam of the radiator in desired directions. Further, proposed solution is discussed. Thus, simple pattern reconfiguration approach of an Ultra Wide Band monopole antenna is presented. By inserting a VIVALDI shape in the CPW ground plane, the pattern reconfiguration is achieved without changing the original size and form of the monopole. Only two switches were used, and the main beam is controlled depending on the state of these switches. Therefore, in the band of reconfiguration, the antenna radiates in three different directions (two directive states and one omnidirectional state). Switches were inserted in specific locations so that to eliminate currents to distribute and to radiate from that side, hence the main pattern is shifted in the other side. Obtained results confirm the effectiveness of the technique. The proposed approach can be applied to different CPW-Fed monopoles, consequently, it may be suitable for domains where dynamic pattern reconfiguration is needed such as tracking, cognitive radio, etc.

Muti-element systems (MIMOs) are also very promising architectures in the improvement of recent wireless systems. The use of antenna arrays is then highlighted and some technical drawbacks are discussed. Phased arrays are extensively needed in diverse applications such as beamforming, however the technique is based on phase shifted antenna

feeding. Phase shifters are then found to be crucial devices in such systems. Three different designs are proposed in this field. The first one concerns a frequency independent 180° planar phase shifter Based on UWB Coupled Sections. In order to obtain good performances, two basic considerations are derived from mathematical analysis. First, we consider the structure in which the main and reference lines are identical, then we consider the structure when two ports in the main line are short-circuited. By doing this, theoretical calculations provide frequency independent differential phase shift equal to 180°. Hence, the proposed design is mainly based on coupled sections which are realized by inserting slots into the common ground plane of the multilayer circuit. Two identical structures, leading to discard parameters depending on frequency, especially the coupling factor, which disturbs greatly the output phase, are introduced in the design. In order to get 180° phase difference shift, via holes are used to perform a short circuit in one of the two coupled sections. The second proposed configuration provides also a novel flowchart design of frequency independent 180° phase shifters. It is based on microstrip slot transition technique as well. The frequency independence feature is due to comparing two quasi-identical structures and the phase inversion (180°) is related to the chosen inverted orientation of the main line compared to the reference one. Another design based on coupled transitions is also proposed, it provides a compact 45° phase shifter. Further, interesting results are obtained.

MIMOs suffer also from element coupling phenomenon. This is a hot topic requiring efficient solutions to keep high performances. The coupling problem have been massively treated and lot of methods were developed in the literature. In the light of aforementioned challenge, a novel antenna decoupling approach is investigated. The introduced new concept is based on expelling the currents flowing between the closely spaced antennas through a tapered slot etched on the array ground plane. The proposed method is free from extra-reactive components and transmission lines. Further, there is no direct contact between the array elements. Although they are closely spaced and strongly coupled, the developed technique allows a high improvement in port isolation. Obtained results are very attractive and high decoupling is achieved with good impedance matching. Moreover, a radiation diversity is obtained. This pattern diversity is still an important purpose of multiple-input-multiple-output (MIMO) communications systems since it allows reducing the channel correlation and consequently, increases the communications data rate. In

addition to its efficient port isolation, the most attractive features of the proposed decoupling technique are simplicity and ease of implementation in diverse miniaturized and compact multi-antenna wireless devices.

As a future work, the proposed solutions may be upgraded. For instance, the pattern reconfiguration of monopoles can be improved using hybrid methods by adding reflectors to achieve higher directivity. The developed approaches of phase shifters can be exploited to achieve different output phase shifts independently from frequency or at least with UWB features. Finally, the decoupling mechanism may be extended to more than two radiators in order to provide significant contribution in massive MIMO topic.

Bibliography

[1] J. Du Preez and S. Sinha, *Millimeter-wave antennas: configurations and applications*. Springer, 2016.

[2] M. Dillinger, K. Madani, and N. Alonistioti, *Software defined radio: Architectures, systems and functions*. John Wiley & Sons, 2005.

[3] H. Sharetechnote. (2012). SDR Overview, [Online]. Available: `http://www.sharetechnote.com/html/SDR_Overview.html`.

[4] E. Buracchini, "The software radio concept," *IEEE Communications Magazine*, vol. 38, no. 9, pp. 138–143, 2000.

[5] T. W. Rondeau and C. W. Bostian, *Artificial intelligence in wireless communications*. Artech House, 2009.

[6] N. USRP, "2920," *NI USRP-2921, Universal Software Radio Peripherals, National Instruments*, 2017.

[7] N. Instrument. (2018). USRP software defined radio reconfigurable device, [Online]. Available: `http://www.ni.com/en-lb/shop/select/usrp-software-defined-radio-reconfigurable-device`.

[8] T. Aboufoul, C. Parini, X. Chen, and A. Alomainy, "Pattern-reconfigurable planar circular ultra-wideband monopole antenna," *IEEE Transactions on Antennas and Propagation*, vol. 61, no. 10, pp. 4973–4980, 2013.

[9] H. A. Majid, M. K. A. Rahim, M. R. Hamid, and M. F. Ismail, "Frequency and pattern reconfigurable slot antenna," *IEEE Trans. Antennas Propag.*, vol. 62, no. 10, pp. 5339–5343, 2014.

[10] X.-S. Yang, B.-Z. Wang, W. Wu, and S. Xiao, "Yagi patch antenna with dual-band and pattern reconfigurable characteristics," *IEEE Antennas and Wireless Propagation Letters*, vol. 6, pp. 168–171, 2007.

[11] Y.-Y. Bai, S Xiao, M.-C. Tang, C Liu, and B.-Z. Wang, "Pattern reconfigurable antenna with wide angle coverage," *Electronics letters*, vol. 47, no. 21, pp. 1163–1164, 2011.

[12] N. Gökalp and Ö. A. Civi, "Beam-steerable meanderline antenna using varactor diodes," *Microwave and Optical Technology Letters*, vol. 53, no. 1, pp. 200–204, 2011.

[13] M. T. Ali, M. R. Kamarudin, T. A. Rahman, R. Sauleau, and M. N. Md Tan, "Design of reconfigurable multiple elements microstrip rectangular linear array antenna," *Progress In Electromagnetics Research*, vol. 6, pp. 21–35, 2009.

[14] Y. Li, Z. Zhang, J. Zheng, Z. Feng, and M. F. Iskander, "Experimental analysis of a wide-band pattern diversity antenna with compact reconfigurable CPW-to-slotline transition feed," *IEEE Transactions on Antennas and Propagation*, vol. 59, no. 11, pp. 4222–4228, 2011.

[15] K.-P. Ma, Y. Qian, and T. Itoh, "Analysis and applications of a new CPW-slotline transition," *IEEE Transactions on Microwave theory and Techniques*, vol. 47, no. 4, pp. 426–432, 1999.

[16] Y. Huang and K. Boyle, *Antennas: from theory to practice*. John Wiley & Sons, 2008.

[17] A. Sabban, *Low-visibility antennas for communication systems*. CRC Press, 2015.

[18] P.-S. Kildal, *Foundations of antenna engineering: a unified approach for line-of-sight and multipath*. Artech House, 2015.

[19] amitec. (2018). Microstrip-patch-antenna-array, [Online]. Available: `https://amitec.co/microstrip-patch-antenna-array-22/`.

[20] A. B. Constantine *et al.*, *Antenna theory: analysis and design*. 2005.

[21] S. X. Ta, H. Choo, and I. Park, "Broadband printed-dipole antenna and its arrays for 5G applications," *IEEE Antennas and Wireless Propagation Letters*, vol. 16, pp. 2183–2186, 2017.

[22] J. L. Allen and B. Diamond, "Mutual coupling in array antennas," MASSACHUSETTS INST OF TECH LEXINGTON LINCOLN LAB, Tech. Rep., 1966.

[23] I. Nadeem and D.-Y. Choi, "Study on Mutual Coupling Reduction Technique for MIMO Antennas," *IEEE Access*, 2018.

[24] S. Xu, M. Zhang, H. Wen, and J. Wang, "Deep-subwavelength decoupling for mimo antennas in mobile handsets with singular medium," *Scientific reports*, vol. 7, no. 1, p. 12 162, 2017.

[25] S.-Y. Eom, "Broadband 180° bit phase shifter using a $\frac{\lambda}{2}$ coupled line and parallel $\frac{\lambda}{8}$ stubs," *IEEE Microwave and wireless components letters*, vol. 14, no. 5, pp. 228–230, 2004.

[26] S. H. Yeung, Z. Mei, T. K. Sarkar, and M. Salazar-Palma, "Design and testing of a single-layer microstrip ultrawideband 90° differential phase shifter," *IEEE Microwave and Wireless Components Letters*, vol. 23, no. 3, pp. 122–124, 2013.

[27] L Guo, H Zhu, and A Abbosh, "Wideband phase shifter with wide phase range using parallel coupled lines and l-shaped networks," *IEEE Microw. Wireless Compon. Lett*, vol. 26, no. 8, pp. 592–594, 2016.

[28] A. M. Abbosh, "Broadband fixed phase shifters," *IEEE microwave and wireless components letters*, vol. 21, no. 1, pp. 22–24, 2011.

[29] Y.-X. Guo, Z.-Y. Zhang, L. C. Ong, *et al.*, "Improved wide-band schiffman phase shifter," *IEEE Transactions on Microwave Theory and Techniques*, vol. 54, no. 3, pp. 1196–1200, 2006.

[30] M. Sorn, R. Lech, and J. Mazur, "Simulation and experiment of a compact wideband 90°differential phase shifter," *IEEE Transactions on Microwave Theory and Techniques*, vol. 60, no. 3, pp. 494–501, 2012.

[31] X. Y. Pu, S. Y. Zheng, J. Liu, Y. Li, and Y. Long, "Novel multi-way broadband differential phase shifter with uniform reference line using coupled line structure," *IEEE Microw. Wireless Compon. Lett.*, vol. 25, no. 3, pp. 166–168, 2015.

[32] A. M. Abbosh, "Broadband fixed phase shifter for c-band applications," *Microwave and Optical Technology Letters*, vol. 50, no. 2, pp. 396–399, 2008.

[33] A. M. Abbosh, "Ultra-wideband phase shifters," *IEEE Transactions on Microwave Theory and Techniques*, vol. 55, no. 9, pp. 1935–1941, 2007.

[34] Y. Wang, M. E. Bialkowski, and A. M. Abbosh, "Double Microstrip-Slot Transitions for Broadband ±90° Microstrip Phase Shifters," *IEEE Microwave and Wireless Components Letters*, vol. 22, no. 2, pp. 58–60, 2012.

[35] N. Seman and M. E. Bialkowski, "Microstrip-slot transition and its applications in multi-layer microwave circuits," in *Passive microwave components and antennas*, InTech, 2010.

[36] P. Sobis, J. Stake, and A. Emrich, "High/low-impedance transmission-line and coupled-line filter networks for differential phase shifters," *IET microwaves, antennas & propagation*, vol. 5, no. 4, pp. 386–392, 2011.

[37] I. Kulandhaisamy, D. B. Rajendran, M. Kanagasabai, B. Moorthy, J. V. George, and L. Lawrance, "Dual-frequency phase shifter deploying complementary split-ring resonator," *International Journal of Microwave and Wireless Technologies*, vol. 8, no. 7, pp. 1045–1050, 2016.

[38] B. Schiffman, "A new class of broad-band microwave 90-degree phase shifters," *IRE Transactions on Microwave Theory and Techniques*, vol. 6, no. 2, pp. 232–237, 1958.

[39] S. Y. Zheng, W. S. Chan, and K. F. Man, "Broadband phase shifter using loaded transmission line," *IEEE Microwave and Wireless Components Letters*, vol. 20, no. 9, pp. 498–500, 2010.

[40] S. H. Yeung, Q. Xue, and K. F. Man, "Broadband 90° differential phase shifter constructed using a pair of multisection radial line stubs," *IEEE Transactions on Microwave Theory and Techniques*, vol. 60, no. 9, pp. 2760–2767, 2012.

[41] J. Sajin, G Praveen, H. Habiba, and P. Rao, "Extremely compact phase delay line with CTSRR loaded transmission line," *Electronics Letters*, vol. 50, no. 3, pp. 190–192, 2014.

[42] Q. Liu, Y. Liu, J. Shen, S. Li, C. Yu, and Y. Lu, "Wideband single-layer 90° phase shifter using stepped impedance open stub and coupled-line with weak coupling," *IEEE Microwave and Wireless Components Letters*, vol. 24, no. 3, pp. 176–178, 2014.

[43] Z. Ying, C.-Y. Chiu, K. Zhao, S. Zhang, and S. He, "Antenna design for diversity and mimo application," *Handbook of Antenna Technologies*, pp. 1–43, 2014.

[44] S Blanch, J Romeu, and I Corbella, "Exact representation of antenna system diversity performance from input parameter description," *Electronics letters*, vol. 39, no. 9, pp. 705–707, 2003.

[45] R. Chandel and A. Gautam, "Compact mimo/diversity slot antenna for uwb applications with band-notched characteristic," *Electronics Letters*, vol. 52, no. 5, pp. 336–338, 2016.

[46] M. Manteghi and Y. Rahmat-Samii, "Multiport characteristics of a wide-band cavity backed annular patch antenna for multipolarization operations," *IEEE Transactions on Antennas and Propagation*, vol. 53, no. 1, pp. 466–474, 2005.

[47] X. Chen, S. Zhang, and Q. Li, "A Review of Mutual Coupling in MIMO Systems," *IEEE Access*, vol. 6, pp. 24 706–24 719, 2018.

[48] A. K. Arya, M. Kartikeyan, and A Patnaik, "Defected ground structure in the perspective of microstrip antennas: A review," *Frequenz*, vol. 64, no. 5-6, pp. 79–84, 2010.

[49] P. R. Prajapati, "Application of defected ground structure to suppress out-of-band harmonics for WLAN microstrip antenna," *International Journal of Microwave Science and Technology*, vol. 2015, 2015.

[50] K. Wei, J. Li, L. Wang, Z. Xing, and R. Xu, "S-shaped periodic defected ground structures to reduce microstrip antenna array mutual coupling," *Electronics Letters*, vol. 52, no. 15, pp. 1288–1290, 2016.

[51] R Anitha, V. Sarin, P Mohanan, and K Vasudevan, "Enhanced isolation with defected ground structure in MIMO antenna," *Electronics letters*, vol. 50, no. 24, pp. 1784–1786, 2014.

[52] C. R. Jetti and V. R. Nandanavanam, "Trident-shape strip loaded dual band-notched UWB MIMO antenna for portable device applications," *AEU-International Journal of Electronics and Communications*, vol. 83, pp. 11–21, 2018.

[53] J Bonache, I Gil, J Garcia-Garcia, and F Martin, "Complementary split rings resonators (CSRRs): Towards the miniaturization of microwave device design," *Journal of computational electronics*, vol. 5, no. 2-3, pp. 193–197, 2006.

[54] R. Selvaraju, M. H. Jamaluddin, M. R. Kamarudin, J. Nasir, and M. H. Dahri, "Complementary Split Ring Resonator for Isolation Enhancement in 5G Communication Antenna Array," *Progress In Electromagnetics Research*, vol. 83, pp. 217–228, 2018.

[55] M. S. Khan, A.-D. Capobianco, S. M. Asif, D. E. Anagnostou, R. M. Shubair, and B. D. Braaten, "A compact CSRR-enabled UWB diversity antenna," *IEEE Antennas and Wireless Propagation Letters*, vol. 16, pp. 808–812, 2017.

[56] A. Diallo, C. Luxey, P. Le Thuc, R. Staraj, and G. Kossiavas, "Study and reduction of the mutual coupling between two mobile phone PIFAs operating in the DCS1800 and UMTS bands," *IEEE Transactions on Antennas and Propagation*, vol. 54, no. 11, pp. 3063–3074, 2006.

[57] Y. Wang and Z. Du, "A wideband printed dual-antenna with three neutralization lines for mobile terminals," *IEEE Transactions on Antennas and Propagation*, vol. 62, no. 3, pp. 1495–1500, 2014.

[58] S.-W. Su, C.-T. Lee, and F.-S. Chang, "Printed MIMO-antenna system using neutralization-line technique for wireless USB-dongle applications," *IEEE Transactions on Antennas and Propagation*, vol. 60, no. 2, pp. 456–463, 2012.

[59] S. Fan, Y. Yin, B Lee, W Hu, and X Yang, "Bandwidth enhancement of a printed slot antenna with a pair of parasitic patches," *IEEE antennas and wireless propagation letters*, vol. 11, pp. 1230–1233, 2012.

[60] J.-S. Row and S.-W. Wu, "Circularly-polarized wide slot antenna loaded with a parasitic patch," *IEEE Transactions on Antennas and propagation*, vol. 56, no. 9, pp. 2826–2832, 2008.

[61] M. S. Khan, A.-D. Capobianco, A. Iftikhar, R. M. Shubair, D. E. Anagnostou, and B. D. Braaten, "Ultra-compact dual-polarised UWB MIMO antenna with meandered feeding lines," *IET Microwaves, Antennas & Propagation*, vol. 11, no. 7, pp. 997–1002, 2017.

[62] M. Alam, N. Misran, B. Yatim, M. T. Islam, *et al.*, "Development of electromagnetic band gap structures in the perspective of microstrip antenna design," *International Journal of Antennas and Propagation*, vol. 2013, 2013.

[63] A. Suntives and R. Abhari, "Miniaturization and isolation improvement of a multiple-patch antenna system using electromagnetic bandgap structures," *Microwave and Optical Technology Letters*, vol. 55, no. 7, pp. 1609–1612, 2013.

[64] S.-C. Chen, Y.-S. Wang, and S.-J. Chung, "A decoupling technique for increasing the port isolation between two strongly coupled antennas," *IEEE transactions on antennas and propagation*, vol. 56, no. 12, pp. 3650–3658, 2008.

[65] C.-H. Wu, G.-T. Zhou, Y.-L. Wu, and T.-G. Ma, "Stub-loaded reactive decoupling network for two-element array using even-odd analysis," *IEEE Antennas and Wireless Propagation Letters*, vol. 12, pp. 452–455, 2013.

[66] G Das, A Sharma, R. Gangwar, and M. Sharawi, "Compact back-to-back DRA-based four-port MIMO antenna system with bi-directional diversity," *Electronics Letters*, vol. 54, no. 14, pp. 884–886, 2018.

[67] S. Soltani, P. Lotfi, and R. D. Murch, "A port and frequency reconfigurable MIMO slot antenna for WLAN applications," *IEEE Transactions on Antennas and Propagation*, vol. 64, no. 4, pp. 1209–1217, 2016.

[68] A. A. Ibrahim and M. A. Abdalla, "CRLH MIMO antenna with reversal configuration," *AEU-International Journal of Electronics and Communications*, vol. 70, no. 9, pp. 1134–1141, 2016.

[69] M. Gallo, E. Antonino-Daviu, M. Ferrando-Bataller, M. Bozzetti, J. M. Molina-Garcia-Pardo, and L. Juan-Llacer, "A broadband pattern diversity annular slot antenna," *IEEE Transactions on Antennas and propagation*, vol. 60, no. 3, pp. 1596–1600, 2012.

[70] Q. Rao and D. Wang, "A compact dual-port diversity antenna for long-term evolution handheld devices," *IEEE transactions on vehicular technology*, vol. 59, no. 3, pp. 1319–1329, 2010.

[71] Y. Ding, Z. Du, K. Gong, and Z. Feng, "A novel dual-band printed diversity antenna for mobile terminals," *IEEE Transactions on Antennas and Propagation*, vol. 55, no. 7, pp. 2088–2096, 2007.

[72] X. Cai, A.-g. Wang, N. Ma, and W. Leng, "A novel planar parasitic array antenna with reconfigurable azimuth pattern," *IEEE Antennas and Wireless Propagation Letters*, vol. 11, pp. 1186–1189, 2012.

[73] T. S. See and Z. N. Chen, "An ultrawideband diversity antenna," *IEEE Transactions on Antennas and Propagation*, vol. 57, no. 6, pp. 1597–1605, 2009.

[74] S Zhang, G. Huff, J Feng, and J. Bernhard, "A pattern reconfigurable microstrip parasitic array," *IEEE Transactions on Antennas and Propagation*, vol. 52, no. 10, pp. 2773–2776, 2004.

[75] W. K. Toh, Z. N. Chen, X. Qing, and T. S. P. See, "A planar uwb diversity antenna," *IEEE Transactions on Antennas and Propagation*, vol. 57, no. 11, pp. 3467–3473, 2009.

[76] Y. Zhou, R. S. Adve, and S. V. Hum, "Design and evaluation of pattern reconfigurable antennas for MIMO applications," *IEEE Transactions on Antennas and Propagation*, vol. 62, no. 3, pp. 1084–1092, 2014.

[77] G.-M. Zhang, J.-S. Hong, B.-Z. Wang, G. Song, and P. Li, "Design and time-domain analysis for a novel pattern reconfigurable antenna," *IEEE Antennas and Wireless Propagation Letters*, vol. 10, pp. 365–368, 2011.

[78] T. Zhang, S.-Y. Yao, and Y. Wang, "Design of radiation-pattern-reconfigurable antenna with four beams," *IEEE Antennas and wireless propagation letters*, vol. 14, pp. 183–186, 2015.

[79] K Yang, A Loutridis, X Bao, G Ruvio, and M. Ammann, "Printed inverted-f antenna with reconfigurable pattern and polarization," in *Antennas and Propagation (EuCAP), 2016 10th European Conference on*, IEEE, 2016, pp. 1–5.

[80] M. Yunita and A. Munir, "Reconfigurable radiation pattern of microstrip antenna using shorting post," in *Information Technology, Computer, and Electrical Engineering (ICITACEE), 2015 2nd International Conference on*, IEEE, 2015, pp. 292–296.

[81] S Zhang, G. Huff, G Cung, and J. Bernhard, "Three variations of a pattern-reconfigurable microstrip parasitic array," *Microwave and optical technology letters*, vol. 45, no. 5, pp. 369–372, 2005.

[82] J. G. Jeong, J. Ahn, and Y. J. Yoon, "Ultra-wideband reconfigurable radiation pattern antenna for diversity applications," *Electronics Letters*, vol. 51, no. 25, pp. 2086–2087, 2015.

[83] G. Huff, J Feng, S Zhang, and J. Bernhard, "A novel radiation pattern and frequency reconfigurable single turn square spiral microstrip antenna," *IEEE Microwave and Wireless Components Letters*, vol. 13, no. 2, pp. 57–59, 2003.

[84] S Zhang, G. Huff, J Feng, and J. Bernhard, "A pattern reconfigurable microstrip parasitic array," *IEEE Transactions on Antennas and Propagation*, vol. 52, no. 10, pp. 2773–2776, 2004.

[85] E. Palantei, D. V. Thiel, and S. G. O'Keefe, "Rectangular patch with parasitic folded dipoles: A reconfigurable antenna," in *Antenna Technology: Small Antennas and Novel Metamaterials, 2008. iWAT 2008. International Workshop on*, IEEE, 2008, pp. 251–254.

[86] W. Kang, J. Park, and Y. Yoon, "Simple reconfigurable antenna with radiation pattern," *Electronics Letters*, vol. 44, no. 3, pp. 182–183, 2008.

[87] J. Dong, A. Wang, and H. Lan, "A simple radiation pattern reconfigurable printed dipole antenna," in *Microwave, Antenna, Propagation and EMC Technologies for Wireless Communications, 2009 3rd IEEE International Symposium on*, IEEE, 2009, pp. 619–622.

[88] M. Donelli, R. Azaro, L. Fimognari, and A. Massa, "A planar electronically reconfigurable wi-fi band antenna based on a parasitic microstrip structure," *IEEE Antennas and Wireless Propagation Letters*, vol. 6, pp. 623–626, 2007.

[89] H. A. Majid, M. K. A. Rahim, M. R. Hamid, and M. F. Ismail, "Frequency and pattern reconfigurable slot antenna," *IEEE Trans. Antennas Propag.*, vol. 62, no. 10, pp. 5339–5343, 2014.

[90] S Raman, P Mohanan, N. Timmons, and J. Morrison, "Microstrip-fed pattern-and polarization-reconfigurable compact truncated monopole antenna," *Ieee antennas and wireless propagation letters*, vol. 12, pp. 710–713, 2013.

[91] Y. P. Selvam, L. Elumalai, M. G. N. Alsath, M. Kanagasabai, S. Subbaraj, and S. Kingsly, "Novel frequency-and pattern-reconfigurable rhombic patch antenna with switchable polarization," *IEEE Antennas and Wireless Propagation Letters*, vol. 16, pp. 1639–1642, 2017.

[92] M. J. Slater, H. K. Pan, and J. T. Bernhard, "Preliminary results in the development of a compound reconfigurable antenna," in *Antennas and Propagation Society International Symposium, 2008. AP-S 2008. IEEE*, IEEE, 2008, pp. 1–4.

[93] A. Ramadan, M. Al-Husseini, Y. Tawk, K. Y. Kabalan, and A. El-Hajj, "A novel frequency/pattern-reconfigurable microstrip antenna for wlan applications," in *Antennas and Propagation (EuCAP), 2010 Proceedings of the Fourth European Conference on*, IEEE, 2010, pp. 1–3.

[94] D. Piazza, P. Mookiah, M. D'Amico, and K. R. Dandekar, "Pattern and polarization reconfigurable circular patch for mimo systems," in *Antennas and Propagation, 2009. EuCAP 2009. 3rd European Conference on*, IEEE, 2009, pp. 1047–1051.

[95] X.-S. Yang, B.-Z. Wang, and W. Wu, "Pattern reconfigurable patch antenna with two orthogonal quasi-yagi arrays," in *Antennas and Propagation Society International Symposium, 2005 IEEE*, IEEE, vol. 2, 2005, pp. 617–620.

[96] C. won Jung, M.-j. Lee, G. Li, and F. De Flaviis, "Reconfigurable scan-beam single-arm spiral antenna integrated with rf-mems switches," *IEEE Transactions on antennas and propagation*, vol. 54, no. 2, pp. 455–463, 2006.

[97] Skyworks. (2004). Skyworks SMP1320 Series Data Sheet, [Online]. Available: `http://www.skyworksinc.com/uploads/documents/SMP1320_Series_200047Q.pdf`.

[98] M. Ali, "Conception et Réalisation d'Antennes Reconfigurables en Fréquence (PhD thesis)," 2016.

[99] J. Liang, L. Guo, C. C. Chiau, and X. Chen, "CPW-fed circular disc monopole antenna for UWB applications," in *Antenna Technology: Small Antennas and Novel Metamaterials, 2005. IWAT 2005. IEEE International Workshop on*, IEEE, 2005, pp. 505–508.

[100] M. Bialkowski and N. Karmakar, "Design of compact l-band 180° phase shifters," *Microwave and optical technology letters*, vol. 22, no. 2, pp. 144–148, 1999.

[101] D. Chai, M. Yim, M. Linh, and G. Yoon, "A miniaturized side-coupled 45° schiffman phase shifter on teflon substrate," *Microwave and Optical Technology Letters*, vol. 38, no. 2, pp. 147–150, 2003.

[102] M. Bialkowski and Y. Wang, "Broadband microstrip phase shifters employing parallel stubs and ground slots," *Microwave and Optical Technology Letters*, vol. 53, no. 4, pp. 723–728, 2011.

[103] X. Tang and K. Mouthaan, "Phase-Shifter Design Using Phase-Slope Alignment With Grounded Shunt $\frac{\lambda}{4}$ Stubs," *IEEE Transactions on Microwave Theory and Techniques*, vol. 58, no. 6, pp. 1573–1583, 2010.

[104] M. A. Abbosh, "Ultra wideband vertical microstrip-microstrip transition," *IET Microwaves, Antennas Propagation*, vol. 1, no. 5, pp. 968–972, 2007.

[105] J. Reed and G. J. Wheeler, "A method of analysis of symmetrical four-port networks," *IRE Transactions on Microwave Theory and Techniques*, vol. 4, no. 4, pp. 246–252, 1956.

[106] H. J. Riblet, "A mathematical theory of directional couplers," *Proceedings of the IRE*, vol. 35, no. 11, pp. 1307–1313, 1947.

[107] F. P. Casares-Miranda, C. Viereck, C. Camacho-Penalosa, and C. Caloz, "Vertical microstrip transition for multilayer microwave circuits with decoupled passive and active layers," *IEEE Microwave and Wireless Components Letters*, vol. 16, no. 7, pp. 401–403, 2006.

[108] A. S. Theodorou and N. K. Uzunoglu, "Transition properties of a vertical conductor connecting two microstrip lines at different planes," *IEEE Transactions on Microwave Theory and Techniques*, vol. 42, no. 12, pp. 2277–2284, 1994.

[109] Q. Gu, Y. E. Yang, and M. A. Tassoudji, "Modeling and analysis of vias in multilayered integrated circuits," *IEEE Transactions on Microwave Theory and Techniques*, vol. 41, no. 2, pp. 206–214, 1993.

[110] D. M. Pozar, *Microwave Engineering. 4th*, 54. 2012, vol. 51, p. 51.

[111] A. M. Abbosh, "Ultrawideband balanced bandpass filter," *IEEE Microwave and Wireless Components Letters*, vol. 21, no. 9, pp. 480–482, 2011.

[112] R. Garg, I. Bahl, and M. Bozzi, *Microstrip lines and slotlines*. Artech house, 2013.

[113] J. Shin and D. H. Schaubert, "A parameter study of stripline-fed vivaldi notch-antenna arrays," *IEEE Transactions on Antennas and Propagation*, vol. 47, no. 5, pp. 879–886, 1999.

[114] X. Y. Zhang, Y. Zhang, Y.-M. Pan, and W. Duan, "Low-profile dual-band filtering patch antenna and its application to lte mimo system," *IEEE Transactions on Antennas and Propagation*, vol. 65, no. 1, pp. 103–113, 2017.

[115] I. T. Elfergani, A. S. Hussaini, J. Rodriguez, R. A. Abd-Alhameed, C. H. See, N. Jan, S. Zhu, and N. J. McEwan, "Compact and closely spaced tunable printed f-slot multiple-input–multiple-output antenna system for portable wireless applications with efficient diversity," *IET Science, Measurement & Technology*, vol. 8, no. 6, pp. 359–369, 2014.

[116] S. Hong, J. Brand, J. I. Choi, M. Jain, J. Mehlman, S. Katti, and P. Levis, "Applications of self-interference cancellation in 5g and beyond," *IEEE Communications Magazine*, vol. 52, no. 2, pp. 114–121, 2014.

[117] M. A. Jensen and J. W. Wallace, "A review of antennas and propagation for mimo wireless communications," *IEEE Transactions on Antennas and Propagation*, vol. 52, no. 11, pp. 2810–2824, 2004.

[118] J. Weber, C. Volmer, K. Blau, R. Stephan, and M. A. Hein, "Miniaturized antenna arrays using decoupling networks with realistic elements," *IEEE Transactions on Microwave Theory and Techniques*, vol. 54, no. 6, pp. 2733–2740, 2006.

[119] H. J. Song, A. Bekaryan, J. H. Schaffner, A. Hussain, and P.-S. Kildal, "Effects of mutual coupling on lte mimo capacity for monopole array: Comparing reverberation chamber tests and drive tests," *IEEE Antennas Wireless Propag. Lett.*, vol. 14, pp. 454–457, 2015.

[120] S. H. Chae, S.-k. Oh, and S.-O. Park, "Analysis of mutual coupling, correlations, and tarc in wibro mimo array antenna," *IEEE Antennas and Wireless Propagation Letters*, vol. 6, pp. 122–125, 2007.

[121] Y. Chen and D. Manteuffel, "A tunable decoupling and matching concept for compact mobile terminal antennas," *IEEE Transactions on Antennas and Propagation*, vol. 65, no. 4, pp. 1570–1578, 2017.

[122] J. Sui and K.-L. Wu, "A general t-stub circuit for decoupling of two dual-band antennas," *IEEE Transactions on Microwave Theory and Techniques*, vol. 65, no. 6, pp. 2111–2121, 2017.

[123] C.-C. Hsu, K.-H. Lin, and H.-L. Su, "Implementation of broadband isolator using metamaterial-inspired resonators and a t-shaped branch for mimo antennas," *IEEE Transactions on Antennas and Propagation*, vol. 59, no. 10, pp. 3936–3939, 2011.

[124] D. Sarkar and K. V. Srivastava, "A compact four-element mimo/diversity antenna with enhanced bandwidth," *IEEE Antennas and Wireless Propagation Letters*, vol. 16, pp. 2469–2472, 2017.

[125] B. C. Pan and T. J. Cui, "Broadband decoupling network for dual-band microstrip patch antennas," *IEEE Transactions on Antennas and Propagation*, vol. 65, no. 10, pp. 5595–5598, 2017.

[126] L. Zhao and K.-L. Wu, "A decoupling technique for four-element symmetric arrays with reactively loaded dummy elements," *IEEE Transactions on Antennas and Propagation*, vol. 62, no. 8, pp. 4416–4421, 2014.

[127] L. Qu, R. Zhang, and H. Kim, "Decoupling between ground radiation antennas with ground-coupled loop-type isolator for wlan applications," *IET Microwaves, Antennas & Propagation*, vol. 10, no. 5, pp. 546–552, 2016.

[128] X.-L. Liu, Z.-D. Wang, Y.-Z. Yin, J Ren, and J.-J. Wu, "A compact ultrawideband mimo antenna using qsca for high isolation," *IEEE Antennas and Wireless Propagation Letters*, vol. 13, pp. 1497–1500, 2014.

[129] Z. Qamar, L. Riaz, M. Chongcheawchamnan, S. A. Khan, and M. F. Shafique, "Slot combined complementary split ring resonators for mutual coupling suppression in microstrip phased arrays," *IET Microwaves, Antennas & Propagation*, vol. 8, no. 15, pp. 1261–1267, 2014.

[130] S. Shoaib, I. Shoaib, N. Shoaib, X. Chen, and C. G. Parini, "Mimo antennas for mobile handsets," *IEEE Antennas and Wireless Propagation Letters*, vol. 14, pp. 799–802, 2015.

[131] J. Tao and Q. Feng, "Compact ultrawideband mimo antenna with half-slot structure," *IEEE Antennas and Wireless Propagation Letters*, vol. 16, pp. 792–795, 2017.

[132] H. Qi, X. Yin, L. Liu, Y. Rong, and H. Qian, "Improving isolation between closely spaced patch antennas using interdigital lines," *IEEE Antennas Wireless Propag. Lett.*, vol. 15, pp. 286–289, 2016.

[133] H. Qi, L. Liu, X. Yin, H. Zhao, and W. J. Kulesza, "Mutual coupling suppression between two closely spaced microstrip antennas with an asymmetrical coplanar strip wall," *IEEE Antennas Wireless Propag. Lett*, vol. 15, pp. 191–194, 2016.

[134] Y. Sharma, D. Sarkar, K. Saurav, and K. V. Srivastava, "Three-element mimo antenna system with pattern and polarization diversity for wlan applications," *IEEE Antennas and Wireless Propagation Letters*, vol. 16, pp. 1163–1166, 2017.

[135] C. H. See, R. A. Abd-Alhameed, Z. Z. Abidin, N. J. McEwan, and P. S. Excell, "Wideband printed mimo/diversity monopole antenna for wifi/wimax applications," *IEEE transactions on antennas and propagation*, vol. 60, no. 4, pp. 2028–2035, 2012.

[136] L. Yang, M. Fan, F. Chen, J. She, and Z. Feng, "A novel compact electromagnetic-bandgap (ebg) structure and its applications for microwave circuits," *IEEE Transactions on Microwave Theory and Techniques*, vol. 53, no. 1, pp. 183–190, 2005.

[137] F Caminita, S Costanzo, G Di Massa, G Guarnieri, S Maci, G Mauriello, and I Venneri, "Reduction of patch antenna coupling by using a compact ebg formed by shorted strips with interlocked branch-stubs," *IEEE Antennas and Wireless Propagation Letters*, vol. 8, pp. 811–814, 2009.

[138] C.-Y. Chiu, C.-H. Cheng, R. D. Murch, and C. R. Rowell, "Reduction of mutual coupling between closely-packed antenna elements," *IEEE Transactions on Antennas and Propagation*, vol. 55, no. 6, pp. 1732–1738, 2007.

[139] Y. Chung, S.-S. Jeon, D. Ahn, J.-I. Choi, and T. Itoh, "High isolation dual-polarized patch antenna using integrated defected ground structure," *IEEE Microwave and Wireless Components Letters*, vol. 14, no. 1, pp. 4–6, 2004.

[140] Y.-F. Cheng and K.-K. M. Cheng, "A novel and simple decoupling method for a three-element antenna array," *IEEE Antennas and Wireless Propagation Letters*, vol. 16, pp. 1072–1075, 2017.

[141] C.-H. Wu, C.-L. Chiu, and T.-G. Ma, "Very compact fully lumped decoupling network for a coupled two-element array," *IEEE Antennas and Wireless Propagation Letters*, vol. 15, pp. 158–161, 2016.

[142] R.-P. Li, P. Wang, Q. Zheng, and R.-Z. Wu, "Compact microstrip decoupling and matching network for two symmetric antennas," *Electronics Letters*, vol. 51, no. 18, pp. 1396–1398, 2015.

[143] K. Qian, L. Zhao, and K.-L. Wu, "An ltcc coupled resonator decoupling network for two antennas," *IEEE Transactions on Microwave Theory and Techniques*, vol. 63, no. 10, pp. 3199–3207, 2015.

[144] H. Meng and K.-L. Wu, "An lc decoupling network for two antennas working at low frequencies," *IEEE Transactions on Microwave Theory and Techniques*, vol. 65, no. 7, pp. 2321–2329, 2017.

[145] H. Makimura, K. Nishimoto, T. Yanagi, T. Fukasawa, and H. Miyashita, "Novel decoupling concept for strongly coupled frequency-dependent antenna arrays," *IEEE Transactions on Antennas and Propagation*, vol. 65, no. 10, pp. 5147–5154, 2017.

[146] X. Tang, X. Qing, and Z. N. Chen, "Simplification and implementation of decoupling and matching network with port pattern-shaping capability for two closely spaced antennas," *IEEE Transactions on Antennas and Propagation*, vol. 63, no. 8, pp. 3695–3699, 2015.

[147] X. Tang, K. Mouthaan, and J. Coetzee, "Tunable decoupling and matching network for diversity enhancement of closely spaced antennas," *IEEE Antennas and Wireless Propagation Letters*, vol. 11, pp. 268–271, 2012.

[148] R.-L. Xia, S.-W. Qu, P.-F. Li, Q. Jiang, and Z.-P. Nie, "An efficient decoupling feeding network for microstrip antenna array," *IEEE Antennas and Wireless Propagation Letters*, vol. 14, pp. 871–874, 2015.

[149] K.-C. Lin, C.-H. Wu, C.-H. Lai, and T.-G. Ma, "Novel dual-band decoupling network for two-element closely spaced array using synthesized microstrip lines," *IEEE Transactions on Antennas and Propagation*, vol. 60, no. 11, pp. 5118–5128, 2012.

[150] J. C. Coetzee and Y. Yu, "Port decoupling for small arrays by means of an eigenmode feed network," *IEEE Transactions on Antennas and Propagation*, vol. 56, no. 6, pp. 1587–1593, 2008.

[151] K.-L. Wu, C. Wei, X. Mei, and Z.-Y. Zhang, "Array-antenna decoupling surface," *IEEE Transactions on Antennas and Propagation*, vol. 65, no. 12, pp. 6728–6738, 2017.

[152] P. Gibson, "The vivaldi aerial," in *Microwave Conference, 1979. 9th European*, IEEE, 1979, pp. 101–105.

[153] E. Gazit, "Improved design of the vivaldi antenna," in *IEE Proceedings H-Microwaves, Antennas and Propagation*, IET, vol. 135, 1988, pp. 89–92.

[154] M. Han and J. Choi, "Small-size printed strip mimo antenna for next generation mobile handset application," *Microwave and Optical Technology Letters*, vol. 53, no. 2, pp. 348–352, 2011.

[155] R. G. Vaughan and J. B. Andersen, "Antenna diversity in mobile communications," *IEEE Transactions on vehicular technology*, vol. 36, no. 4, pp. 149–172, 1987.

[156] B. C. Ng and C. M. S. See, "Sensor-array calibration using a maximum-likelihood approach," *IEEE Transactions on Antennas and Propagation*, vol. 44, no. 6, pp. 827–835, 1996.

Publications

"Scientists discover the world that exists, Engineers create the world that never was."

Theodore Von Karman (1881-1963).

Publications

Journals

- **S. Tebache**, A. Belouchrani, F. Ghanem, and A. Mansoul, "Novel reliable and practical decoupling mechanism for strongly coupled antenna arrays," *IEEE Transactions on Antennas and Propagation*, vol. 67, no. 9, pp.5892-5899, 2019.

- **S. Tebache**, F. Ghanem, A. Belouchrani, and A. Mansoul, "Novel flowchart design of frequency independent 180° phase shifters," *Microwave and Optical Technology Letters*, vol. 61, no. 1, pp. 136–140, 2019.

- **S. Tebache**, F. Ghanem, A. Belouchrani, and A. Mansoul, "Frequency independent 180 ° phase shifter based on UWB coupled sections," *Microwave and Optical Technology Letters*, vol. 59, no. 12, pp. 3185–3189, 2017.

International conferences

- **S. Tebache**, A. Belouchrani, F. Ghanem, and A. Mansoul, "Compact 45° phase shifter based on coupled tapered transition for UWB applications," *in 2017 5th International Conference on Electrical Engineering-Boumerdes (ICEE-B), IEEE*, 2017, pp. 1–4.

- **S. Tebache**, F. Ghanem, and A. Belouchrani, "Novel and simple approach for reconfiguring the pattern of an UWB $CPW-Fed$ monopole antenna," *in Detection Systems Architectures and Technologies (DAT), Seminar on, IEEE*, 2017, pp. 1–5.